Knockdown of Plakophilin 2 Downregulates miR-184 Through CpG Hypermethylation and Suppression of the E2F1 Pathway and Leads to Enhanced Adipogenesis In Vitro

Priyatansh Gurha,* Xiaofan Chen,* Raffaella Lombardi, James T. Willerson, Ali J. Marian

Rationale: ***PKP2*, encoding plakophilin 2 (PKP2), is the most common causal gene for arrhythmogenic cardiomyopathy.**

Objective: **To characterize miRNA expression profile in PKP2-deficient cells.**

Methods and Results: **Control and PKP2-knockdown HL-1 (HL-1$^{Pkp2\text{-}shRNA}$) cells were screened for 750 miRNAs using low-density microfluidic panels. Fifty-nine miRNAs were differentially expressed. MiR-184 was the most downregulated miRNA. Expression of miR-184 in the heart and cardiac myocyte was developmentally downregulated and was low in mature myocytes. MicroRNA-184 was predominantly expressed in cardiac mesenchymal progenitor cells. Knockdown of *Pkp2* in cardiac mesenchymal progenitor cells also reduced miR-184 levels. Expression of miR-184 was transcriptionally regulated by the E2F1 pathway, which was suppressed in PKP2-deficient cells. Activation of E2F1, on overexpression of its activator CCND1 (cyclin D1) or knockdown of its inhibitor retinoblastoma 1, partially rescued miR-184 levels. In addition, DNA methyltransferase-1 was recruited to the promoter region of miR-184, and the CpG sites at the upstream region of miR-184 were hypermethylated. Treatment with 5-aza-2′-deoxycytidine, a demethylation agent, and knockdown of DNA methyltransferase-1 partially rescued miR-184 level. Pathway analysis of paired miR-184:mRNA targets identified cell proliferation, differentiation, and death as the main affected biological processes. Knockdown of miR-184 in HL-1 cells and mesenchymal progenitor cells induced and, conversely, its overexpression attenuated adipogenesis.**

Conclusions: **PKP2 deficiency leads to suppression of the E2F1 pathway and hypermethylation of the CpG sites at miR-184 promoter, resulting in downregulation of miR-184 levels. Suppression of miR-184 enhances and its activation attenuates adipogenesis in vitro. Thus, miR-184 contributes to the pathogenesis of adipogenesis in PKP2-deficient cells. (*Circ Res*. 2016;119:731-750. DOI: 10.1161/CIRCRESAHA.116.308422.)**

Key Words: cardiomyopathy ■ DNA methylation ■ epigenetics ■ gene expression ■ heart failure ■ microRNA

Arrhythmogenic cardiomyopathy (AC) is a hereditary cardiomyopathy that manifests with ventricular arrhythmias, sudden cardiac death, and heart failure.[1,2] The pathological hallmark of AC is a gradual and progressive replacement of cardiac myocytes by fibro-adipocytes, which classically shows a predilection toward involvement of the right ventricle and, hence, the term arrhythmogenic right ventricular cardiomyopathy.[3,4] AC is an enigmatic disease with an inadequately understood pathogenesis. Recent molecular genetic discoveries have led to partial elucidation of the causal genes and identification of mutations in genes encoding the protein constituents of the intercalated disks (IDs).[5–9] IDs are cell–cell adhesion structures composed of desmosomes, adherens junctions, and gap junctions. IDs not only provide mechanical integrity to the myocardium but also control contact-regulated signal transduction.[10] Mutations in Lamin A/C and transmembrane protein 43 are also associated with AC.[11,12] Overall, *PKP2* gene encoding plakophilin 2 (PKP2), a constituent of the IDs, is the most common causal gene for AC.[13,14]

In This Issue, see p 697

The molecular links between the mutant causal proteins and the ensuing cardiac phenotype in AC are not fully known. Extensive molecular remodeling of the IDs in AC impairs mechanotransduction and is associated with activation of the

Original received January 24, 2016; revision received July 16, 2016; accepted July 28, 2016. In June 2016, the average time from submission to first decision for all original research papers submitted to *Circulation Research* was 13.08 days.

From the Center for Cardiovascular Genetics, Institute of Molecular Medicine and Department of Medicine, University of Texas Health Sciences Center at Houston, and Texas Heart Institute.

*These authors are joint first authors.

This article was sent to Mark A. Sussman, Consulting Editor, for review by expert referees, editorial decision, and final disposition.

The online-only Data Supplement is available with this article at http://circres.ahajournals.org/lookup/suppl/doi:10.1161/CIRCRESAHA.116.308422/-/DC1.

Correspondence to Dr Ali J. Marian, Center for Cardiovascular Genetics, 6770 Bertner St, Suite C900A, Houston, TX 77030. E-mail Ali.J.Marian@uth.tmc.edu; or Dr Priyatansh Gurha, Center for Cardiovascular Genetics, 6770 Bertner St, Suite C905, Houston, TX 77030. E-mail Priyatansh.Gurha@uth.tmc.edu

Nonstandard Abbreviations and Acronyms

5-aza-D	5-aza-2′-deoxycytidine
AC	arrhythmogenic cardiomyopathy
Agpat1	acylglycerolphosphate acyltransferase
Agpat3	acylglycerolphosphate acyltransferase
DNMT	DNA methyltransferase
FABP4	fatty acid–binding protein 4
IDs	intercalated disk
JUP	junction plakoglobin
MPCs	mesenchymal progenitor cells
miR	microRNA
PDGFRA	platelet-derived growth factor α
PKP2	plakophilin-2
PPARG	peroxisome proliferator-activated receptor gamma
RB1	retinoblastoma 1
RNA-Seq	RNA sequencing
ShRNA	short hairpin RNA
TCF7L2	transcription factor 7-like 2 (T cell–specific, HMG-box)
TEAD	TEA domain family member (SV40 transcriptional enhancer factor)
YAP	Yes-associated protein

Hippo pathway, a contact-regulated signaling pathway involved in cellular growth, differentiation, and proliferation.[15] Activation of the Hippo pathway results in suppression of gene expression through its downstream effector, the Yes-associated protein–TEA domain family member (YAP–TEAD) complex, as well as suppression of the canonical Wnt signaling through the β catenin (CTNNB1)-TCF7L2 (transcription factor 7-like 2 [T cell–specific, HMG-box]) transcriptional machinery.[15–17] Collectively, these cell-signaling events impart transcriptional changes that regulate cell growth, proliferation, and differentiation, leading to phenotypic expression of AC.[15]

MicroRNAs (miRNAs) are small 22 nucleotide molecules that regulate gene expression and impact various biological processes, including cardiac hypertrophy, myocyte differentiation, and proliferation..[18–20] MiRNAs are largely nudgers and tweakers of genome management because their effects on transcript levels, by-and-large, are modest.[21] Because of multiplicity of their targets, however, miRNAs influence various molecular networks and biological processes.[20,22–30] MiRNAs are also targets of various signaling pathways, including Hippo and the canonical Wnt pathways, which are implicated in AC.[20,22–30] Moreover, miRNAs are implicated in the pathogenesis of heart failure, fibrosis, and adipogenesis,[18,31–33] phenotypes typically observed in patients with cardiomyopathies.[2–4] Thus, we hypothesized that miRNAs are also involved in the pathogenesis of AC. To test this hypothesis, we screened for the differentially expressed miRNAs and characterized functional and biological effects of the most downregulated miRNA in HL-1 and cardiac mesenchymal progenitor cells (MPCs).

Methods

An expanded version of Material and Methods is provided as Online Data Supplement.

Recombinant Viral Constructs

Recombinant lentiviruses were generated as published.[15] The miR-Zip vector contained short hairpin RNAs (shRNAs) positioned in tandem with a GFP expression cassette downstream to an H1 promoter. MiR-184 overexpression vector contained a 500-bp genomic fragment of miR-184 in the miR-Express vector. Commercially available lentiviruses expressing shRNAs against target transcripts and prepackaged recombinant adenoviral constructs were used. HL-1 cells at 70% to 90% confluence were transduced with the recombinant viruses. Transduction efficiency was determined by detecting the GFP signal under fluorescence microscopy, fluorescence-activated cell sorter analysis, and quantification of the target transcript levels.

Suppression of Expression of PKP2 in the HL-1 Cells

Two independent PKP2-deficient HL-1 lines (HL-1$^{Pkp2\text{-}shRNA}$) were established using 2 different shRNAs, as published.[15] Knockdown of *Pkp2* mRNA and PKP2 protein levels were detected by quantitative polymerase chain reaction (qPCR) and immunoblotting, respectively.

Isolation of Cardiac Myocytes and MPCs

To isolate cardiac myocytes, explanted hearts were perfused with a Ca^{2+}-free perfusion buffer and subjected to digestion in a collagenase buffer. Myocytes were dissociated and gravity precipitated in the presence of 200 mmol/L ATP and centrifugation at 20*g*. The isolated myocytes were reintroduced to increasing concentrations of calcium at a final concentration of 1.5 mmol/L of $CaCl_2$ and placed in culture dishes or cover glasses coated with laminin.

Cardiac MPCs were isolated by sorting of nonmyocyte fraction of cardiac cells against anti-CD44 and antiplatelet-derived growth factor α (PDGFRA) antibodies, per published protocols.[34–36]

Mouse Models of AC

Myh6:Jup^{Tr} mice have been published.[16,37,38] To knock down *Pkp2* gene in the heart, an shRNA targeting the *Pkp2* mRNA (position 1154–1174) was cloned into the U6-LoxP-Neo vector.[39,40] *Nkx2-5:Cre* deleter mice was used to remove a LoxP neo cassette and conditionally activate expression of the shRNA against *Pkp2* mRNA (*Pkp2*^{shRNA}) in the cardiogenic lineage.[41]

MicroRNA Expression Profiling

Expression profile of miRNAs was determined using TaqMan low-density array microfluidic cards (Rodent miRNA v3.0 Card A and Card B; Applied Biosystems). The panels contain a total of 750 mature miRNAs of which 641 are annotated and curated in the mouse genome. Mouse small nucleolar RNA (*MammU6*) was used for data normalization and relative quantification because it was spotted 3 times in each card, as opposed to other controls. In brief, aliquots of RNA isolated from the HL-1 and HL-1$^{Pkp2\text{-}shRNA}$ cells from 2 independent experiments were reverse-transcribed into cDNAs and amplified by qPCR. MiRNAs with *C*t values of >35 were excluded.

Immunoblotting and Immunofluorescence Staining

Immunoblotting and immunofluorescence were performed as per the conventional methods.[15,36] The list of the primary and secondary antibodies used is provided in the Online Table I.

In Situ Hybridization

In situ hybridization was performed as per a published protocol.[42] In brief, thin myocardial sections were hybridized with a 5′ and 3′ dual DIG-labeled detection probe against miR-184 or a control scrambled probe. Sections were washed in PBS after overnight hybridization, mounted, and examined under light microscopy.

Quantitative PCR

Total RNA (including miRNA) was extracted and reverse transcribed. MiRNAs were amplified using specific TaqMan gene expression assays and TaqMan MicroRNA assays (Online Table I). *Gapdh* and *snoRNA202* transcript levels were used for normalization for mRNA and miRNA levels, respectively. $2^{\Delta\Delta Ct}$ method was used to calculate the normalized gene expression values.

MicroRNA Targets and miRNA–mRNA Pairing

Global gene expression patterns were determined by whole transcriptome sequencing, as published.[15] Predicted miR-184 targets were identified using miRWalk online software (www.umm.uni-heidelberg.

de/apps/zmf/mirwalk/). Genes that were identified as targets in at least 2 different databases were analyzed. MiRNA–mRNA pairing was performed using the ingenuity pathway analysis software (www.ingenuity.com). All putative targets of miR-184 were identified using the miRwalk and ingenuity pathway analysis software. Targets that were identified by at least 2 programs and had a seed length of 6 nucleotides or longer were included for further analyses. The candidate target mRNAs and differentially expressed mRNAs were matched, and those mRNAs that had a minimum fragments per kilobase of transcript per million fragments mapped value of 1 in at least one sample and showed a reciprocal expression to its corresponding miRNA were considered as targets. Finally, target gene expression cutoff was set at 1.2-fold expression, and the *q* value at 0.05. To examine the potential biological significance of paired changes, gene ontology over-representation analysis, upstream regulator, and canonical pathway analyses were performed using ingenuity pathway analysis.

Adiogenesis Network Analysis

A protein functional association network was constructed for miR-184 targets that were involved in adipogenesis, namely, AGPAT1, AGPAT3, NCOA1, and peroxisome proliferator-activated receptor gamma (PPARG)C1B, using the STRING online tool. The medium confidence score for interaction was set at 0.4, and the option for all active prediction method was included. Direct interactions are depicted as colored nodes in the Network. Gene that are identified as members of the network and were found to be upregulated in the HL-1$^{Pkp2\text{-}shRNA}$ cells in RNA-sequencing data were further validated to build an miR-184 target network for adipogenesis.

Adipogenesis

Induction and quantification of adipogenesis in the HL-1 cells and MPCs cells were as described.[15] In brief, ≈5×10^4 HL-1 cells or MPCs were treated with an adipogenesis induction medium for 7 to 14 days. qPCR and immunoblotting were used to quantify transcript and protein levels of selected genes that regulate adipogenesis, respectively. Accumulation of fat droplets was assessed by Oil Red O staining and expression of adipogenic transcription factors CEBPA (CCAAT/enhancer binding protein alpha) and PPARG expression by immunofluorescence.

Activation and Suppression of Selected Signaling Pathways

To determine the effect of activation of the E2F signaling pathway on miR-184 levels, HL-1 cells were transduced with recombinant adenoviruses expressing CCND1 (cyclin D1). Likewise, a siRNA construct was used to target retinoblastoma (RB1), an inhibitor of E2F1 pathway. Control viruses and viruses expressing no-target or scrambled shRNAs and nontargeting siRNAs were included as controls.

To activate the canonical Wnt signaling, cells were treated with Wnt-3A at 40, 80, and 120 ng/mL for 24 hours. To suppress the canonical Wnt signaling pathway, HL-1 cells were transduced with recombinant lentiviruses expressing shRNA against *Tcf7l2* (Lenti:*Tcf7l2*^{shRNA}). Activation or suppression of the canonical Wnt signaling pathway was also confirmed by quantifying protein levels of TCF7L2, mRNA levels of *Axin2* and *Ccnd1*, and a *Tcf7l2*-luciferase reporter assay.

To activate gene expression through the Hippo pathway, HL-1 cells were treated with 1 µmol/L of 1-Oleoyl lysophosphatidic acid for 1, 2, and 4 hours. To suppress gene expression through the Hippo pathway, cells were transduced with the recombinant lentiviruses expressing an shRNA against *Yap* (Lenti:*Yap*^{shRNA}). Activity state of the Hippo pathway was confirmed by quantifying levels of YAP protein by immunoblotting, mRNA levels of target transcripts *Ctgf* and *Cry61* by qPCR, and a TEAD luciferase assay.

DNA Methylation Assay

To determine whether suppression of miR-184 was a consequence of DNA methylation–dependent epigenetic silencing of the locus, the genomic sequence upstream of the pre-miR-184 transcription start site was analyzed for the presence of CpG-rich regions. Using EMBOSS Cpgplot (http://www.ebi.ac.uk/Tools/seqstats/emboss_cpgplot/), 15 CpG sites with observed/expected ratio of >0.60, located 500- to 800-bp upstream to the pre-miRNA start site, were identified. This region was used for DNA methylation analysis by bisulfite conversion, cloning, and sequencing of individual clones. Genomic DNA was extracted from the HL-1 and HL-1$^{Pkp2\text{-}shRNA}$ cells, treated for bisulfite conversion, and PCR-amplified using primers specific to the miR-184 upstream region (Online Table I). PCR products were cloned using a TA cloning strategy and then sequenced. Methylation of CpG sites was analyzed using QUMA online tool (http://quma.cdb.riken.jp/).

To determine effects of DNA methylation, *Dnmt1* was knocked down using recombinant lentiviruses expressing respective shRNAs, as described earlier.

Statistics

Data were presented as mean±SD. Differences in the continuous variables between the 2 groups were compared by *t* test or Mann–Whitney U test and among multiple groups by 1-way ANOVA. Whenever applicable, multiple groups Dunnett's corrected *P* values for pairwise comparisons were presented. Differences among the categorical values were compared by Kruskall–Wallis test. Statistical significance for methylation at each CpG sites was calculated by Fisher exact test (QUMA online tool).

Results

Differentially Expressed miRNAs in HL-1$^{Pkp2\text{-}shRNA}$ Cells

Two independent lines of HL-1$^{Pkp2\text{-}shRNA}$ were generated using 2 different sets of shRNAs that target *Pkp2* transcript (Figure 1A). qPCR showed reduced *Pkp2* mRNA levels by 3.7±0.5-fold (shRNA no 1, N=6; *P*<0.001) and 2.4±0.4-fold (shRNA no 2, N=5; *P*<0.001), as compared with control HL-1 cells (Figure 1B). Likewise, PKP2 protein levels were reduced by 81.1±10.4% (shRNA no 1, N=5; *P*<0.0001) and 77.8±15.6% (shRNA no 2, N=5; *P*<0.0001), as compared with control cells (Figure 1C and 1D).

To identify differentially expressed miRNAs in the HL-1$^{Pkp2\text{-}shRNA}$ cells, miRNAs were screened using TaqMan low-density array microfluidic panels comprising 641 unique miRNAs. A total of 292 miRNAs were expressed in the HL-1 cells at a threshold *C*t value of ≤35. Thirty-one miRNAs were upregulated, 28 were downregulated, and 233 were unchanged in the HL-1$^{Pkp2\text{-}shRNA}$ cells as compared with control HL-1 cells (Figure 1E and 1F; Online Table II).

MiR-200b, miR-487b, and miR-429 were the most upregulated, whereas miR-184 and miR-881 were the most downregulated miRNAs (Figure 1F). MiR-184, an independently transcribed miRNA, was the most downregulated miRNA in both lines of HL-1$^{Pkp2\text{-}shRNA}$ cells (Figure 1E, 1F, and 1G). It was reduced by more than ≈14-fold (N=24; *P*<0.0001). Likewise, transcript levels of miR-881 were reduced by 64.14±19.9% in the HL-1$^{Pkp2\text{-}shRNA}$ cells (*P*<0.0001). qPCR validation of top upregulated miRNAs showed that miR-200b levels were increased by 7.99±0.27 (N=4; *P*<0.0001) and miR-429 by 7.98±0.37 (N=4; *P*<0.0001) in the HL-1$^{Pkp2\text{-}shRNA}$ cells (Figure 1H). Given robust and consistent downregulation of miR-184 levels in the PKP2-deficient HL-1 cells and in view of a paucity of data on the biological functions of miR-184 in the heart, it was further characterized.

Generation and Characterization of an Nkx2.5-Cre:Pkp2^{shRNA} Mouse Model of AC

To extend the in vitro findings to in vivo models of AC, expression of *PKP2*, the most common causal gene for AC,[13,14] was conditionally knocked down in the mouse heart on expression of an shRNA against *Pkp2* mRNA, under the transcriptional

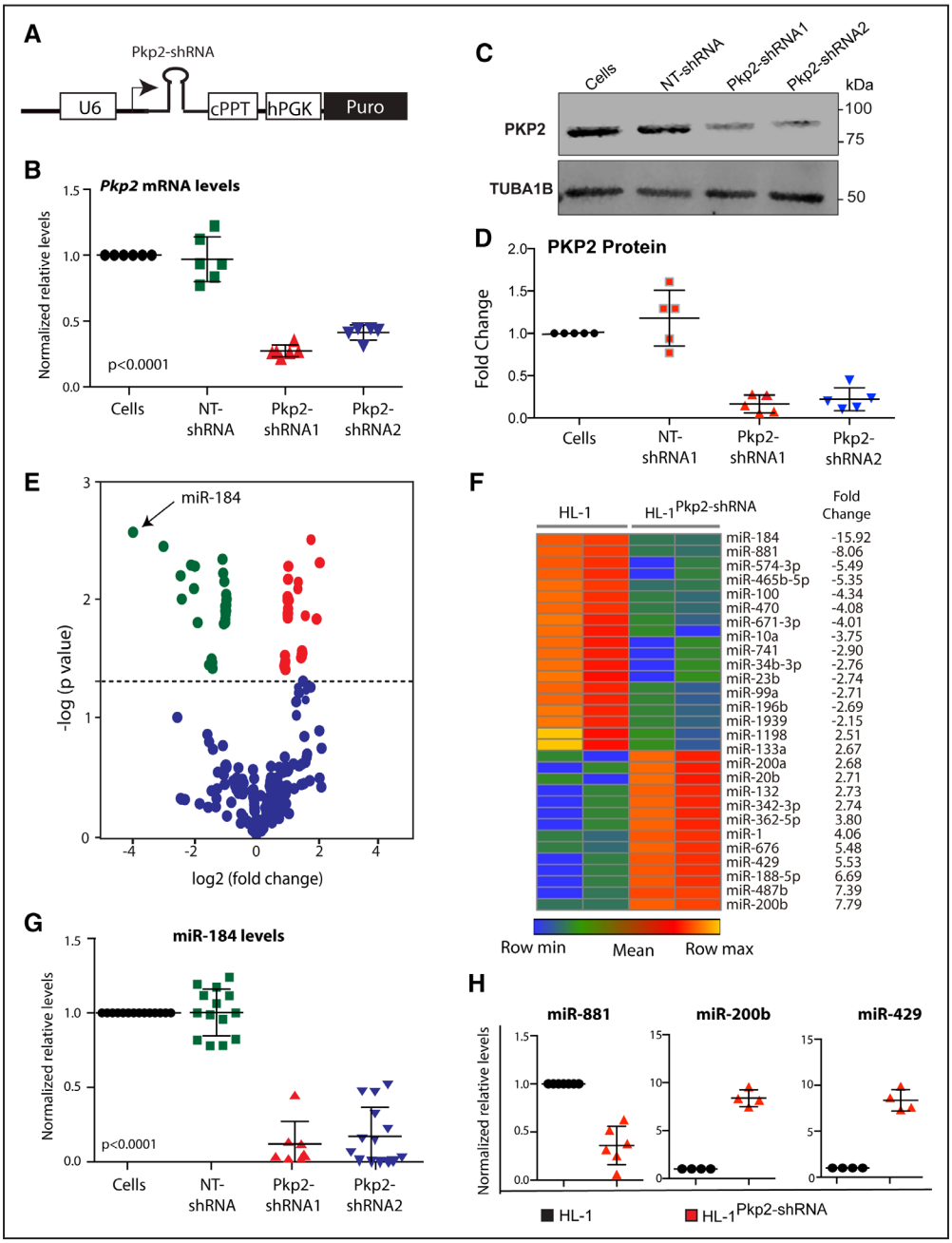

Figure 1. Differentially expressed microRNA (miRNAs) in arrhythmogenic cardiomyopathy (AC) models. A, Schematic representation of shRNA constructs used to knockdown *Pkp2* in the HL-1 (HL-1$^{Pkp2\text{-}shRNA}$) cells. **B**, Quantitative polymerase chain reaction (qPCR) analysis of *Pkp2* mRNA in HL-1 cells expressing 2 independent shRNAs targeting *Pkp2*. An shRNA with no targeting site in the mammalian genome (NT-shRNA) was used as a control (N=6 per group; $P<0.0001$ between HL-1 and HL-1$^{Pkp2\text{-}shRNA1}$ or HL-1$^{Pkp2\text{-}shRNA2}$ and $P=0.27$ between nontransduced HL-1 and HL-1 cells transduced with NT-shRNA by Dunnett's multiple comparisons test). There were no differences in the expression levels of *Pkp2* or selected genes, including miRNAs between the NT-shRNA and HL-1 control cells. Therefore, control PKP2-competent HL-1 cells were used as control. **C** and **D**, Immunoblots (IB) and quantification graph showing suppression of PKP2 protein in the HL-1$^{Pkp2\text{-}shRNA}$ cells (N=5 per group; $P<0.0001$ between control cells and cells transduced with shRNA1 and 2 constructs and $P=0.8$ for nontransduced cells vs cells transduced with the NT-shRNA construct). **E**, Volcano plot of Taqman low-density array data showing log 2-fold change vs –log *P* values for all miRNAs in control HL-1 vs HL-1$^{Pkp2\text{-}shRNA}$ cells. MiR-184, the most differentially expressed miRNA (16-fold downregulation in the HL-1$^{Pkp2\text{-}shRNA}$ cells), is marked. **F**, Heat map of differentially expressed miRNAs (a 2-fold change cutoff point) between control HL-1 and HL-1$^{Pkp2\text{-}shRNA}$ cells. **G**, qPCR data showing suppressed miR-184 expression levels in 2 independent lines of HL-1$^{Pkp2\text{-}shRNA}$ cells (fshRNA no 1 vs control: 5.86±4.5-fold, N=7, $P<0.0001$ and shRNA no 2 vs control, 14.2±9.2-fold, N=24, $P<0.001$). **H**, qPCR confirming reduced levels of miR-881 and increased levels of miR-200b and miR-429 in the HL-1$^{Pkp2\text{-}shRNA}$ cells (N=4–6 per group and all *P* values <0.001). cPPT indicates central polypurine tract; hPGK, human phosphoglycerate kinase; PKP2, plakophilin 2; shRNA, short hairpin RNA; and TUBA1B, tubulin alpha 1B.

regulation of the *Nkx2-5* locus (Figure 2A). *Pkp2* mRNA and PKP2 protein levels were reduced by 41±10% and 54±21%, respectively, in the *Nkx2.5*-Cre:*Pkp2*^{shRNA} mice, as compared with wild-type mice (Figure 2B–2D). The *Nkx2.5*-Cre:*Pkp2*^{shRNA} mice survived normally but exhibited significantly enlarged left ventricle and decreased cardiac systolic

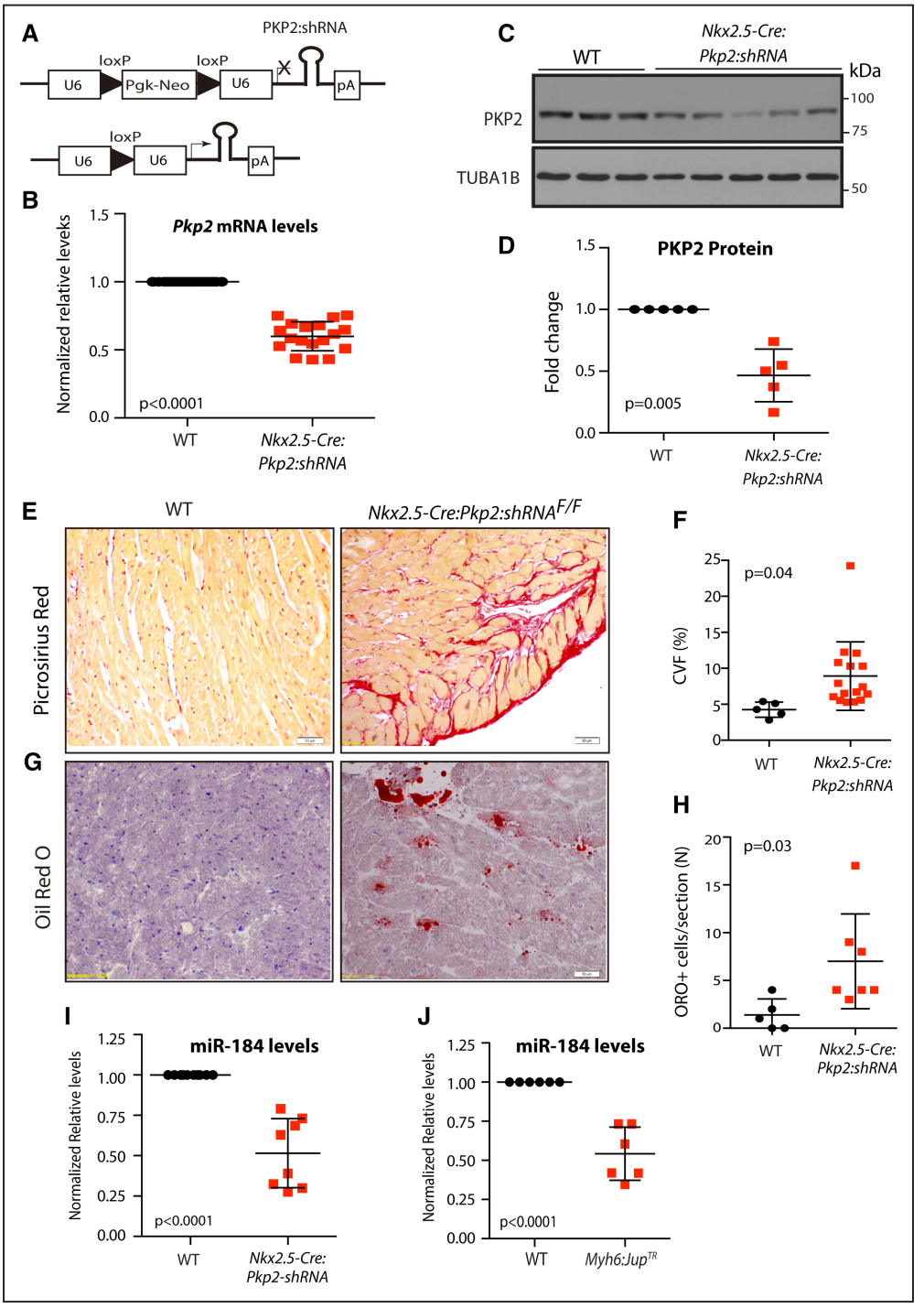

Figure 2. *Pkp2* knockdown mouse model of arrhythmogenic cardiomyopathy (AC). A, Schematic representation of the shRNA construct used to knock down PKP2 conditionally in the mouse heart. **B**, Quantitative polymerase chain reaction (qPCR) data showing efficient *Pkp2* mRNA knockdown in the heart in the *Nkx2.5-Cre:Pkp2*^{shRNA} mice as compared with wild-type (WT) control (41±10%, N=19; *P*<0.0001). **C** and **D**, Immunoblots (IB) and quantification graph showing suppression of PKP2 protein in the *Nkx2.5-Cre:Pkp2*^{shRNA} mice, as compared with WT control (54±21%, N=5; *P*=0.005). **E** and **F**, Thin myocardial sections stained for Picro-Sirius Red showing increased fibrosis in the *Nkx2.5-Cre:Pkp2*^{shRNA} mouse hearts, as compared with WT mice (2.1±1.1-fold increase, N=5 WT and 16 *Nkx2.5-Cre:Pkp2*^{shRNA} mice). **G** and **H**, Oil Red O (ORO)–stained thin myocardial sections and quantitative data, respectively, showing increased number of adipocytes in the heart of *Nkx2.5-Cre:Pkp2*^{shRNA} mice (5.1±3.4-fold, N=5–7 per group). **I** and **J**, Data showing reduced levels of miR-184 in 2 independent mouse models of AC. MiR-184 levels were reduced in the PKP2-deficient mice (*Nkx2-5-Cre*$^{Pkp2\text{-}shRNA}$, 2.2±0.97-fold, N=8 per group; *P*=0.0001) and mice expressing a truncated junction protein plakoglobin (*Myh6:Jup*^{Tr}, 1.99±0.63-fold, N=6 per group; *P*<0.0001). CVF indicates collagen volume fraction; PKP2, plakophilin 2; shRNA, short hairpin RNA; and TUBA1B, tubulin alpha 1B.

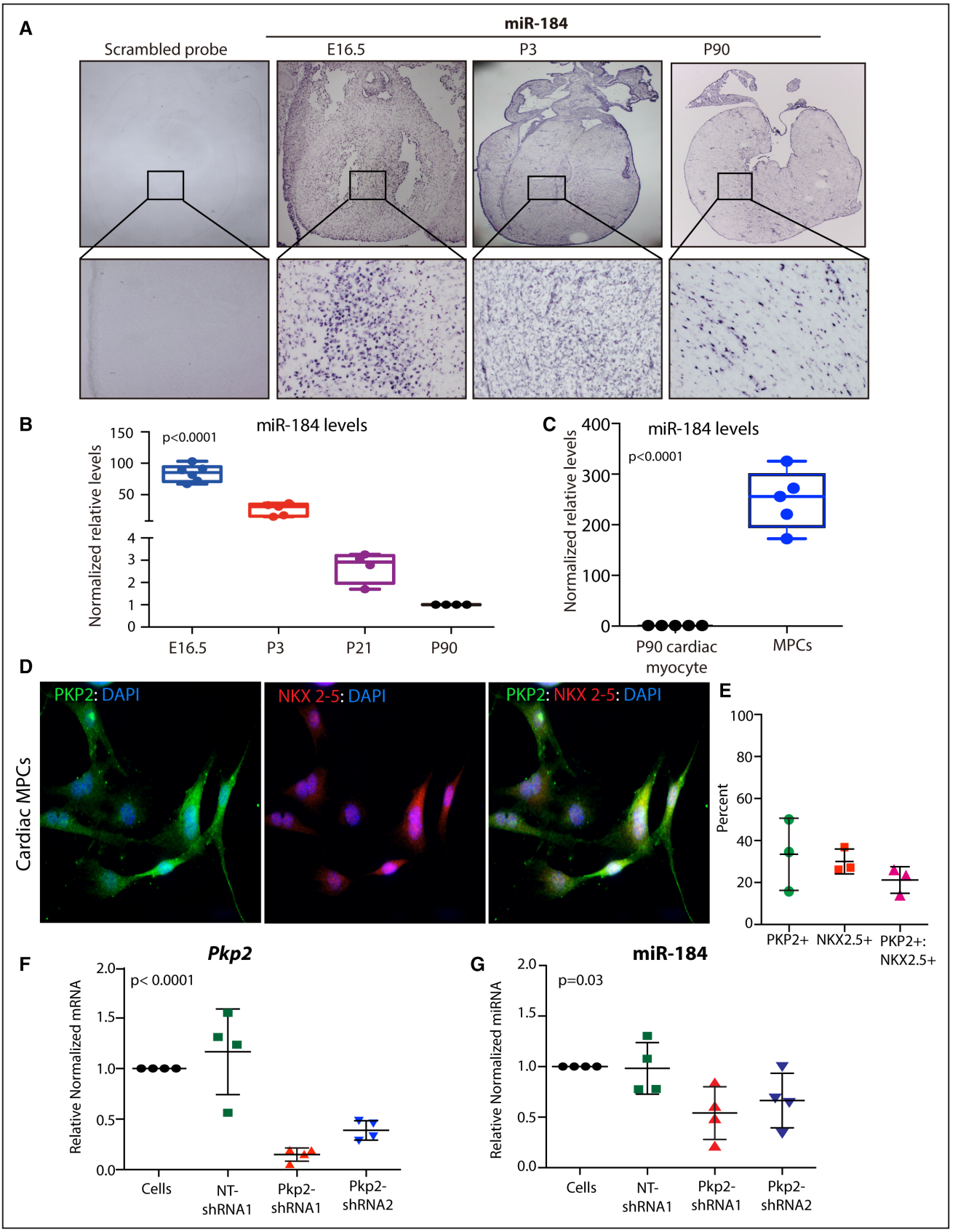

Figure 3. Expression and developmental downregulation of miR-184 in the heart and cardiac mesenchymal progenitor cells (MPCs). A, In situ hybridization showing expression and progressive reduction in miR-184 levels in E16.5, P3, and P90 hearts. **B**, Quantitative polymerase chain reaction (qPCR) data showing progressive downregulation of miR-184 levels in E16.5, P3, P21, and P90 hearts (N=4–6 per group; $P<0.001$ for all groups compared with E16.5 group, $P<0.001$ between P90 and E16.5, $P=0.002$ (*Continued*)

Figure 3 Continued. between P90 and P3, and *P*=0.1 between P90 and P21). **C**, Expression levels of miR-184 in cardiac MPCs showing 249.4±57.17-fold higher levels in cardiac MPCs, as compared with adult cardiac myocytes (N=5; *P*<0.0001). **D**, Expression of PKP2 (green) and NKX2-5 (red) in isolated cardiac MPCs, as detected by immunofluorescence staining. **E**, Quantitative data showing 33.45±17.13% of cardiac MPC expressing PKP2, 30.0±5.9% expressing NKX2-5, and 21.2±6.3% expressing both PKP2 and NKX2-5. **F**, Knockdown of *Pkp2* in cardiac MPCs using 2 independent sets of shRNAs. *Pkp2* mRNA levels were reduced by 85±6.4% and 61.2±9.5% with shRNAs 1 and 2, respectively (N=4 per each set; *P*<0.0001 for each knockdown groups compared with nontransduced cells). **G**, Reduced miR-184 transcript levels on knockdown of *Pkp2* in 2 independent lines in cardiac MPCs (N=4; *P*=0.03 and *P*=0.02 for pairwise comparisons between the control and Pkp2-shRNA1 groups and *P*=0.10 between control and Pkp2-shRNA1 groups). The control NT-shRNA vector had a backbone identical to that in the viral constructs used to suppress *Pkp2* expression. NKX indicates NK2 homeobox 5; NT, no target; PKP2, plakophilin 2; and shRNA, short hairpin RNA.

function (Online Table III). Right ventricular function could not be reliable evaluated by echocardiography. Interstitial fibrosis was increased by 2.1±1.2-fold (Figure 2E and 2F). Likewise, the number of cells accumulating fat droplets was increased by 5.1±3.5-fold (N=7; *P*=0.037) in the hearts of *Nkx2.5*-Cre:*Pkp2*^{shRNA} mice (Figure 2G and 2H). The observed phenotype is similar to that in the previously described mouse models of AC.[16,37]

Suppressed miR-184 Levels in Independent Mouse Models of AC

Expression levels of miRNA-184 were determined by qPCR in the heart of the *Nkx2.5*-Cre:*Pkp2*^{shRNA} and the *Myh6-Jup*^{Tr} mice.[37] Levels of miR-184 were reduced by 52±21% in the hearts of 4-week-old *Nkx2.5-Cre:Pkp2*^{shRNA} mice (Figure 2I, N=9; *P*=0.004) and by 49±10% (N=6, *P*=0.0048) in the hearts of *Myh6:Jup*^{Tr} mice compared with age- and sex-matched wild-type mouse hearts (Figure 2J).

Developmental Downregulation of miR-184 Expression in the Heart

In situ hybridization detected expression of miR-184 in E16.5, P3, and P90 hearts (Figure 3A). MiR-184 was abundantly expressed in the embryonic hearts and exhibited progressive downregulation from embryonic to P90 adult hearts (Figure 3A). To further quantify miR-184 levels during cardiac myocyte differentiation, its levels were quantified in E16.5, P3, P21, and P90 hearts. As shown in Figure 3B, miR-184 levels were ≈100-fold higher in E16.5 hearts than in P90 adult hearts and were progressively reduced in E16.5, P3, P21, and P90 hearts (Figure 3B).

Differential Downregulation of miR-184 in Cardiac Myocytes Isolated From the Nkx2.5-Cre:Pkp2^{shRNA} Mice

To further corroborate differential expression of miR-184 in AC, cardiac myocytes were isolated from P3, P21, and P90 wild-type and *Nkx2.5-Cre:Pkp2*^{shRNA} mice. Levels of *Pkp2* mRNA were reduced by 40% to 50% in cardiac myocytes isolated from the heart of *Nkx2.5-Cre:Pkp2*^{shRNA} mice as compared with wild-type mice at all 3 stages of development (Online Figure IA). MiR-184 levels were the highest in the neonatal (P3) cardiac myocytes, intermediary in P21 cardiac myocytes (4-fold reduction from P3 to P21), and the lowest in P90 cardiac myocytes (10-fold reduction; Online Figure IB). Developmental downregulation of miR-184 expression in cardiac myocytes was differential between the wild-type and the *Nkx2.5-Cre:Pkp2*^{shRNA} mice because miR-184 levels were consistently lower by ≈40% in cardiac myocytes isolated from the *Nkx2.5-Cre:Pkp2*^{shRNA} mice in all 3 development ages as compared with the corresponding levels in the wild-type mice (Online Figure IB).

Expression of miR-184, PKP2, and NKX2-5 in Cardiac MPCs

Given that miR-184 was expressed at higher levels in immature cardiac cells and was downregulated in mature myocytes, we quantified miR-184 levels in cardiac MPCs, identified as Lin^{neg};PDGFRA^{pos}:CD44^{pos} cells. Consistent with the higher expression levels of miR-184 in the embryonic heart and immature myocytes, miR-184 levels were higher (249.4±57.17-fold) in cardiac MPCs as compared with isolated P90 cardiac myocytes (Figure 3C).

To determine whether PKP2 is also expressed in cardiac MPCs, in addition to cardiac myocytes, MPCs were isolated from the hearts of wild-type mice and stained for the expression of PKP2. Likewise, isolated cardiac MPCs were also stained for the expression of NKX2-5, which drives expression of an shRNA against *Pkp2* transcript in the *Nkx2.5*-Cre:*Pkp2*^{shRNA} mice. Consistent with our recent data on the expression of desmosome proteins in nonmyocyte cells in the heart,[36] PKP2 as well as NKX2-5 were expressed in isolated cardiac MPCs (Figure 3D). Quantitatively 33.45±17.13% of cardiac MPCs express PKP2, 30.0±5.9% express NKX2-5, and only 21.2±6.3% of MPCs stained for both PKP2 and NKX2.5 (Figure 3E).

Given heterogeneous expression of PKP2 in cardiac MPCs, to further define the role of miR-184 in differentiation of cardiac MPCs to adipocytes, *Pkp2* transcript was targeted in isolated cardiac MPCs, using 2 sets of lentiviruses expressing distinct *Pkp2*-specific shRNAs (Figure 3F). Knockdown of *Pkp2* with both shRNAs (85±6.4% with shRNA1 and 61.2±9.5% with shRNA2) was associated with reduced expression levels of miR-184 (46±26% and 33.6±27%, respectively) in cardiac MPCs (Figure 3F and 3G).

Regulation of Expression of miR-184 by the E2F1 Pathway

To gain insights into the mechanisms responsible for downregulation of miR-184 in the AC models, we analyzed differentially expressed transcripts in the HL-1$^{Pkp2\text{-}shRNA}$ cells by RNA sequencing.[15] Pathway analysis led to identification of multiple perturbed signaling pathways, including the Hippo, canonical Wnt, and integrin signaling pathways in the HL-1$^{Pkp2\text{-}shRNA}$ cells.[15] Notable among the target genes was *Ccnd1*, whose expression was consistently reduced by >10-fold. CCND1 is a regulatory subunit of cyclin-dependent kinases 4 and 6, which target RB1 for inactivation by phosphorylation and, hence, removal of the inhibitory effects of RB1 on E2F transcription factors (Online Figure II). Thus, a dramatic reduction in *Ccnd1* expression is expected to lead to activation of RB1 and suppression of the E2F1 pathway. In accord with the above, gene set enrichment analysis showed significant downregulation of the E2F1 targets (Figure 4A). Likewise, E2F1 target genes were significantly downregulated in

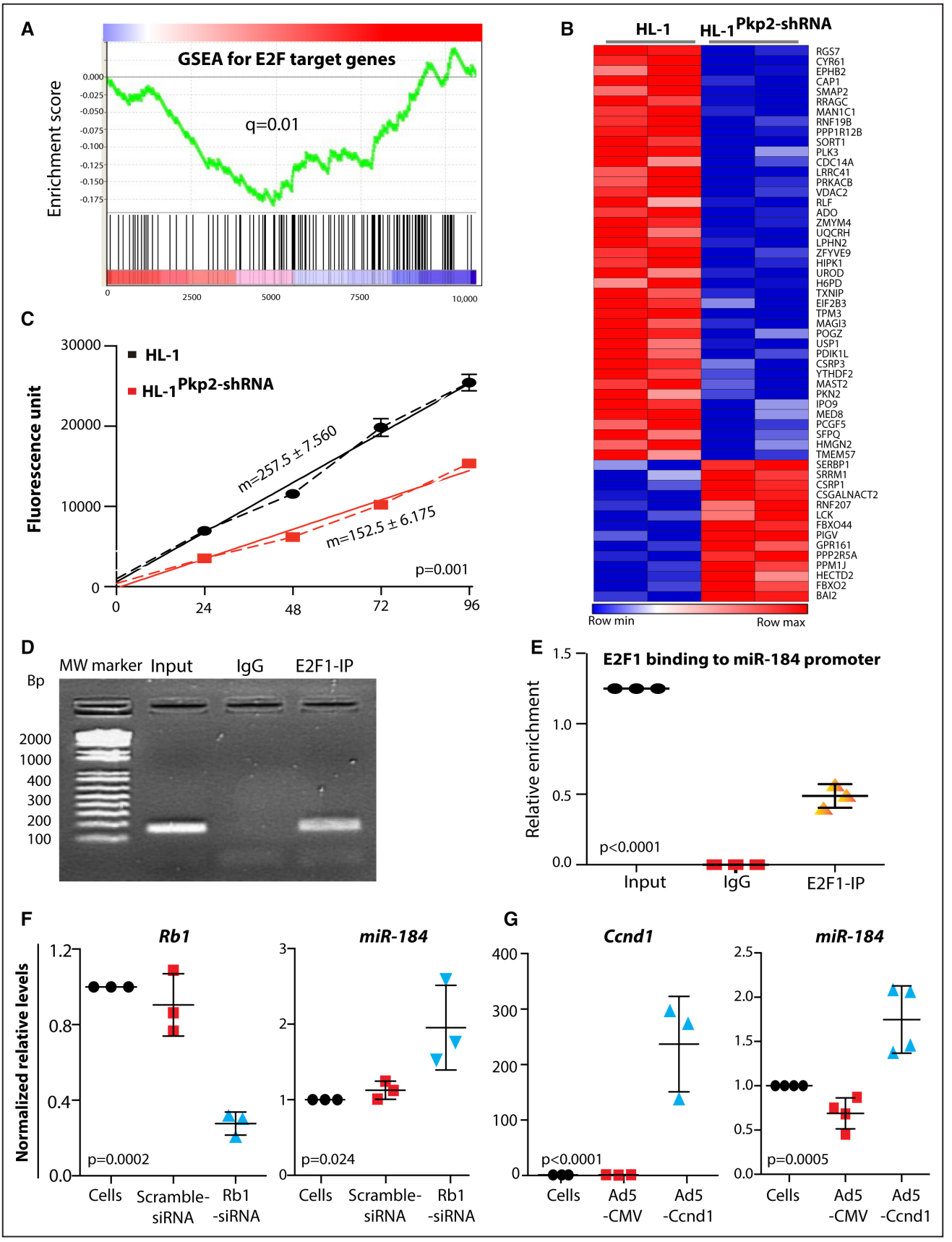

Figure 4. Regulation of miR-184 levels by E2F1 transcription factor. A, Gene set enrichment analysis (GSEA) of the differentially expressed transcripts between wild-type (WT) HL-1 and HL-1$^{Pkp2\text{-}shRNA}$ cells showing a significant enrichment of the E2F1 target genes. **B**, Heat map of E2F enrichment profile showing the predominantly downregulated transcripts (false discovery rate [FDR] is (*Continued*)

Figure 4 Continued. set at 0.01). **C**, Proliferation rate of wild-type and HL-1$^{Pkp2\text{-}shRNA}$ cells, as determined by CellTiter Blue assay. Dotted lines show the growth curves at 4 different time points and straight lines the linear regression fit depicting slope of each curve (*m* value). **D**, Agarose gel electrophoresis photograph showing a 160-bp miR-184 5′ genomic region amplified after precipitation of DNA with an anti-E2F1 antibody in a ChIP assay. **E**, Quantitative data showing precipitated 5′ genomic region of miR-184 relative to input in the ChIP assay. **F**, Rescue of miR-184 levels on siRNA-mediated knockdown of retinoblastoma 1 (RB1) in HL-1 cells. Cells treated with a scrambled siRNA are included as controls. As shown, *Rb1* transcript levels were reduced by 3.7±0.6-fold compared with control nontransfected cells (N=3 per group; *P*=0.0002). **Right**, Increased miR-184 levels by 1.95±0.56 on knockdown of *Rb1* (N=3; *P*=0.024). **G**, Rescue of miR-184 on overexpression of CCND1, which activates the E2F1 pathway and inactivates RB on phosphorylation by CDK4/6. Levels of *Ccnd1* mRNA were increased by 236±85-fold on transduction of HL-1 cells with recombinant adenoviruses, as shown in the graph to the left (N=3; *P*<0.001). In accord with increased *Ccnd1* levels, miR-184 levels were changed in a similar direction and increased by 1.74±0.38-fold (N=4; *P*=0.005). CCND1 indicates cyclin D1; ChIP, chromatin immunoprecipitation; CMV, cytomegalovirus; E2F1, E2F transcription factor 1; IP, immunoprecipitation; MW, molecular weight; PKP2, plakophilin 2; and shRNA, short hairpin RNA.

the HL-1$^{Pkp2\text{-}shRNA}$ cells (Figure 4B). Consistent with suppressed E2F1 transcriptional activity and reduced CCND1 levels, proliferation rate of HL-1$^{Pkp2\text{-}shRNA}$ cells was considerably slower as compared with wild-type HL-1 cells (Figure 4C).[15] To determine whether E2F1 directly regulated expression of miR-184, its binding to the promoter region of miR-184 was analyzed by ChIP (chromatin immunoprecipitation) assay. Genomic DNA was precipitated with an anti-E2F1 antibody, and miR-184 promoter region was amplified by PCR. The finding indicated binding of E2F1 transcription factor to the promoter region of miR-184 (Figure 4D and 4E). To further support the role of E2F1 in transcriptional regulation of miR-184, expression of RB1, an inhibitor of E2F1, was suppressed by siRNA targeting. Suppression of *Rb1* expression (3.7±0.6) led to an ≈ 2-fold increase in miR-184 transcript levels (Figure 4F). In a complementary set of studies, HL-1$^{Pkp2\text{-}shRNA}$ cells were transduced with recombinant adenoviruses expressing CCND1, which activates the E2F1 transcription factor pathway. Overexpression of CCND1 in HL-1$^{Pkp2\text{-}shRNA}$ cells led to a 1.7-fold increase in the miR-184 transcript levels (Figure 4G).

Effects of the Hippo Pathway on miR-184 Levels

To determine whether activation of the Hippo pathway, observed in AC,[15] was responsible for suppressed miR-184 levels, the Hippo pathway kinases LATS1/2 were inactivated to activate gene expression through YAP–TEAD transcription factors, on treatment of the cells with 1 μM of lysophosphatidic acid for 1, 2, and 4 hours. Treatment with lysophosphatidic acid increased nuclear localization of YAP (Online Figure IIIA and IIIB), TEAD transcriptional activity, as detected by a luciferase assay (Online Figure IIIC), and YAP–TEAD target transcript levels (Online Figure IIID). However, despite increased YAP–TEAD transcriptional activity, levels of miR-184 were unchanged (Online Figure IIIE–IIIG).

In a complementary set of studies, the YAP–TEAD complex was transcriptionally inactivated on transduction of the HL-1 cells with Lenti:*Yap*^{shRNA} construct, which expresses an shRNA against *Yap* mRNA. YAP protein levels were reduced by 41% (Online Figure IIIH), as were the transcript levels of its downstream targets *Ctgf* and *Cyr61* (Online Figure III-I). However, despite knockdown of the YAP–TEAD transcriptional activity, levels of miR-184 remained unchanged as compared with control nontransduced cells or cells transduced with a control shRNA (Online Figure IIIJ).

Effects of the Canonical Wnt Signaling Pathway on miR-184 Levels

To ascertain whether suppressed canonical Wnt signaling was responsible for reduced miR-184 levels, the canonical Wnt signaling was activated by treating the HL-1 and HL-1$^{PKP2\text{-}shRNA}$ cells with 40, 80, and 120 ng/mL of the purified Wnt-3A protein. Activation of the canonical Wnt signaling led to a dose-dependent increase in the TCF7L2 luciferase activity (Online Figure IVA) and levels of selected canonical Wnt target transcripts *Ccnd1* and *Axin2* by 2- to 5-fold (Online Figure IVB). However, activation of the canonical Wnt signaling had no effect on miR-184 levels in the HL-1 cells (Online Figure IVC). Likewise, treatment with Wnt-3A increased TFC7L2 luciferase activity (Online Figure IVD) and levels of the established canonical Wnt targets in HL-1$^{Pkp2\text{-}shRNA}$ cells (Online Figure IVE). MiR-184 levels were increased only modestly (1.6-fold, N=5; *P*=0.06; Online Figure IVF). In a complementary set of studies, the canonical Wnt signaling was inactivated on transduction of the cells with a Lenti:*Tcf7l2*^{shRNA} construct expressing an shRNA targeted to *Tcf7l2* transcription factor. Lentiviral transduction effectively reduced TCF7L2 protein levels by ≈50% in the HL-1 cells (Online Figure IVG) and the transcripts levels of canonical Wnt targets *Ccnd1* and *Axin2* (Online Figure IVH). However, suppression of the canonical Wnt signaling had no discernible effect on the expression levels of miR-184 (Online Figure IV-I).

Effects of miR-184 on Hippo and Canonical Wnt Signaling

To determine whether miR-184 was involved in suppression of gene expression through the YAP–TEAD and CTNNB1–TCF7L2 transcription factors, HL-1 cells were transduced with Lenti-miR-184^{shRNA} or Lenti-pre-miR-184 constructs to knock down or overexpress miR-184 in HL-1 cells, respectively (Online VA–VG). Transduction efficiency was determined by flow cytometric analysis of cells expressing the reporter protein GFP (Online Figure VD and VE). Knockdown and overexpression of miR-184 were verified by quantification of miR-184 transcript levels (Online Figure VF and VG). Neither suppression nor increased expression of miR-184 had any effects on expression levels of selected targets of the Hippo (TEAD-YAP) and canonical Wnt (CTNNB1-TCF7L2) signaling pathways (Online Figure VH and V-I).

Epigenetic Silencing of the miR-184 Locus by Hypermethylation

Because activation of E2F1 only partially rescued miR-184 levels and given that modulation of the Hippo and canonical Wnt had no significant effect on miR-184 expression, we surmised that additional mechanism(s) might contribute to suppressed miR-184 levels in the HL-1$^{Pkp2\text{-}shRNA}$ cells. The E2F/RB1 complex is known to recruit DNA methyltransferases (DNMTs) to gene promoters.[43] Given that miR-184 resides

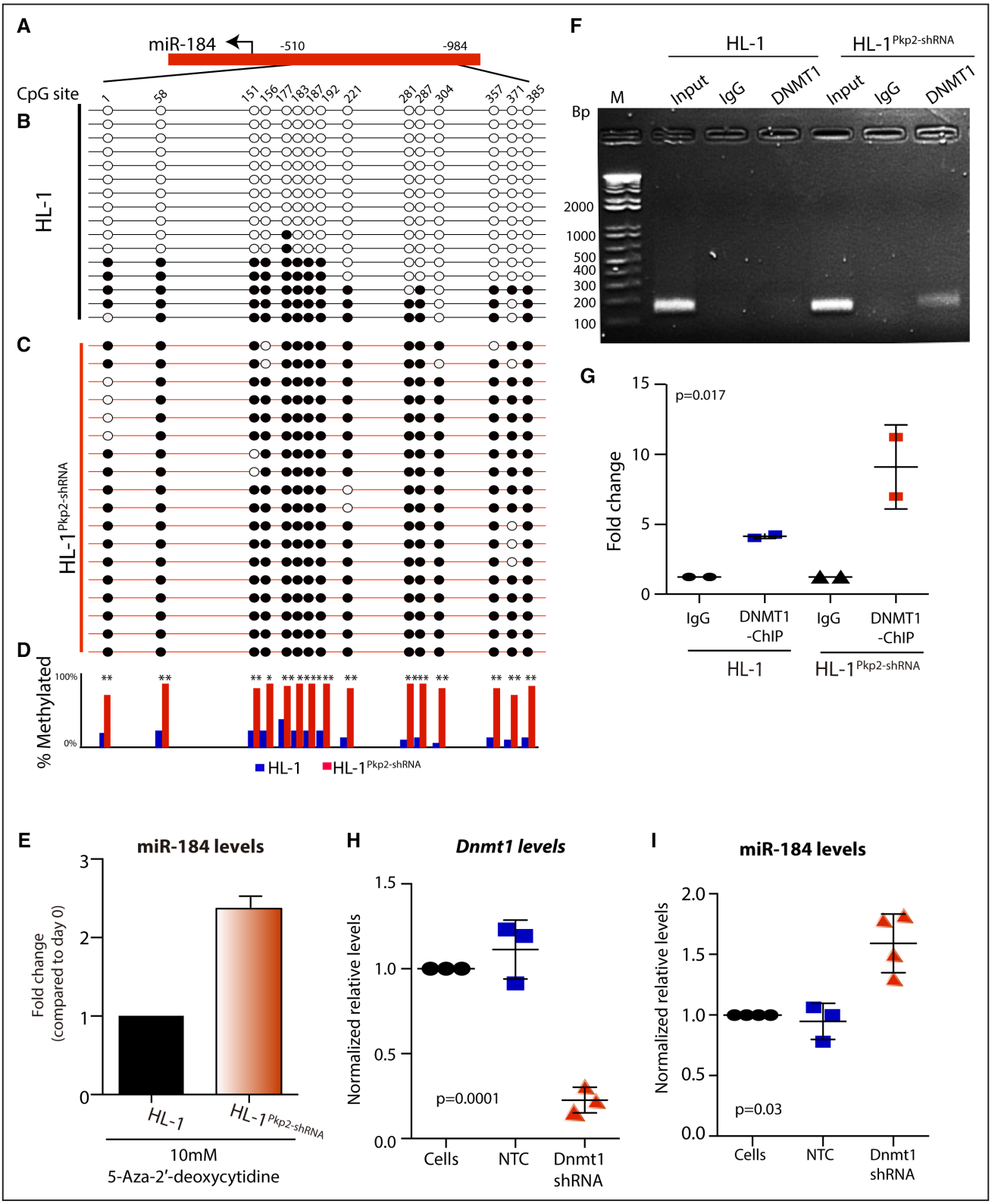

Figure 5. Epigenetic regulation of miR-184 in arrhythmogenic cardiomyopathy (AC). A, Position of the CpG sites at the upstream regulatory genomic locus of miR-184. **B** and **C,** Analysis of DNA methylation at the mouse miR-184 locus by sodium bisulfite treatment and sequencing of PCR clones from HL-1 (**B**) and HL-1$^{Pkp2\text{-}shRNA}$ cells (**C**). Each row represents CpG methylation status of a randomly selected independent clone. **D**, Bar graph showing percent methylation of all CpG site in HL-1 and HL-1$^{Pkp2\text{-}shRNA}$ cells. All analyzed CpG sites show significant hypermethylation in the HL-1$^{Pkp2\text{-}shRNA}$ cells as compared with HL-1 cells alone (*P<0.01 and **P<0.001). **E**, Effects of treatment of HL-1 and HL-1$^{Pkp2\text{-}shRNA}$ cells with 10 μm 5-aza-2′-deoxycytidine (5-azaD) on miR-184 levels determined daily. MiR-184 levels were increased after treatment with 5-azaD in both HL-1 and HL-1$^{Pkp2\text{-}shRNA}$ cells at 5 days post aza-C treatment. Magnitude of the induction in the HL-1$^{Pkp2\text{-}shRNA}$ was greater than that in the HL-1 cells (N=3, P<0.01). **F**, Photograph of agarose gel showing (*Continued*)

Figure 5 Continued. precipitation and amplification of a 160-bp genomic region of miR-184 with an anti–DNA methyltransferase 1 (DNMT1) antibody in a ChIP (chromatin immunoprecipitation) assay. **G**, Quantitative data from ChIP assay showing binding and fold increase in miR-184 5′ genomic region precipitated in ChIP assay (N=2). **H** and **I**, Rescue of miR-184 levels on knockdown of *Dnmt1* transcript by 4.5±1.4-fold (N=3; *P*=0.0001) and increased miR-184 levels (1.6±0.2-fold, N=4; *P*=0.03) on knockdown of *Dnmt1* RNA. PKP2 indicates plakophilin 2; and shRNA, short hairpin RNA.

in an imprinted locus, regulated by methyl-CpG–binding domain protein 1 and methyl-CpG–binding protein 2, we determined methylation state of miR-184 5′ genomic region. A total of 15 CpG-rich regions were identified in the upstream regulatory region of miR-184 locus, which were screened for methylation (Figure 5A). Bisulfite conversion, cloning, and sequencing showed that the CpG sites were predominantly unmethylated in the control HL-1 cells (Figure 5B). In contrast, the vast majority of the CpG sites were hypermethylated in HL-1$^{Pkp2\text{-}shRNA}$ cells (Figure 5C). On average, HL-1 cells showed 23% CpG methylation in miR-184 regulatory region, in contrast to 90% CpG methylation in the HL-1^{Pkp2shRNA} cells (Figure 5D). All the 15 identified CpGs showed greater hypermethylation in the HL-1^{Pkp2shRNA} cells (Online Table IV).

To further validate the role of CpG methylation in miR-184 expression, control HL-1 and HL-1$^{PKP2\text{-}shRNA}$ cells were treated with the nucleotide analogue 5-aza-2′-deoxycytidine for 5 days. Treatment with 5-aza-2′-deoxycytidine increased miR-184 levels in the control HL-1 and HL-1$^{PKP2\text{-}shRNA}$ cells. However, the magnitude of induction was greater in the HL-1$^{PKP2\text{-}shRNA,}$ as compared with control HL-1 cells (2.4±0.2-fold versus 1.8±0.1-fold, respectively, N=3; *P*=0.004; Figure 5E). Nevertheless, despite increased expression of miR-184 on treatment with 5-aza-2′-deoxycytidine , its level in the HL-1$^{PKP2\text{-}shRNA}$ cells remained reduced as compared with the control HL-1 cells, indicating a partial rescue.

To delineate the mechanism(s) responsible for hypermethylation of the CpG site in the 5-genomic region of miR-184, we analyzed recruitment of DNMT1 to the promoter region of miR-184 by ChIP assay. As shown in Figure 5F, genomic fragment of miR-184 was precipitated with an anti-DNMT1 antibody, and the magnitude of the precipitated DNA was greater in HL-1$^{PKP2\text{-}shRNA}$ cells as compared with wild-type HL-1 cells (Figure 5G; 2.1±0.8–fold; *P*=0.0.17). To further substantiate the role of DNMT1 in suppression of miR-184 levels, DNMT1 was targeted by recombinant lenti-viruses expressing an shRNA against *Dnmt1* transcript. Knockdown of *Dnmt1* by shRNA led to increased miR-184 levels (Figure 5H and 5I; 1.6±0.2-fold, N=4; *P*=0.03).

Integrated miRNA–mRNA Analysis

To delineate biological significance of downregulation of miR-184 in AC models and considering pleiotropic targeting of multiple mRNAs by a single miRNA, we performed a pairwise analysis of miR-184 and the differentially expressed mRNA targets in the HL-1$^{PKP2\text{-}shRNA}$ cells (Figure 6A and 6B). Only mRNA transcripts that met the target selection criteria were curated. Pairing of miR-184 and its known and predicted target mRNAs led to identification of 145 genes, whose expression levels were increased by 1.2-fold, and 40 genes, whose expression levels were increased by at least 2-fold (Figure 6C). Gene ontology over-representation analysis (Figure 6D) identified mRNA clusters that were enriched for cellular death and survival (51 transcripts), growth and differentiation (51 transcripts), and cellular development (11 transcripts). MiR-184 target genes involved specifically in cellular differentiation were further curated, and their subcellular localization map is depicted in Figure 6E.

MiR-184 and Transcriptional Switch to Adipogenesis

Pathway analysis of paired miR-184 and its mRNA targets also identified networks of genes involved in lipid biosynthesis (Figure 7A). Analysis of target transcripts in the networks showed upregulation of more than a dozen genes involved in lipid biosynthesis in the HL-1$^{PKP2\text{-}shRNA}$ as compared with the control cells (Figure 7B). *Agpat1*, *Agpat3*, *Ncoa3*, *Ppargc1b*, *Dgat1*, *Dgat2*, and *Lpl*, regulators of lipid biosynthesis, were upregulated by 2- to 4-fold (Figure 7B). Upregulation of a selected number of genes in the lipid biosynthesis networks was also validated by qPCR (Figure 7C). Moreover, expression of the adipogenic transcription factor PPARG was increased, and fat droplets were accumulated in the HL-1$^{Pkp2\text{-}shRNA}$ cells (Figure 7D–7G). Knockdown of *Pkp2* in MPCs also led to enhanced adipogenesis, as evidenced by increased number of cells expressing CEBPA (Figure 7H and 7J) and accumulating fat droplets (Figure 7I and 7K).

To determine whether the adipogenic genes identified in the pairwise miR-184-mRNA analysis were directly targeted by miR-184, the 3′ untranslated regions of the candidate genes were analyzed for the presence of miR-184 seed sequence. The 3′ untranslated regions of *Agpat3, Ncoa3, Ppargc1b*, and *Dgat1* are conserved in mouse and human and were aligned with miR-184 seed sequence (Online Figure VI).

To validate the findings experimentally, HL-1 cells were transduced with recombinant lentiviruses expressing either an shRNA against miR-184 (Lenti:*miR-184^{shRNA}*) or *pre-miR-184* to suppress or increase miR-184 levels, respectively (Online Figure V). Suppression and overexpression of miR-184 was confirmed by qPCR (Figure 7L). Knockdown of miR-184 was associated with increased transcript levels of *Agpat1* and *Agpat3* (Figure 7M). In contrast, overexpression of miR-184 was associated with a modest but a significant decrease in the transcript levels of *Agpat1* and *Agpat 3* (Figure 7M). However, knockdown and overexpression of miR-184 did not affect *Ncoa3* and *Ppargc1b* transcript levels, suggesting that mRNAs of these 2 genes were not directly targeted for degradation by miR-184 (Figure 7M).

Effects of miR-184 on Adipogenesis

To further substantiate the causal role of miR-184 in adipogenic differentiation, expression of adipogenic markers and accumulation of fat droplets were analyzed after suppression and overexpression of miR-184 in HL-1 cells and cardiac MPCs (Figure 8). Knockdown of miR-184 (Figure 8A) increased transcript levels of *Agpat1* (24% increase, N=3; *P*=0.001), *Agpat3* (20% increase, N=3; *P*=0.007), *Pparg* (2.1±0.6-fold, N=4; *P*=0.002), and *Fabp4* (fatty acid–binding protein 4), a

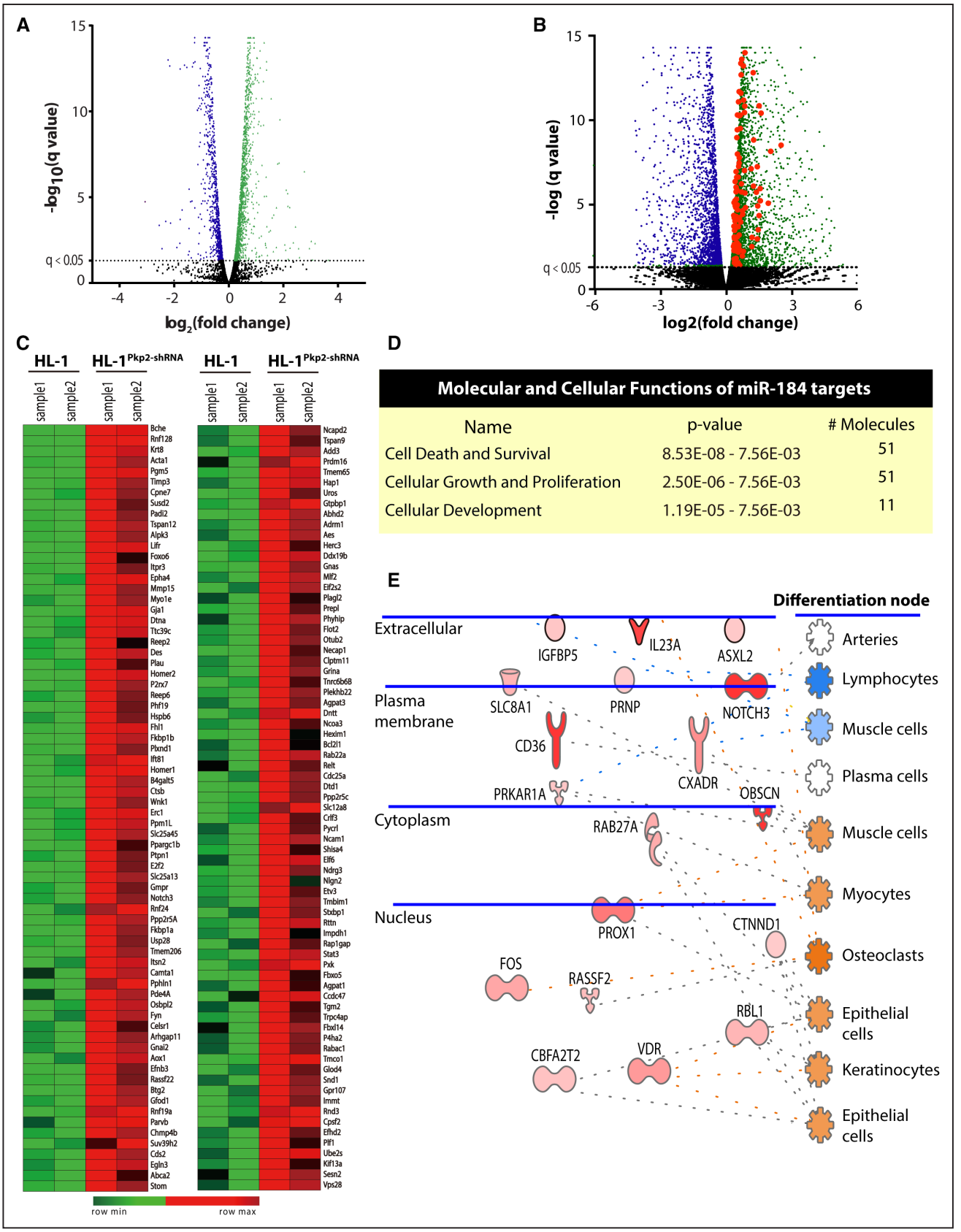

Figure 6. MiR-184:mRNA paired analysis. A, Volcano plot showing log2-fold change vs –log10 *q* values for differentially expressed mRNAs levels as quantified by RNA sequencing from HL-1 and HL-1$^{Pkp2\text{-}shRNA}$ cells. The dotted line shows a *q* value of <0.05. **B**, Volcano plot of differentially expressed miR-184 targets (red dots) superimposed on volcano plot of the differentially expressed transcripts showing miR-184 targets were upregulated in the HL-1$^{Pkp2\text{-}shRNA}$ cells. **C**, Heat plots of mRNA transcripts that were (*Continued*)

Figure 6 Continued. upregulated by >1.3-fold in HL-1$^{Pkp2\text{-}shRNA}$ cells and predicted to be the targets of miR-184 by at least 2 different target prediction programs. **D**, Prediction of molecular and cellular functions regulated by the miR-184 targets as determined by the ingenuity pathway analysis (IPA). Top 3 functions are listed along with their corresponding *P* values and the number of affected genes. **E**, Gene network display from the IPA analysis of miR-184 targets showing the subcellular distribution and upregulation of miR-184 targets involved in cell differentiation. ASXL2 indicates additional sex comb-like 2; CBFA2T2, core-binding factor runt domain alpha subunit 2; CD36, cell differentiation 36; CTNND1, catenin delta 1; CXADR, coxsackie virus and adenovirus receptor; FOS, FBJ osteosarcoma oncogene; IGFBP5, insulin growth factor binding protein 5; IL23A, interleukin 23, subunit alpha; NOTCH3, notch 3; OBSCN, obscurin; PKP2, plakophilin 2; PRNP, prion protein; PROX1, prospero homeobox 1; RAB27A, RAB27A, member RAS oncogene family; RASSF2, Ras association domain family member 2; RBL1, retinoblastoma-like 1; shRNA, short hairpin RNA; SLC8A1, solute carrier family 8 member A1; VDR, vitamin D receptor.

downstream target of PPARG (4.1±3.1-fold, N=4; *P*=0.02) in HL-1 cells (Figure 8B). Knockdown of miR-184 in cardiac MPCs (Figure 8C) also had similar effects on the transcript levels of the above adipogenic genes (Figure 8D). In contrast, overexpression of miR-184 had the opposite effects in both HL-1 cells and cardiac MPCs (Figure 8C and 8D). Immunofluorescence staining of HL-1 cells and cardiac MPCs for the expression of adipogenic transcription factors PPARG and CEBPA showed increased and decreased levels of the adipogenic transcription factors on knockdown and overexpression of miR-184, respectively (Figure 8E–8H). Finally, suppression of expression of miR-184 was associated with increased accumulation of fat droplets in HL-1 cells and in cardiac MPCs, whereas overexpression had the opposite effects (Figure 8I–8L).

Rescue of Adipogenesis on Overexpression of miR-184 in PKP2-Deficient HL-1 Cells

To rescue enhanced adipogenesis in the HL-1$^{PKP2\text{-}shRNA}$ cells, cells were transduced with the Lenti:*pre-miR-184* construct to overexpress miR-184 (Figure 9A). Expression of miR-184 was evaluated by qPCR, fluorescence-activated cell sorting of GFP+ cells, and quantification of miR-184 target transcript levels (Figure 9B–9D). As shown in Figure 9A, overexpression of miR-184 was associated with a significant reduction in the transcript levels of *Pparg* (25±10%, N=5; *P*=0.008), *Fabp4* (25±7%, N=5; *P*=0.02), *Agpat1* (28±9%, N=5; *P*=0.0002), and *Agpat3* (25±7%, N=5; *P*=0.0005). Likewise, the number of cells that contained fat droplets was decreased on overexpression of miR-184, as compared with nontransduced HL-1$^{PKP2\text{-}shRNA}$ cells (25±3% versus 17.6±4%, respectively, N=3200 cells per group per experiment; *P*=0.01; Figure 9E and 9F). Moreover, overexpression of miR-184 reduced the number of PPARG expressing HL-1$^{Pkp2\text{-}shRNA}$ cells (18.43±2.5% versus 14.37±1.5%, N=5; *P*=0.045; Figure 9G and 9H). Overexpression of miR-184 only attenuated and did not completely rescue enhanced adipogenesis in the PKP2-deficient cells because the number of cells with fat droplet remained greater in the transduced HL-1$^{PKP2\text{-}shRNA}$ cells as opposed to the nontransduced control HL-1 levels (25±3% versus 5.4±1.0%, respectively, N=5; *P*=0.001).

Discussion

The findings of the present study implicate miR-184, whose expression is progressively reduced in cardiac myocytes during cardiac development, in the pathogenesis of enhanced adipogenesis in PKP2-deficient cells. Levels of miR-184 were markedly reduced in in vitro and in vivo models, including a new *Pkp2*-knockdown mouse model of AC. The mechanisms responsible for downregulation of miR-184 levels included suppression of the E2F1 pathway, which regulates miR-184 expression on binding of E2F1 to its 5′ genomic region (Online Figure II). In addition, recruitment of DNMT1 leads to epigenetic silencing of the miR-184 locus on hypermethylation of the CpG-rich regions. Downregulation of miR-184 levels was associated with upregulation of its target genes involved in cell death, growth, proliferation, and differentiation. Notable among the perturbed pathways was upregulation of genes involved in lipid synthesis and enhanced adipogenesis. Overexpression and knockdown of miR-184 suppressed and enhanced adipogenesis, respectively, in HL-1 cells and cardiac MPCs. These findings collectively implicate miR-184 in the pathogenesis of excess adipogenesis in PKP2-deficient cells.

MicroRNA profiling and the mechanistic studies were performed in the HL-1 cells, and selected findings, including the effects of miR-184 on adipogenesis, were confirmed in cardiac MPCs. The approach was in keeping with the higher expression levels of miR-184 in cardiac MPCs and murine embryonic hearts, as opposed to mature cardiac myocytes, which expressed miR-184 at low levels. Moreover, adult cardiac myocytes are terminally differentiated cells with limited, if any, capacity for fate switch. In contrast, MPCs have the potential to differentiate to different lineages and been identified as a cell source of adipocytes in AC.[36,44] Nevertheless, despite demonstration of the role of MiR-184 in regulating cell fate in 2 different cell types, the findings merit testing in in vivo models to determine contributions of miR-184 to adipogenesis in AC.

The study by no means is designed to identify all differentially expressed miRNAs or mRNAs in the PKP2-deficient cells or mouse models of AC. The small sample size in the miRNA screening study is expected to lead to underdetection of differentially expressed miRNAs as well as mRNAs (type II statistical error). Nevertheless, differential expressions of the candidate miRNAs, including miR-184, and mRNAs of interest were verified by qPCR in multiple sets of independent experiments. Differentially expressed miRs and mRNA were detected on comparing the PKP2-competent and PKP2-deficient cells but not PKP2-deficient HL-1 cells and cells transfected with a no-target shRNA vector. The latter had no discernible effects on the transcript levels of selected miRs and mRNAs.

The current gene transfer and genetic engineering methods do not afford the opportunity to manipulate expression of miR-184 in the subset of CD44^{pos}/PDGFRA^{pos}/NKX2-5^{pos} cardiac MPCs specifically and efficiently to assess in vivo phenotypic effects of manipulation of miR-184 levels. Moreover, it is also not feasible to isolate and further characterize the CD44^{pos}/PDGFRA^{pos}/NKX2-5^{pos} cells in vitro. Consequently, the relevance of the mechanistic studies, performed in cell culture systems to in vivo models and human AC, remains to be determined. Additional studies in in vivo models would be needed to delineate the role of miR-184 in the pathogenesis of AC.

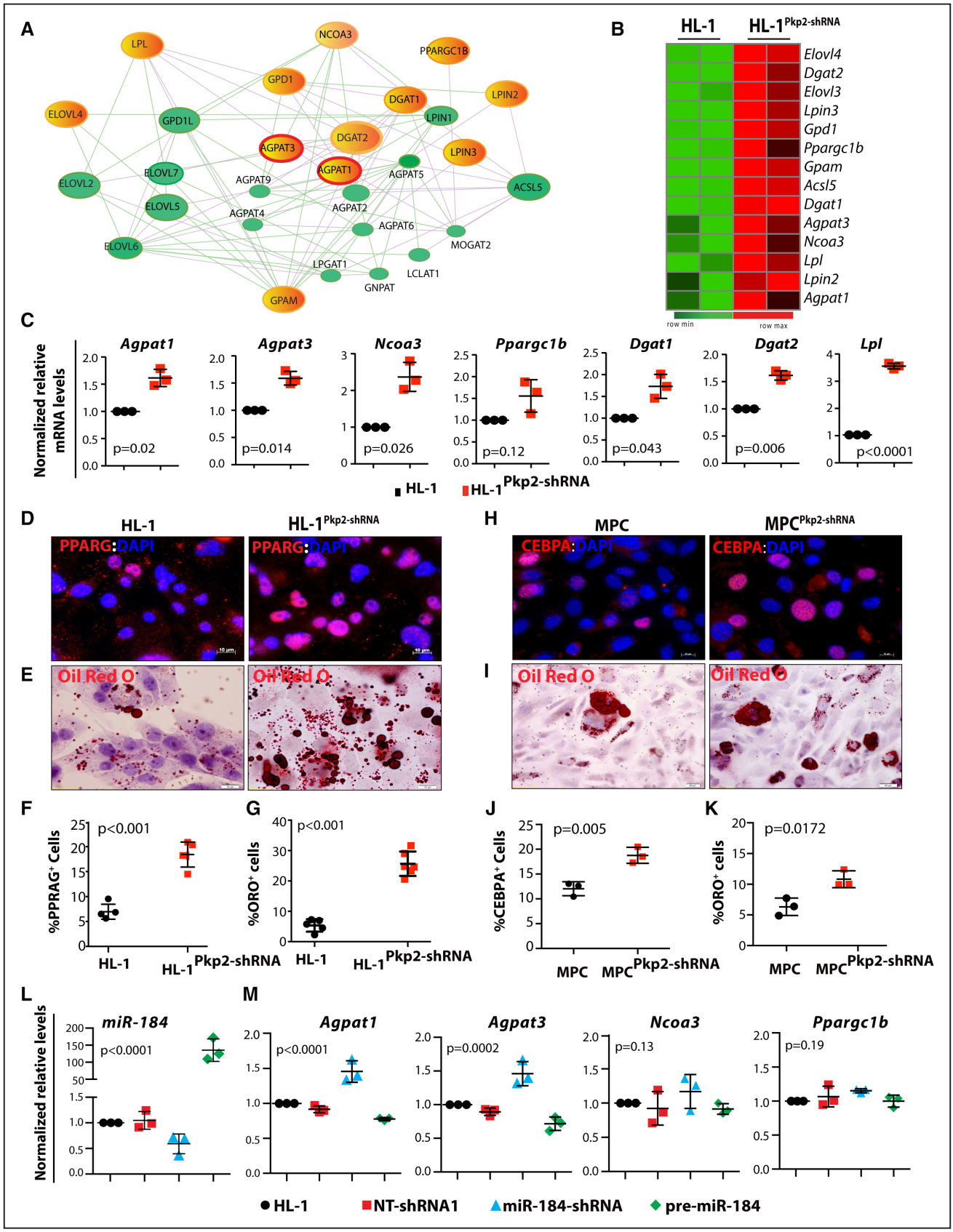

Figure 7. Adipogenic genes as targets of miR-184. Protein functional association network, constructed using STRING online tool for paired analysis of miR-184 and its mRNA transcripts involved in triglyceride synthesis, including *Agpat1*, *Agpat3*, *Ncoa3*, and *Ppargc1b*. Genes directly targeted by miR-184 are highlighted as orange color. **B**, Heat plot constructed for paired analysis of miR-184 and its mRNA target networks involved in adipogenesis, which were upregulated in the HL-1$^{Pkp2\text{-}shRNA}$ cells. **C**, Confirmation of increased (*Continued*)

Figure 7 Continued. transcript levels of selected miR-184 targets involved in lipid metabolism (N=4). **D**, Immunofluorescence (IF) panels showing expression of nuclear peroxisome proliferator-activated receptor gamma (PPARG), an adipogenic transcription factor, in the control HL-1 and HL-1$^{Pkp2\text{-}shRNA}$ cells 14 days after induction of adipogenesis. **E**, Oil Red O (ORO)–stained panels showing increased lipid accumulation in the HL-1$^{Pkp2\text{-}shRNA}$ as compared with the control HL-1 cells 14 days after induction with an adipogenic medium. **F** and **G**, Corresponding quantitative data showing a 2.6±0.16-fold increase in the number of PPARG expressing HL-1$^{Pkp2\text{-}shRNA}$ and 4.7±0.4-fold higher number of HL-1$^{Pkp2\text{-}shRNA}$ cells accumulating fat droplets, as compared with the control HL-1 cells (N=5, P<0.0001 and N=6, P<0.0001, respectively). **H** and **I**, CEBPA (CCAAT/enhancer binding protein alpha) expression and fat droplet accumulation in cardiac mesenchymal progenitor cells (MPCs) and MPCs knockdown for *Pkp2* (MPC$^{Pkp2\text{-}shRNA}$) after 5 days of adipogenic induction. **J**, Quantitative data showing 1.7±0.13-fold increase in number of cells expressing adipogenic transcription factor CEBPA in the MPC$^{Pkp2\text{-}shRNA}$ cells, as compared with control MPCs (N=3600 cells/group). **K**, Enhanced fat droplet accumulation (1.6±0.23-fold) in MPC$^{Pkp2\text{-}shRNA}$ (N=3800 cells/group) as compared with controls. **L**, Effects of knockdown and overexpression of miR-184 on selected target genes involved in adipogenesis. Transcript levels of *Agpat1* and *Agpat3* were increased by ≈2-fold in HL-1 cells transduced with Lenti:miR-184^{shRNA} as compared nontransduced HL-1 cells (N=3 per group; P<0.05). Conversely, overexpression of miR-184 was associated with ≈25% decrease in the *Agpat1* and *Agpat3* mRNA levels (N=3; P=0.04), identifying these genes as the targets of miR-184. However, levels of *Ncoa3* and *Ppargc1b* were not changed on overexpression or knockdown of miR-184. To avoid potential confounding effects of the vector backbones, experiments were repeated with the viral constructs that had identical viral backbones in the control NT-shRNA, knockdown, and overexpression groups. Similar results were obtained for changes in the transcript levels of selected adipogenic markers in cardiac MPCs (Online Figure VII). NT indicates no target; PKP2, plakophilin 2; and shRNA, short hairpin RNA.

MiR-184, an evolutionary conserved intergenic single-copy miR, was the most differentially expressed miRNA in 2 independent lines of HL-1$^{Pkp2\text{-}shRNA}$ cells. PKP2 levels were reduced similarly between the 2 lines. Hence, a dose-dependent effect of PKP2 suppression on miR-184 levels could not be determined. The initial studies were performed in the HL-1 cells, and the findings provided the impetus for generation and characterization of the *Pkp2*-deficient mice. Ab initio studies in cardiac MPCs are considered more pertinent and aligned with the working hypothesis. MicroRNA-184 was also downregulated in cardiac myocytes isolated from the AC models and in 2 independent mouse models of AC, including the new *Nkx2.5*-Cre:*Pkp2*^{shRNA} and the established *Jup* transgenic (*Myh6:Jup*^{Tr}) mouse models.[37] Whether mechanisms similar to those observed in the PKP2-deficiency models are also responsible for downregulation of miR-184 in the heart in the *Myh6:Jup*^{Tr} mice remain to be determined. Several other miRNAs were also dysregulated in the HL-1$^{Pkp2\text{-}shRNA}$ cells. However, among the most dysregulated miRNAs, expression of miR-184 was consistently suppressed in the HL-1 cells and mouse models. The magnitude of reduction was greater in the HL-1$^{Pkp2\text{-}shRNA}$ cells by ≈16-fold as compared with ≈2-fold reduction in the heart of the genetic mouse models. Milder reductions in the heart of transgenic models likely reflect cellular heterogeneity of the heart, expression of miR-184 only in a subset of cardiac cells, and downregulation of miR-184 levels in the adult heart. Knockdown of the *Pkp2* gene under transcriptional regulation of the *Nkx2.5* locus predominantly deletes *Pkp2* in cardiac myocytes. NKX2-5 and PKP2, despite being predominantly expressed in the cardiac myocyte lineage, are also expressed in nonmyocyte cells in the heart, including a subset of cardiac MPCs, as shown in the present and previous studies.[36] Such cellular heterogeneity in the expression of the key molecules relevant to the pathogenesis of AC may account for the discrepancy in the magnitude of reductions of miR-184 levels in in vitro and in vivo models. Nevertheless, the findings are in agreement with the notion that only a subset of cardiac progenitor cells differentiates to fibro-adipocytes in AC.[2,36,45]

In view of a more pronounced reduction of miR-184 levels in the HL-1$^{Pkp2\text{-}shRNA}$ cells, phenotypic effects and the mechanistic studies were performed primarily in the HL-1 cells and subsequently in cardiac MPCs, surmising that the in vitro studies would provide a more sensitive platform for delineating the underpinning mechanisms than studies performed on the whole heart. These data are in keeping with our hypothesis that it is a subset of cardiac progenitor cells and not mature cardiac myocytes that differentiate to adipocytes in AC.[2,37,38,45] To strengthen the evidence for the observed effects, the biological effects of miR-184 were analyzed by complementary methods of overexpression and knockdown approaches in 2 independent cell types. Phenotypic consequences, including adipogenesis were detected by independent complementary methods, such as qPCR of the genes involved in lipid biosynthesis, immunofluorescence staining for adipogenic transcription factors, and Oil Red O staining of fat droplets. Collectively, the findings provide strong evidence for the role of miR-184 in the pathogenesis of AC.

In accord with targeting of multiple mRNAs by a single miR and, hence, phenotypic pleiotropy of each miRNA, miR-184 is also implicated in various biological processes, notable among them is cell lineage specification.[46–48] Suppression of miR-184 has been associated with reduced cellular proliferation, clonal expansion, and differentiation of several progenitor and precursor cells.[46–48] Consistent with the role of miR-184 in cell fate determination, suppressed expression of miR-184, whether on shRNA-mediated targeting or indirectly on knockdown of PKP2, was associated with a transcriptional switch to adipogenesis and enhanced fat accumulation. At the molecular level, genes encoding AGPAT1 and AGPAT3, which convert lysophosphatidic acid into phosphatidic acid in lipid biosynthetic pathways, were identified as novel targets of miR-184.[49] In accord with these findings, overexpression of AGPAT1 is shown to increase fatty acid uptake, triacylglycerol production, and accumulation of fat droplets in the 3T3-L1 and C2C12 cells.[50] Likewise, *Ncoa3* and *Ppargc1b,* which have prominent roles in adipogenic differentiation, along with several other adipogenic genes were upregulated on knockdown of PKP2. Transcriptionally, miR-184 targets *Numbl*, *Sox17*, *Ncor2*, and *Akt2* are known to regulate cellular differentiation.[47,51] In view of multiplicity of miRNA targets, the phenotype consequent to downregulation of miR-184 in HL-1$^{Pkp2\text{-}shRNA}$ cells or cardiac MPCs is the collective effects of changes in the expression levels of multiple targets and not a

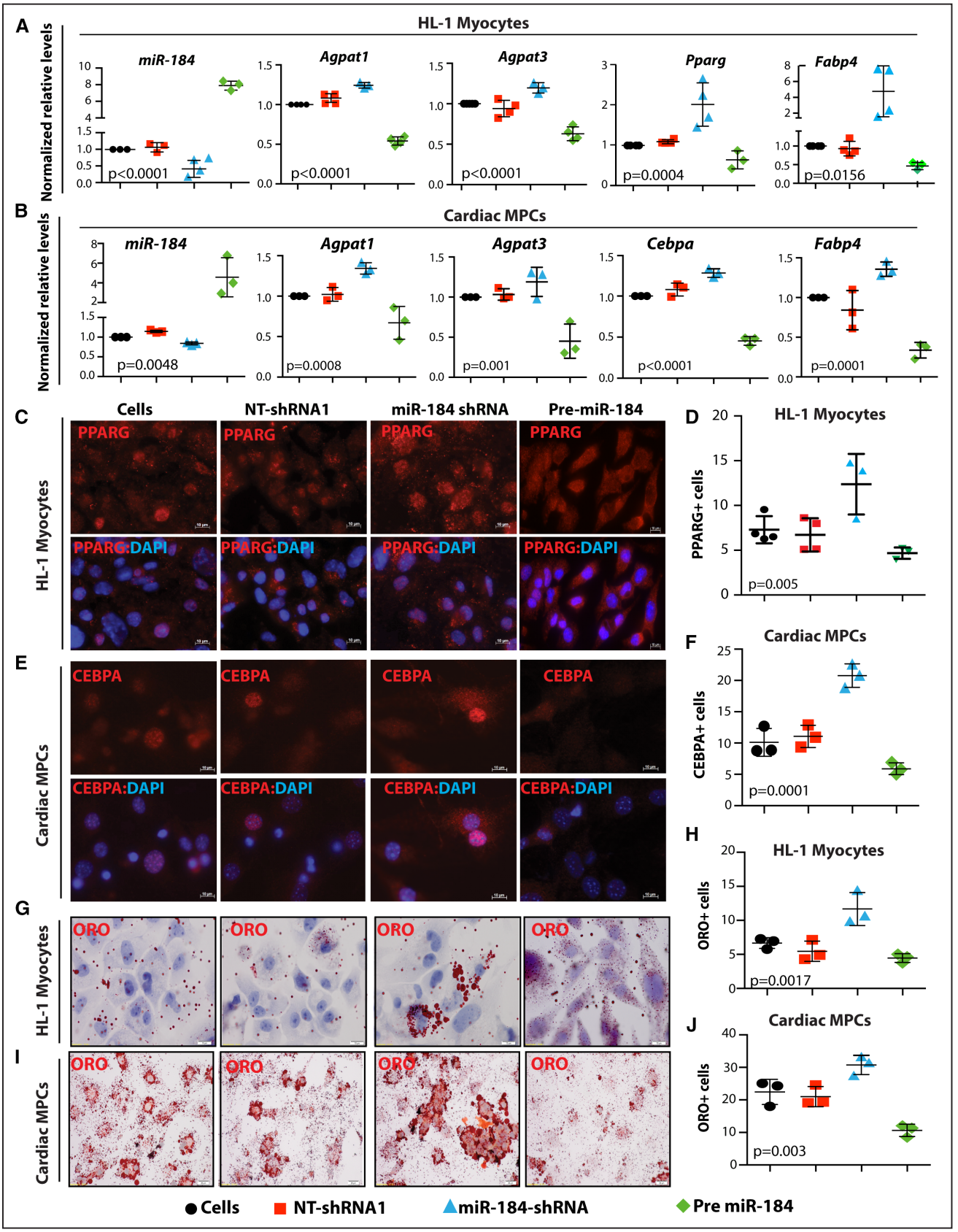

Figure 8. Effects of knockdown and overexpression of miR-184 on adipogenesis. A–D, Transcript levels of miR-184 and its targets showing knockdown (Lenti:miR-184^{shRNA}) and overexpression (Lenti:*pre-miR-184*) of miR-184 in HL-1 cells and mesenchymal progenitor cells (MPCs) isolated from the heart. Levels normalized to nontransduced cells are presented as fold change. **A**, Transduction of HL-1 cells with Lenti:miR-184^{shRNA} construct, leading to increased transcript levels of several adipogenic genes (*Pparg:* 2.15±0.56, (*Continued*)

Figure 8 Continued. $P<0.05$; *Fabp4:* 4.1±3.1, $P<0.05$; *Agpat*1: 1.3±0.1, $P<0.001$; and *Agpat3:* 1.2±0.1, $P=0.007$), as compared with control or the Lenti:NT^{shRNA} groups. In contrast, overexpression of miR-184, on transduction of HL-1 cells with Lenti:*pre-miR-184*, was associated with decreased transcript levels of the adipogenic genes. **B**, Overexpression and knockdown of miR-184 levels in cardiac MPCs led to changes in the transcript levels of the selected miR-184 target genes, similar to those observed in the HL-1 cells. **C** and **D**, Immunofluorescence (IF) panels showing staining of adipogenic transcription factor PPARG and the corresponding quantification data in HL-1 cells. The number of HL-1 cells expressing PPARG was increased by 1.8±0.4-fold in the Lenti:miR-184^{shRNA} group, as compared with the control groups. In contrast, overexpression of miR-184 was associated with reduced number of HL-1 cells expressing PPARG (average of 200 cells per group, N=3–4; $P<0.05$). **E** and **F**, IF panels show staining for CEBPA (CCAAT/enhancer binding protein alpha) and the corresponding quantitative data in cardiac MPCs. The number of CEBPA expressing MPCs was increased on knockdown of miR-184 (2.03±0.18-fold, N=3; $P=0.0002$) and decreased on overexpression of miR-184 (≈200 cells per group, 1.74±0.27-fold, N=3; $P=0.046$). **G** and **H**, Representative Oil Red O (ORO)–stained panels and the corresponding quantitative showing increased and decreased number of cells accumulating fat droplets in HL-1 cells transduced with Lenti:*miR-184^{shRNA}* and Lenti:*pre-miR-184*, respectively, as compared with the control groups (250 cells per group; N=3, $P<0.05$). **I** and **J**, Knockdown and overexpression of miR-184 in MPCs was associated with increase (1.35±0.13-fold, N=3; $P=0.02$) and decrease (2.2±0.4, N=3; $P=0.004$) of fat droplet accumulation, respectively. NT indicates no target; PPARG, peroxisome proliferator-activated receptor gamma; and shRNA, short hairpin RNA.

single target. The pleiotropic of effects hinders from manipulation of a single miR-184 target as a means of phenotypic rescue. Consequently, the rescue experiments were performed on overexpression of miR-184 in the HL-1$^{Pkp2\text{-}shRNA}$ cells, which exhibit suppressed miR-184 levels. Collectively, the new findings along with the existing data support a role of miR-184 as a homeostatic balancer of proliferation and differentiation.

The effect size of miR-184 on the levels of its target transcripts were relatively modest, a finding that is consistent with the established role of miRNAs as nudgers and tweakers of genome management.[21] These subtle changes in gene expression and phenotype are inherent to miRNA regulatory networks that are not only dependent on the changes in miRNA concentration but also dependent on stoichiometric amounts of its target. Furthermore, miRs, in general, behave as a temporal agent to control targets or signaling networks by setting a threshold of expression, thus, allowing or amplifying a signal in cohort with other transcription factors. Accordingly, in a complex phenotype such as AC, the phenotype is the consequence of a myriad of molecular changes that occur, including changes in the levels of multiple miRNA, as observed in the present study, each contributing to the phenotype, and none alone is a sole determinant.

MiR-184 is located in an imprinted locus on mouse chromosome 9, and it is repressed on methylation of the CpG-rich sequences at its promoter region.[47] In accord with the epigenetic silencing of the miR-184 locus, the upstream regulatory sites of miR-184 were hypermethylated in the HL-1$^{Pkp2\text{-}shRNA}$ cells. DNA methylation-dependent repression of miR-184 transcription occurs by binding of methyl-CpG–binding protein 1 and methyl-CpG protein binding to the methylated regions.[47,52] Treatment with 5-aza-2′-deoxycytidine-D and suppression of DNMT1, as well as activation of the E2F1 transcription pathway, induced expression of miR-184 levels in HL-1 cells. Nevertheless, the magnitude of induction was insufficient to normalize the miR-184 levels in the HL-1$^{Pkp2\text{-}shRNA}$ cells. Failure to completely rescue suppressed miR-184 levels might reflect irreversible epigenetic silencing of this locus in the HL-1$^{Pkp2\text{-}shRNA}$ cells. Moreover, several other mechanisms that were delineated, particularly cell contact regulators, such as integrins, might contribute to downregulation of the miR-184 levels in the PKP2-deficient HL-1 cells, which were not studied. The mechanism(s) by which PKP2 impacts methylation of the miR-184 locus is likely related to recruitment of DNMT1 by the RB1/E2F1 complex to the 5′ genomic region of miR-184 (Online Figure II). The 2 delineated mechanisms, namely suppression of E2F1 and hypermethylation of 5′ genomic region of miR-184, offer a unifying mechanism regulated by CCND1, which is markedly suppressed in the AC models.[15] CCND1 is a regulator of CDK4/6, which target RB1 for inactivation on phosphorylation and, hence, gene expression through E2F1 transcription factor (Online Figure II). Consequently, reduced CCND1 levels and activation of RB1 might enhance recruitment of DNMT1 to the genomic regions.[43] Finally, given that PKP2 is known to localize to the nucleus in addition to the IDs,[53,54] it is intriguing to postulate a role of the PKP2 in recruitment and assembly of DNMTs, directly or through interactions with other proteins in the promoter complex. As a whole, the findings suggest a primary role for increased CpG methylation, but also the involvement of multiple mechanisms including suppression of E2F1 pathway in downregulation of miR-184 levels in the HL-1$^{Pkp2\text{-}shRNA}$ cells.

Activation of the Hippo pathway and reduced gene expression through its downstream effectors YAP-TEAD and the canonical Wnt signaling, which are impaired in the HL-1$^{Pkp2\text{-}shRNA}$ cells,[15,16] did not significantly influence miR-184 levels. Likewise, overexpression or knockdown of miR-184 did not affect transcriptional activities of these pathways. In contrast to a recent report indicating that miR-184 suppresses the canonical Wnt signaling in retina,[55] overexpression of miR-184 had no discernible effects on the transcript levels of selected canonical Wnt signaling targets in HL-1 cells. By-and-large, suppressed expression levels of miR-184 were independent of the Hippo and canonical Wnt signaling pathway transcriptional activities in HL-1 cells.

In conclusion, the findings of the present study show pathogenic downregulation of miR-184 in PKP2-deficient cells and mouse models of AC. The responsible mechanisms include suppression of the E2F1 transcription factor pathway and epigenetic silencing of miR-184 genomic locus on CpG methylation. MiR-184 regulates adipogenesis in HL-1 cells and a subset of cardiac MPCs that express intercalated disc protein PKP2. The findings illustrate a pathogenic role for miR-184 in cellular proliferation and enhanced adipogenesis PKP2 deficiency.

Sources of Funding

This work was supported in part by grants from National Institutes of Health (NIH), National Heart, Lung and Blood Institute (NHLBI, R01 HL088498, 1R01HL132401, and R34 HL105563), Leducq Foundation (14 CVD 03), Roderick MacDonald Foundation (13RDM005), TexGen Fund from Greater Houston Community Foundation, Texas Heart Institute Foundation, and George and Mary Josephine Hamman Foundation. Dr Chen was supported as a PhD student for his work at the Center for Cardiovascular Genetics, the University of Texas Health

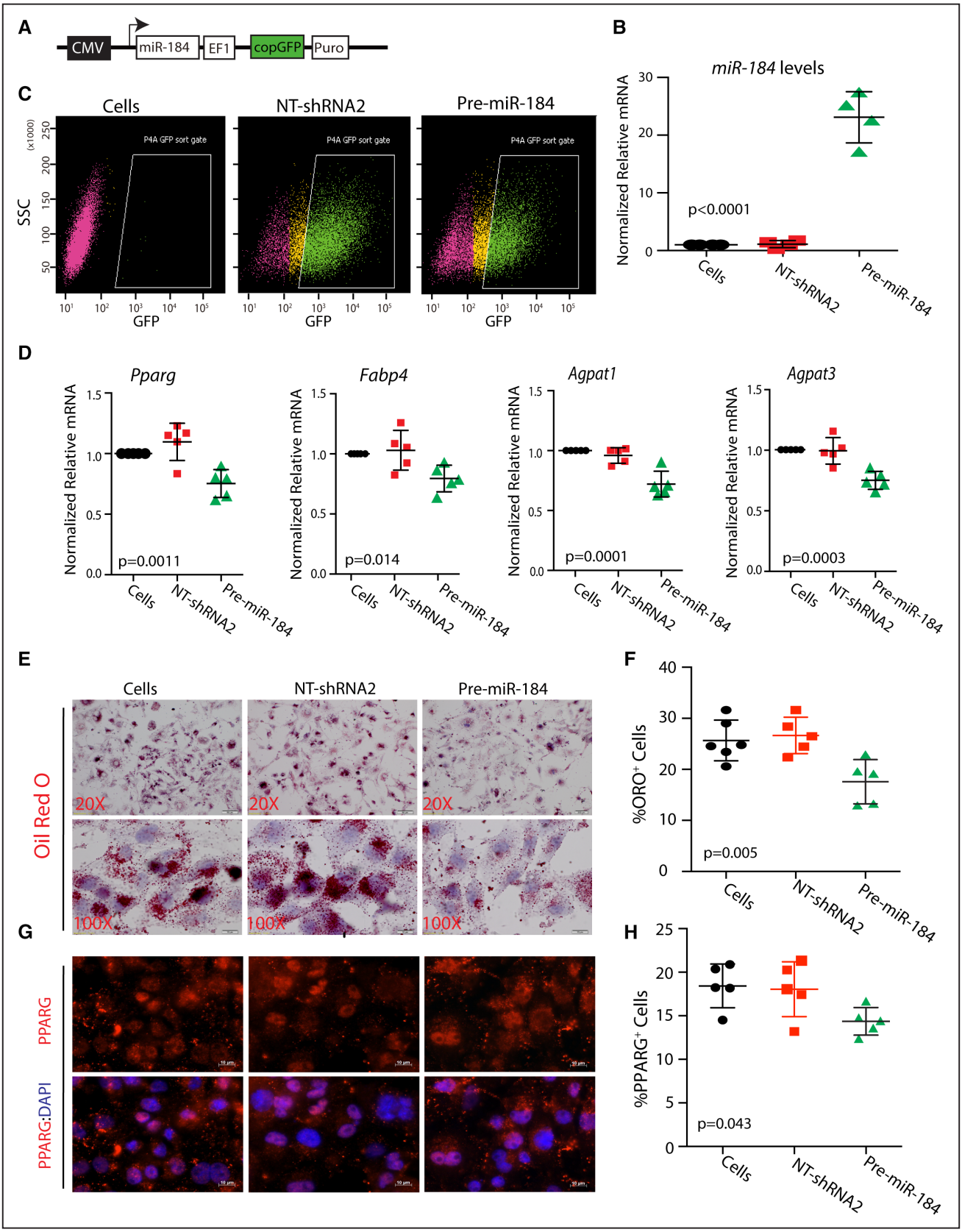

Figure 9. Attenuation of adipogenesis on overexpression of miR-184 in the HL-1$^{Pkp2\text{-}shRNA}$ cells. A, Schematic of pre-miR-184 expression construct showing expression regulation of miR by the CMV promoter and GFP by the EF1 promoter. **B,** Flow cytometry plot depicting GFP expressing in HL-1$^{Pkp2\text{-}shRNA}$ cells transduced with nontargeting control (NT-shRNA2) or Lenti:*pre-miR*-184 viruses. **C**, Quantitative polymerase chain reaction (qPCR) analysis of miR-184 levels in HL-1$^{Pkp2\text{-}shRNA}$ cells transduced with Lenti:*pre-miR-184* (N=3, *P*<0.0001). **D**, Reduced mRNA levels of *Pparg* (27±10%), *Fabp4* (25±12%), *Agpat1* (26±13%), and *Agpat3* (25±9%) in (*Continued*)

Figure 9 Continued. the HL-1$^{Pkp2\text{-}shRNA}$ cells transduced with Lenti:*pre-miR-184*, as compared with the control groups (N=5; $P<0.05$). **E** and **F**, Reduced accumulation of fat droplets on overexpression of miR-184 (Lenti:*pre-miR-184*) as detected by Oil Red O (ORO; **E**) and the corresponding quantitative data (**F**). **G** and **H,** Immunofluorescence (IF) staining and quantification of cells expressing PPARG in the experimental groups (N=5, $P=0.043$). CMV indicates cytomegalovirus; GFP, green fluorescent protein; PKP2, plakophilin 2; PPARG, peroxisome proliferator-activated receptor gamma; and shRNA, short hairpin RNA.

Science Center-Houston, for 1 year by a grant from China Scholarship Council, sponsored by Dr Yiming Ni at the Zhejiang University, China.

Disclosures

None.

References

1. Delmar M, McKenna WJ. The cardiac desmosome and arrhythmogenic cardiomyopathies: from gene to disease. *Circ Res*. 2010;107:700–714. doi: 10.1161/CIRCRESAHA.110.223412.
2. Lombardi R, Marian AJ. Molecular genetics and pathogenesis of arrhythmogenic right ventricular cardiomyopathy: a disease of cardiac stem cells. *Pediatr Cardiol*. 2011;32:360–365. doi: 10.1007/s00246-011-9890-2.
3. Basso C, Thiene G, Corrado D, Angelini A, Nava A, Valente M. Arrhythmogenic right ventricular cardiomyopathy. Dysplasia, dystrophy, or myocarditis? *Circulation*. 1996;94:983–991.
4. Corrado D, Basso C, Thiene G, McKenna WJ, Davies MJ, Fontaliran F, Nava A, Silvestri F, Blomstrom-Lundqvist C, Wlodarska EK, Fontaine G, Camerini F. Spectrum of clinicopathologic manifestations of arrhythmogenic right ventricular cardiomyopathy/dysplasia: a multicenter study. *J Am Coll Cardiol*. 1997;30:1512–1520.
5. McKoy G, Protonotarios N, Crosby A, Tsatsopoulou A, Anastasakis A, Coonar A, Norman M, Baboonian C, Jeffery S, McKenna WJ. Identification of a deletion in plakoglobin in arrhythmogenic right ventricular cardiomyopathy with palmoplantar keratoderma and woolly hair (Naxos disease). *Lancet*. 2000;355:2119–2124. doi: 10.1016/S0140-6736(00)02379-5.
6. Rampazzo A, Nava A, Malacrida S, Beffagna G, Bauce B, Rossi V, Zimbello R, Simionati B, Basso C, Thiene G, Towbin JA, Danieli GA. Mutation in human desmoplakin domain binding to plakoglobin causes a dominant form of arrhythmogenic right ventricular cardiomyopathy. *Am J Hum Genet*. 2002;71:1200–1206. doi: 10.1086/344208.
7. den Haan AD, Tan BY, Zikusoka MN, Lladó LI, Jain R, Daly A, Tichnell C, James C, Amat-Alarcon N, Abraham T, Russell SD, Bluemke DA, Calkins H, Dalal D, Judge DP. Comprehensive desmosome mutation analysis in north americans with arrhythmogenic right ventricular dysplasia/cardiomyopathy. *Circ Cardiovasc Genet*. 2009;2:428–435. doi: 10.1161/CIRCGENETICS.109.858217.
8. Heuser A, Plovie ER, Ellinor PT, Grossmann KS, Shin JT, Wichter T, Basson CT, Lerman BB, Sasse-Klaassen S, Thierfelder L, MacRae CA, Gerull B. Mutant desmocollin-2 causes arrhythmogenic right ventricular cardiomyopathy. *Am J Hum Genet*. 2006;79:1081–1088. doi: 10.1086/509044.
9. Syrris P, Ward D, Evans A, Asimaki A, Gandjbakhch E, Sen-Chowdhry S, McKenna WJ. Arrhythmogenic right ventricular dysplasia/cardiomyopathy associated with mutations in the desmosomal gene desmocollin-2. *Am J Hum Genet*. 2006;79:978–984. doi: 10.1086/509122.
10. Li J, Radice GL. A new perspective on intercalated disc organization: implications for heart disease. *Dermatol Res Pract*. 2010;2010:207835. doi: 10.1155/2010/207835.
11. Quarta G, Syrris P, Ashworth M, Jenkins S, Zuborne Alapi K, Morgan J, Muir A, Pantazis A, McKenna WJ, Elliott PM. Mutations in the Lamin A/C gene mimic arrhythmogenic right ventricular cardiomyopathy. *Eur Heart J*. 2012;33:1128–1136. doi: 10.1093/eurheartj/ehr451.
12. Merner ND, Hodgkinson KA, Haywood AF, Connors S, French VM, Drenckhahn JD, Kupprion C, Ramadanova K, Thierfelder L, McKenna W, Gallagher B, Morris-Larkin L, Bassett AS, Parfrey PS, Young TL. Arrhythmogenic right ventricular cardiomyopathy type 5 is a fully penetrant, lethal arrhythmic disorder caused by a missense mutation in the TMEM43 gene. *Am J Hum Genet*. 2008;82:809–821. doi: 10.1016/j.ajhg.2008.01.010.
13. Gerull B, Heuser A, Wichter T, et al. Mutations in the desmosomal protein plakophilin-2 are common in arrhythmogenic right ventricular cardiomyopathy. *Nat Genet*. 2004;36:1162–1164. doi: 10.1038/ng1461.
14. van Tintelen JP, Entius MM, Bhuiyan ZA, et al. Plakophilin-2 mutations are the major determinant of familial arrhythmogenic right ventricular dysplasia/cardiomyopathy. *Circulation*. 2006;113:1650–1658. doi: 10.1161/CIRCULATIONAHA.105.609719.
15. Chen SN, Gurha P, Lombardi R, Ruggiero A, Willerson JT, Marian AJ. The hippo pathway is activated and is a causal mechanism for adipogenesis in arrhythmogenic cardiomyopathy. *Circ Res*. 2014;114:454–468. doi: 10.1161/CIRCRESAHA.114.302810.
16. Garcia-Gras E, Lombardi R, Giocondo MJ, Willerson JT, Schneider MD, Khoury DS, Marian AJ. Suppression of canonical Wnt/beta-catenin signaling by nuclear plakoglobin recapitulates phenotype of arrhythmogenic right ventricular cardiomyopathy. *J Clin Invest*. 2006;116:2012–2021. doi: 10.1172/JCI27751.
17. Heallen T, Zhang M, Wang J, Bonilla-Claudio M, Klysik E, Johnson RL, Martin JF. Hippo pathway inhibits Wnt signaling to restrain cardiomyocyte proliferation and heart size. *Science*. 2011;332:458–461. doi: 10.1126/science.1199010.
18. Thum T, Condorelli G. Long noncoding RNAs and microRNAs in cardiovascular pathophysiology. *Circ Res*. 2015;116:751–762. doi: 10.1161/CIRCRESAHA.116.303549.
19. Gurha P, Marian AJ. Noncoding RNAs in cardiovascular biology and disease. *Circ Res*. 2013;113:e115–e120. doi: 10.1161/CIRCRESAHA.113.302988.
20. Lu TY, Lin B, Li Y, Arora A, Han L, Cui C, Coronnello C, Sheng Y, Benos PV, Yang L. Overexpression of microRNA-1 promotes cardiomyocyte commitment from human cardiovascular progenitors via suppressing WNT and FGF signaling pathways. *J Mol Cell Cardiol*. 2013;63:146–154. doi: 10.1016/j.yjmcc.2013.07.019.
21. Bird A. Genome biology: not drowning but waving. *Cell*. 2013;154:951–952. doi: 10.1016/j.cell.2013.08.010.
22. Tian Y, Liu Y, Wang T, Zhou N, Kong J, Chen L, Snitow M, Morley M, Li D, Petrenko N, Zhou S, Lu M, Gao E, Koch WJ, Stewart KM, Morrisey EE. A microrna-hippo pathway that promotes cardiomyocyte proliferation and cardiac regeneration in mice. *Sci Transl Med*. 2015;7:279ra238.
23. Thompson BJ, Cohen SM. The Hippo pathway regulates the bantam microRNA to control cell proliferation and apoptosis in Drosophila. *Cell*. 2006;126:767–774. doi: 10.1016/j.cell.2006.07.013.
24. Kim IM, Wang Y, Park KM, Tang Y, Teoh JP, Vinson J, Traynham CJ, Pironti G, Mao L, Su H, Johnson JA, Koch WJ, Rockman HA. β-arrestin1-biased β1-adrenergic receptor signaling regulates microRNA processing. *Circ Res*. 2014;114:833–844. doi: 10.1161/CIRCRESAHA.114.302766.
25. Wang D, Zhang H, Li M, Frid MG, Flockton AR, McKeon BA, Yeager ME, Fini MA, Morrell NW, Pullamsetti SS, Velegala S, Seeger W, McKinsey TA, Sucharov CC, Stenmark KR. MicroRNA-124 controls the proliferative, migratory, and inflammatory phenotype of pulmonary vascular fibroblasts. *Circ Res*. 2014;114:67–78. doi: 10.1161/CIRCRESAHA.114.301633.
26. Castaldi A, Zaglia T, Di Mauro V, et al. MicroRNA-133 modulates the β1-adrenergic receptor transduction cascade. *Circ Res*. 2014;115:273–283. doi: 10.1161/CIRCRESAHA.115.303252.
27. Harada M, Luo X, Murohara T, Yang B, Dobrev D, Nattel S. MicroRNA regulation and cardiac calcium signaling: role in cardiac disease and therapeutic potential. *Circ Res*. 2014;114:689–705. doi: 10.1161/CIRCRESAHA.114.301798.
28. Sun X, He S, Wara AK, Icli B, Shvartz E, Tesmenitsky Y, Belkin N, Li D, Blackwell TS, Sukhova GK, Croce K, Feinberg MW. Systemic delivery of microRNA-181b inhibits nuclear factor-κB activation, vascular inflammation, and atherosclerosis in apolipoprotein E-deficient mice. *Circ Res*. 2014;114:32–40. doi: 10.1161/CIRCRESAHA.113.302089.
29. Icli B, Wara AK, Moslehi J, et al. MicroRNA-26a regulates pathological and physiological angiogenesis by targeting BMP/SMAD1 signaling. *Circ Res*. 2013;113:1231–1241. doi: 10.1161/CIRCRESAHA.113.301780.
30. Yang Y, Del Re DP, Nakano N, Sciarretta S, Zhai P, Park J, Sayed D, Shirakabe A, Matsushima S, Park Y, Tian B, Abdellatif M, Sadoshima J. miR-206 mediates YAP-induced cardiac hypertrophy and survival. *Circ Res*. 2015;117:891–904. doi: 10.1161/CIRCRESAHA.115.306624.
31. Bush EW, van Rooij E. miR-25 in heart failure. *Circ Res*. 2014;115:610–612. doi: 10.1161/CIRCRESAHA.114.304909.
32. Kuwabara Y, Horie T, Baba O, Watanabe S, Nishiga M, Usami S, Izuhara M, Nakao T, Nishino T, Otsu K, Kita T, Kimura T, Ono K. MicroRNA-451 exacerbates lipotoxicity in cardiac myocytes and high-fat diet-induced cardiac hypertrophy in mice through suppression of the LKB1/AMPK pathway. *Circ Res*. 2015;116:279–288. doi: 10.1161/CIRCRESAHA.116.304707.

33. Li CJ, Cheng P, Liang MK, Chen YS, Lu Q, Wang JY, Xia ZY, Zhou HD, Cao X, Xie H, Liao EY, Luo XH. MicroRNA-188 regulates age-related switch between osteoblast and adipocyte differentiation. *J Clin Invest*. 2015;125:1509–1522. doi: 10.1172/JCI77716.
34. Carlson S, Trial J, Soeller C, Entman ML. Cardiac mesenchymal stem cells contribute to scar formation after myocardial infarction. *Cardiovasc Res*. 2011;91:99–107. doi: 10.1093/cvr/cvr061.
35. Cieslik KA, Trial J, Entman ML. Defective myofibroblast formation from mesenchymal stem cells in the aging murine heart rescue by activation of the AMPK pathway. *Am J Pathol*. 2011;179:1792–1806. doi: 10.1016/j.ajpath.2011.06.022.
36. Lombardi R, Chen SN, Ruggiero A, Gurha P, Czernuszewicz GZ, Willerson JT, Marian AJ. Cardiac fibro-adipocyte progenitors express desmosome proteins and preferentially differentiate to adipocytes upon deletion of the Desmoplakin gene. *Circ Res*. 2016;119:41–54. doi: 10.1161/CIRCRESAHA.115.308136.
37. Lombardi R, da Graca Cabreira-Hansen M, Bell A, Fromm RR, Willerson JT, Marian AJ. Nuclear plakoglobin is essential for differentiation of cardiac progenitor cells to adipocytes in arrhythmogenic right ventricular cardiomyopathy. *Circ Res*. 2011;109:1342–1353. doi: 10.1161/CIRCRESAHA.111.255075.
38. Lombardi R, Dong J, Rodriguez G, Bell A, Leung TK, Schwartz RJ, Willerson JT, Brugada R, Marian AJ. Genetic fate mapping identifies second heart field progenitor cells as a source of adipocytes in arrhythmogenic right ventricular cardiomyopathy. *Circ Res*. 2009;104:1076–1084. doi: 10.1161/CIRCRESAHA.109.196899.
39. Shukla V, Coumoul X, Wang RH, Kim HS, Deng CX. RNA interference and inhibition of MEK-ERK signaling prevent abnormal skeletal phenotypes in a mouse model of craniosynostosis. *Nat Genet*. 2007;39:1145–1150. doi: 10.1038/ng2096.
40. Shukla V, Coumoul X, Deng CX. RNAi-based conditional gene knockdown in mice using a U6 promoter driven vector. *Int J Biol Sci*. 2007;3:91–99.
41. Moses KA, DeMayo F, Braun RM, Reecy JL, Schwartz RJ. Embryonic expression of an Nkx2-5/Cre gene using ROSA26 reporter mice. *Genesis*. 2001;31:176–180.
42. Yaylaoglu MB, Titmus A, Visel A, Alvarez-Bolado G, Thaller C, Eichele G. Comprehensive expression atlas of fibroblast growth factors and their receptors generated by a novel robotic in situ hybridization platform. *Dev Dyn*. 2005;234:371–386. doi: 10.1002/dvdy.20441.
43. Robertson KD, Ait-Si-Ali S, Yokochi T, Wade PA, Jones PL, Wolffe AP. DNMT1 forms a complex with Rb, E2F1 and HDAC1 and represses transcription from E2F-responsive promoters. *Nat Genet*. 2000;25:338–342. doi: 10.1038/77124.
44. Sommariva E, Brambilla S, Carbucicchio C, et al. Cardiac mesenchymal stromal cells are a source of adipocytes in arrhythmogenic cardiomyopathy. *Eur Heart J*. 2016;37:1835–1846. doi: 10.1093/eurheartj/ehv579.
45. Lombardi R, Marian AJ. Arrhythmogenic right ventricular cardiomyopathy is a disease of cardiac stem cells. *Curr Opin Cardiol*. 2010;25:222–228. doi: 10.1097/HCO.0b013e3283376daf.
46. Shalom-Feuerstein R, Serror L, De La Forest Divonne S, Petit I, Aberdam E, Camargo L, Damour O, Vigouroux C, Solomon A, Gaggioli C, Itskovitz-Eldor J, Ahmad S, Aberdam D. Pluripotent stem cell model reveals essential roles for miR-450b-5p and miR-184 in embryonic corneal lineage specification. *Stem Cells*. 2012;30:898–909. doi: 10.1002/stem.1068.
47. Liu C, Teng ZQ, Santistevan NJ, Szulwach KE, Guo W, Jin P, Zhao X. Epigenetic regulation of miR-184 by MBD1 governs neural stem cell proliferation and differentiation. *Cell Stem Cell*. 2010;6:433–444. doi: 10.1016/j.stem.2010.02.017.
48. Iovino N, Pane A, Gaul U. miR-184 has multiple roles in Drosophila female germline development. *Dev Cell*. 2009;17:123–133. doi: 10.1016/j.devcel.2009.06.008.
49. Wilfling F, Wang H, Haas JT, et al. Triacylglycerol synthesis enzymes mediate lipid droplet growth by relocalizing from the ER to lipid droplets. *Dev Cell*. 2013;24:384–399. doi: 10.1016/j.devcel.2013.01.013.
50. Ruan H, Pownall HJ. Overexpression of 1-acyl-glycerol-3-phosphate acyltransferase-alpha enhances lipid storage in cellular models of adipose tissue and skeletal muscle. *Diabetes*. 2001;50:233–240.
51. Wu GG, Li WH, He WG, Jiang N, Zhang GX, Chen W, Yang HF, Liu QL, Huang YN, Zhang L, Zhang T, Zeng XC. Mir-184 post-transcriptionally regulates SOX7 expression and promotes cell proliferation in human hepatocellular carcinoma. *PLoS One*. 2014;9:e88796. doi: 10.1371/journal.pone.0088796.
52. Nomura T, Kimura M, Horii T, Morita S, Soejima H, Kudo S, Hatada I. MeCP2-dependent repression of an imprinted miR-184 released by depolarization. *Hum Mol Genet*. 2008;17:1192–1199. doi: 10.1093/hmg/ddn011.
53. Mertens C, Hofmann I, Wang Z, Teichmann M, Sepehri Chong S, Schnolzer M, Franke WW. Nuclear particles containing rna polymerase iii complexes associated with the junctional plaque protein plakophilin 2. *Proc Natl Acad Sci U S A*. 2001;98:7795–7800.
54. Chen X, Bonne S, Hatzfeld M, van Roy F, Green KJ. Protein binding and functional characterization of plakophilin 2. Evidence for its diverse roles in desmosomes and beta -catenin signaling. *J Biol Chem*. 2002;277:10512–10522. doi: 10.1074/jbc.M108765200.
55. Takahashi Y, Chen Q, Rajala RV, Ma JX. MicroRNA-184 modulates canonical Wnt signaling through the regulation of frizzled-7 expression in the retina with ischemia-induced neovascularization. *FEBS Lett*. 2015;589:1143–1149. doi: 10.1016/j.febslet.2015.03.010.

Novelty and Significance

What Is Known?

- Arrhythmogenic cardiomyopathy (AC) is a genetic disease that clinically manifests with ventricular arrhythmias, heart failure, and sudden cardiac death.
- Pathological hallmark of AC is replacement of cardiac myocytes by fibro-adipocytes, particularly in the right ventricle.
- Mutations in genes encoding desmosome (intercalated disk) proteins are identified in approximately half of the families with AC.
- *PKP2*, encoding plakophilin 2 (PKP2), is the most common causal gene for AC.

What New Information Does This Article Contribute?

- Knockdown of *Pkp2* in HL-1 cells led to dysregulation of 59 microRNAs.
- MicroRNA-184 was the most downregulated, whereas the miR-200 family was the most upregulated microRNAs in the *Pkp2*-knockdown HL-1 cells.
- Knock down of *Pkp2* in the mouse heart was also associated with downregulation of miR-184.
- Expression of miR-184 was progressively downregulated during cardiac development, being the highest in early embryonic heart and in cardiac mesenchymal progenitor cells and lowest in adult cardiac myocytes.
- Knock down of PKP2 led to epigenetic silencing of miR-184 through increased recruitment of DNA methyltransferase 1 and hypermethylation of the CpG sites at its 5′ genomic region, as well as suppression of the E2F1 transcription factor, which regulated miR-184 on direct binding to the 5′ genomic region.
- Suppression of miR-184 enhanced and its activation attenuated adipogenesis through direct targeting of adipogenic genes in mesenchymal progenitor cells and HL-1 cells.

MicroRNA-184 is a developmentally regulated miR, whose expression is highest in the embryonic heart and cardiac mesenchymal progenitor cells and lowest in adult cardiac myocytes. Developmental downregulation of miR-184 is enhanced in PKP2-deficient myocytes. Expression of miR-184 is regulated by the E2F1 transcription factor and CpG hypermethylation at its 5′ genomic region, which are suppressed and enhanced, respectively, in PKP2 deficiency. MiR-184 regulates proliferation and adipogenesis in HL-1 cells and cardiac mesenchymal progenitor cells. The findings suggest a role for miR-184 in the molecular pathogenesis of adipogenesis in PKP2 deficiency. The findings set the stage for additional studies in in vivo models and humans with AC.

Circulation Research
JOURNAL OF THE AMERICAN HEART ASSOCIATION

Knockdown of Plakophilin 2 Downregulates miR-184 Through CpG Hypermethylation and Suppression of the E2F1 Pathway and Leads to Enhanced Adipogenesis In Vitro

Priyatansh Gurha, Xiaofan Chen, Raffaella Lombardi, James T. Willerson and Ali J. Marian

Circ Res. 2016;119:731-750; originally published online July 28, 2016;
doi: 10.1161/CIRCRESAHA.116.308422
Circulation Research is published by the American Heart Association, 7272 Greenville Avenue, Dallas, TX 75231

Print ISSN: 0009-7330. Online ISSN: 1524-4571

Knock Down of Plakophilin 2 Downregulates miR-184 Through CpG Hypermethylation and Suppression of the E2F1 Pathway and Leads to Enhanced Adipogenesis *In Vitro*

Priyatansh Gurha, Ph.D.*, Xiaofan Chen, M.D.*, Raffaella Lombardi, M.D., Ph.D., James T. Willerson, M.D., A J Marian, M.D.

Center for Cardiovascular Genetics, Institute of Molecular Medicine and Department of Medicine, University of Texas Health Sciences Center at Houston, and Texas Heart Institute, Houston, TX 77030

*** Co-first authors**

Running title: miR-184 and Adipogenesis

Address for Correspondence:

AJ Marian, M.D.

Center for Cardiovascular Genetics

6770 Bertner Street

Suite C900A

Houston, TX 77030

713 500 2350

Ali.J.Marian@uth.tmc.edu

Priyatansh Gurha, Ph.D.

Center for Cardiovascular Genetics

6770 Bertner Street

Suite C905

Houston, TX 77030

713 500 2335

Priyatansh.Gurha@uth.tmc.edu

MATERIAL AND METHODS

The investigation conforms to the Guide for the Care and Use of Laboratory Animals published by the US National Institutes of Health. The Animal Care and Use Committee and Review Board as well as Biological Safety Committee of the University of Texas Health Science Center-Houston approved the studies.

Recombinant viruses: Recombinant lentiviruses were generated as published [1]. In brief, the shRNAs were cloned into a miR-Zip vector downstream to an H1 promoter for miRNA knockdown and a CMV7 promoter for miRNA overexpression studies. Two shRNAs with no known targeting sequence in mammalian genome were used as controls (NT-shRNA1 as a control for knock down and NT-shRNA 2 for overexpression studies). The vector also expresses a Green Fluorescence Protein cloned form copepod *Pontellina plumata* (copGFP, henceforth GFP) reporter to facilitate identification of the transfected cells (modified from System Biosciences, cat # MZIP-184-PA-1, www.systembio.com). MiR-184 overexpression construct was generated by inserting a 500bp genomic fragment of miR-184 (250bp upstream and 250bp downstream to mature transcript) into the miR-Express vector (modified from System Biosciences, cat#MMIR-200b-PA-1 from System Biosciences). DNMT1, DNMT3A, and DNMT3B proteins where knocked down using commercially available lentiviral shRNA constructs (Mission shRNAs, Sigma-Aldrich). Sequence data for the shRNAs are presented in Online Table I. For virus production the plasmids were transfected into 293T cells using X-tremeGENE9 DNA transfection reagent (Roche Life Science, Product # 06365787001, www.roche.com). The infectious lentiviral particles were harvested at 48h and 72h post transfection, cleared by precipitation of cell debris and then filtered through 0.45-μm-pore cellulose acetate filters (VWR International, cat # 28145-479). To transduce the HL-1 cells (a mouse atrial cardiac myocyte AT-1 tumor lineage cell line [2]), cells were grown to 70-90% confluence in the Claycomb medium (Sigma, www.sigmaaldrich.com, cat # 51800C), infected with the recombinant viruses for 48h, and then were cultured in the virus free Claycomb medium

for another 24h. Transduction efficiency was determined by detection of the GFP signal under fluorescence microscopy or by FACS analysis. A pre-packaged ready-to-use Adenoviral construct expressing CCND1 was used to over express CCND1 (Vector Biolabs, http://www.vectorbiolabs.com/Recombinant-Adenovirus/1517/Ad-Cyclin-D1/Cyclin-D1, Catalog: 1517).

Suppression of expression of PKP2 in the HL-1 cells: The HL-1 cell lines deficient in PKP2 (HL-1$^{Pkp2\text{-}shRNA}$) were generated as published [1]. In brief, HL-1 cells were cultured in the Claycomb Medium on tissue culture plates coated with gelatin and fibronectin. Cells were transduced with the recombinant lentiviruses expressing an shRNA that targets the *Pkp2* mRNA (Lenti:*Pkp2*^{shRNA}). Two HL-1$^{PKP2\text{-}shRNA}$ lines were established using two independent shRNAs (TRCN000012335, targeting position 251-271, and TRCN0000123351, targeting position 1126-46) by culturing the cells on a growth medium supplemented with 50 ug/ml puromycin for 2 weeks. Independent shRNAs that had no potential target sites in the mammalian genome (Lenti:non-target^{shRNA} abbreviated as NT-shRNAs) were used as controls in these experiments (Sigma, www.sigmaaldrich.com, cat. # SHC016). Knockdown of *Pkp2* mRNA and PKP2 protein levels were detected by qPCR and immunoblotting (IB), respectively.

Isolation of cardiac myocytes: Mice were anesthetized by intra-peritoneal (I.P.) injection of pentobarbital at 62 mg/Kg. An aliquot of 200U of heparin was injected IP to prevent clot formation. The heart was removed and placed in a Ca^{2+} free perfusion buffer [120 mM NaCl, 15 mM KCl, 0.6 mM KH2PO4, 0.6 mM Na2HPO4, 1.2 mM MgSO4□7H2O, 30 mM Taurine, 4.6 mM NaHCO3, 10 mM HEPES, 10 mM 2,3-Butanedione monoxime (BDM), and 5.5 mM Glucose; pH 7.0]. The heart was perfused through ascending aorta with the perfusion buffer for 2 minutes at a constant rate of 4 mL/min. Then the heart was perfused with a digestion buffer containing 624 U/mL of collagenase II solution (Worthington, Lakewood, NJ) for 2 minutes. Following the above 10 ul of 100 mM CaCl2 was added to the digestion buffer until complete digestion. The

heart was then cut into small pieces in the presence of the digestion buffer and cells were dissociated by gentle pipetting. Upon complete dissociation of the cells, a stop buffer (10% calf serum and 12.5 μM CaCl2 in the perfusion buffer) was added, cells were passed through a 100 μm nylon mesh, and transferred to a 15 ml polypropylene conical tube. Myocytes were let to sediment by gravity in the presence of 200 mM ATP and centrifugation at 20 g for 3 min. The precipitated cells were re-introduced to calcium upon incubation in the stop buffer containing 200 μM, 500 μM, 1 mM and 1.5 mM of CaCl2 sequentially. The final isolate was resuspended in a plating media (MEM media, 1% penicillin-streptomyocin, 10% Calf serum, 10 mM BDM, and 2 mM ATP) in culture dishes or cover glasses coated with laminin in a 2% CO2 incubator at 37 ^{o}C.

Isolation of mesenchymal progenitor Cells (MPCs): CD44 and PDGFRA (CD140A) enriched cardiac MPCs were isolated from adult murine hearts upon treatment of myocardial tissues with liberase (Liberase TM Research Grade, Roche, CA, 05401119001*)* and sorting of the dissociated non-myocyte cell fraction against anti CD44 (eBioscience, San Diego, CA 17-0441-81) anti PDGFRA (eBioscience, San Diego, CA 92121) antibodies. Cells were also sorted against hematopoietic lineage antibodies cocktail to exclude such cells (BD Pharmingen, BD Horizon™ V450 Mouse Lineage Antibody Cocktail, with Isotype Control, cat #561301) [3-5]. Isolated Lin^{neg}:CD44^{pos}:PDGFRA^{pos} cells were plated at the density of 2.5 x 10^4/cm^2 in a growth medium (DMEM/F12 media supplemented with 1XB27) also containing mouse basic Fibroblast Growth Factor (bFGF) at 10 ng/mL concentration (R&D, Minneapolis, MN; cat #3139-FB), 1000 U/mL of mouse Leukemia Inhibitory Factor (mLIF) (Millipore; cat # ESG1106) and 1% Antibiotic-Antimycotic solution. Cells were incubated at 37 °C in a 5% CO2 humidified incubator.

PKP2 was knocked down in the MPCs using the same shRNAs that were used to generate HL-1$^{PKP2\text{-}shRNA}$ cells (TRCN000012335, targeting position 251-271 , and TRCN0000123351, targeting position 1126-46). An shRNA that has no potential target site in the mammalian genome (Lenti:non-target^{shRNA} abbreviated as NT-shRNA) was used as a control

(Sigma, www.sigmaaldrich.com, cat. # SHC016). Knockdown of *Pkp2* mRNA were detected by qPCR. To avoid potential confounding effects resulting from different viral backbones among the groups, transduction studies were performed with vectors with identical backbones or the experiments were repeated using control viral vectors with a backbone identical to that used in the knock down and over-expression constructs.

Mouse models of AC: *Myh6:Jup*^{Tr} mice have been published [6-8]. To knock down the *Pkp2* gene in the heart, an shRNA targeting the *Pkp2* mRNA (position 1154-1174) was cloned into the U6-LoxP-Neo vector [9, 10]. The construct contains a LoxP neo cassette downstream to the U6 promoter and is inactive unless the LoxP-Neo cassette is removed upon expression of the Cre recombinase. *Nkx2-5:Cre* deleter mice was used to conditionally express the *Pkp2*^{shRNA} and suppress expression of the *Pkp2* in the cardiogenic lineage [11].

MicroRNA expression profiling: Expression profile of miRNAs was determined using TaqMan low-density (TLDA) microfluidic cards (Rodent miRNA v3.0 Card A and Card B Applied Biosystems). The panels contain a total of 750 mature miRNAs of which 641 are annotated and curated in the mouse genome. The panel also contains the mouse small nucleolar RNAs (MammU6), for data normalization and relative quantification. Each panel includes four sets of control assays, three candidate endogenous control assays and one negative control assay. Among the four control assays, *MammU6* is spotted in triplicate in each card and provides a more reliable indicator for normalization of the miRNA levels. In brief, 500 ng aliquots of RNA isolated from the HL-1 and HL-1$^{Pkp2\text{-}shRNA}$ cells from two independent experiments were reverse-transcribed using Megaplex Primer Pools (Rodent Pools Set v3.0, cat#4444766). MiRNA cDNAs were loaded into the wells and subjected to qPCR on a 7900HT system per the manufacturer's protocol (Life Biotechnology, www.lifetechnologies.com). Raw TLDA data files were quality controlled and miRNA with Ct values greater than 36 were excluded from further analysis. Heat plots for differentially expressed miRNAs were plotted using Gene-E (http://www.broadinstitute.org/cancer/software/GENE-E/index.html).

***In situ* hybridization:** In situ hybridization was performed at Baylor College of Medicine Core laboratory per a published protocol [12]. In brief, to detect expression for miR-184, thin myocardial sections were embedded in optimal cutting temperature (OCT) compound (Sakura Finetek Inc, Torrance, CA). Tissue sections were then acetylated for 10 min in freshly prepared TEA buffer (4.63 g triethanolamine HCl, 0.56 ml 10N NaOH and DEPC treated H_2O up to 250 ml) and washed in PBS for three minutes. The slides were then pre-hybridized with the hybridization solution (4°C Formamide 100%, SSC 20x, Denhart's reagent, Yeast tRNA at 10mg/ml, Herring sperm DNA at 500 µg/ml, EDTA at 2.5 mM, Tween-20 at 10%, CHAPS at 0.25% and H_2O). Slides were then incubated for 24 h at 65°C and wash 3 times each for 20 minutes in 0.2x SSC at 65°C, blocked in 1x PBS, 0.1% Triton X-100, and 1% blocking reagent for 1 hour at RT. Slides were then hybridized with aliquots of 15-60 nM of 5' and 3' DIG-labeled miRCURY LNA™ Detection probe (Exiqon, Catalog Product no.: 18072-15) in the hybridization buffer. Following hybridization slides were washed PBS and 0.1% Triton X-100 for 20 min, placed in an amplification buffer, and mount in Vectastain with DAPI, seal with nail varnish.

ChIP Assays: ChIP assays were performed using a ChIP-IT High Sensitivity kit (Active Motif, Catalog number: 53040). Briefly, HL-1 and HL-1$^{Pkp2\text{-}shRNA}$ cells were cross-linked in 1% formaldehyde for 10 minutes. DNA-protein cross-linking was stopped by incubation the samples in 0.125 M glycine. Cells were then washed, and recovered for chromatin preparation and lysis using ACTIVE MOTIF ChIP-IT High Sensitivity Kit (Catalog # 53040). Lysates were sonicated using a cell disruptor (Fisher Scientific Model 500 Sonic Dismembrator) for 10 cycles of 30 sec ON and 60 sec OFF yielding a genomic DNA fragments of ~200-1000 bp size. Chromatin immunoprecipitation and washing where performed as described in the manufactures protocol. Aliquots of 5 ug of anti E2F1 and anti DNMT1 antibodies where used in the ChIP assays (Online Table I). Quantitative PCR analysis of ChIP assays was performed using 2 µL of the ChIP DNA and SYBR green master mix. Enrichment of binding on the miR-184 promoter was presented,

as normalized to Input amount and relative to a control IgG group. All primers sequences are listed in Online Table I.

IB: IB was performed per the conventional methods [1]. In brief, total cellular protein was extracted using a RIPA lysis buffer in the presence of protease and phosphatase inhibitors. Protein concentration was measured using the Bio-Rad DC Protein Assay Kit (Bio-Rad Laboratories, www.bio-rad.com, cat # 5000111). Following denaturation in a 4X Laemmli buffer at 95 °C for 5min, extracts were subjected to electrophoresis on the SDS/PAGE gel and transferred to a nitrocellulose membrane. The membranes, after blocking in 5% milk, were incubated with the primary antibody overnight (primary and secondary antibody list is available in Online Table I), followed by incubating with the corresponding HRP conjugated secondary antibody. Signal was detected by chemiluminescence.

Immunofluorescence staining: Cells were fixed in 4% paraformaldehyde for 15 minutes, washed 3X for 5 minutes each, and blocked in 5% donkey serum in PBS containing 0.3% Triton X-100 (0.03% Triton X-100 for PKP2 staining) for 60 minutes at room temperature. After blocking, cells were incubated with the primary antibody (Online Table I) with 1% BSA and 0.3% Triton X-100 (0.03% for PKP2 staining) overnight at 4 °C. After 3 washes, cells were incubated with corresponding secondary antibody in 1% BSA and 0.3% Triton X-100 for 1 hour at room temperature. Cells were then washed for 3 times and stained with DAPI. Slides were analyzed using Axioplan Fluorescence Microscope (Zeiss). Cells showing fluorescence signals beyond the levels detected for the IgG isotype of the corresponding antibody were considered as stained positive for that specific antigen.

Quantitative PCR (qPCR): Total RNA (including miRNA) was extracted using miRNeasy kit (Qiagen, www.quiagen.com, cat # 271004) and cDNA was synthesized using either a high-capacity cDNA Reverse Transcription Kit (Life technology, cat # 4368814) for mRNA conversion or a MicroRNA Reverse Transcription Kit (Life technology, cat # 4366596) for miRNA conversion. Quantitative PCR was performed using specific TaqMan gene express

assays and TaqMan MicroRNA assay. *Gapdh* and *snoRNA202* expression levels were measured for normalization for mRNA and miRNA levels, respectively. ΔΔCt (2^{DDCt}) method was used to calculate the normalized gene expression values.

Transcript levels of *snoRNA202* showed minimum variability in the HL-1 and mouse heart RNA samples. The mean Ct ± SD value of *snoRNA202* transcript levels in 50 experiments (150 triplicates) in the HL-1 cells was 23.13 ± 0.62. Likewise, the mean Ct ± SD value of *snoRNA-202* transcript levels in 25 experiments in the mouse heart samples was 21.80 ± 0.37. These data show a modest variability in the *snoRNA202* levels in the HL-1 cells and myocardial samples, which bode confidence in the use of *snoRNA292* levels in normalization of the miRNA levels.

Raw expression values, presented as ΔΔCt, were used for statistical analysis. For graphical representation the data in the experimental groups were normalized to the average expression value in the control samples and present as relative fold change to the control samples. The later was normalized and set at 1.

MicroRNA targets and miRNA-mRNA pairing: Global gene expression patterns in the HL-1 and HL-$1^{Pkp2\text{-}shRNA}$ cells, determined by whole transcriptome sequencing (RNA-Seq), were compared to identify differentially expressed mRNA transcripts and are published [1]. Predicted miR-184 targets were identified using miRWalk online software (www.umm.uni-heidelberg.de/apps/zmf/mirwalk/). Genes that were identified as targets in at least 2 different databases were included in the subsequent analysis. MiRNA-mRNA pairing was carried out using the Ingenuity Pathway Analysis (IPA) software (www.ingenuity.com). Pairing of miRNA-mRNA for all differentially expressed miRNAs was performed using the following criteria: First, all putative target of a given miRNA were identified using the miRwalk software. Targets that were identified by at least 2 programs and had a seed length of 6 nucleotides or longer were included for further analyses. The heat maps of the RNA-seq data were generated based on differentially expressed transcripts that are statistically significant at a stringent false discovery

rate of less than 5% (q value <0.05), had a FPKM value of at least 1 in one of the samples, and showed a reciprocal expression to that of the corresponding miRNAs. Finally, target gene expression cutoff was set at 1.2 fold expression and a q value of 0.05. Based on these benchmarks potential miR-184 targets where identified and included them in subsequent analysis. To examine the potential biological significance of paired changes, gene ontology over-representation analysis, upstream regulator and canonical pathway analysis was performed using IPA.

Heat plot and Gene network analysis: A heat map depicting miRNA expression levels was generated using the expression values obtained from the $2^{\Delta\Delta Ct}$ method and plotted for the expression value for each miRNAs. Each value was normalized to the mean value of the transcript in that row. Heat plots for mRNAs where generated from the raw FPKM values obtained by RNA-seq experiment. Heat plot were generated using the GENE-E software (http://www.broadinstitute.org/cancer/software/GENE-E).

A protein functional association network for miR-184 targets involved in adipogenesis, *Agpat1*, *Agat3*, *Ncoa1,* and *Ppargc1b,* was constructed using the STRING online tool. The medium confidence score for interaction was set at 0.4 and the option for all active prediction method was included. Direct interactions are depicted as colored nodes in the Network. Gene that are identified as members of the network and were found to be up-regulated in the HL-$1^{Pkp2\text{-}shRNA}$ cells in RNA-seq data were further validated to build a miR-184 target network for adipogenesis.

Proliferation, viability and apoptosis: Cells were plated in triplicate in 96-well plate at a density of $5x10^3$ to $10x10^3$ cells per well. Cell viability was determined by CellTiter-Blue Cell Viability Assay (Promega Corporation, www.promega.com, cat # G8080) every 24h for 72 hours. At each time point, 20µl of CellTiter-Blue reagent was added to the cells, and incubated at the culture conditions for 1 hour followed by measurement of the fluorescence signal at

560/590nm wavelength. Cell growth curve was generated using the corresponding fluorescence value at each time point. Cell doubling time was calculated using an exponential growth equation based on the fluorescence value at each time point.

Adipogenesis: Induction and quantification of adipogenesis was as described [1]. In brief, ~5 x10^4 HL-1 cells were plated on gelatin and fibronectin coated cover glass, and treated with an adipogenesis induction medium [HL-1 media supplemented with 1uM dexamethasone (Sigma, cat # D8893), 0.5mM 3-isobutyl-1-methylxanthine (Sigma, cat # I7018) and 10ug/mL insulin (Cayman Chemical, cat # 10008979)] for 14 days. Quantitative PCR and IB were used to quantify transcript and protein levels of selected genes that regulate adipogenesis, respectively.

To induce adipogenesis in MSC, cells were plated at a density of ~5 x10^4 cells on gelatin-coated plates in DMEM/F12 media supplemented with 1XB27 and 1uM dexamethasone, 0.5mM 3-isobutyl-1-methylxanthine and 10ug/mL insulin for 5 to 14 days.

Accumulation of fat droplets was assessed by Oil Red O staining, and the number of cells stained positive for Oil Red O was determined in at least 15 to 20 randomly selected high (100X) magnification fields and in 3-5 independent experiments. PPARG staining (for HL-1 cells) and CEBPA staining for (MSCs) was performed as described in the IF section and CEBPA or PPARG$^+$ cells where counted from 10-15 randomly selected field (200 to 600 cells /group) from 3 independent experiments.

Activation and suppression of selected signaling pathways: To delineate the mechanism of suppression of miR-184 in AC models, we determined the effect of activation and suppression of the RB1/E2F signaling pathway on miR-184 levels. To activate the E2F1 pathway, suppressed in the HL-1$^{Pkp2\text{-}shRNA}$ cells, serum starved HL-1 cells, plated at a density of 2 - 4 × 10^5 cells, were transduced with recombinant adenoviruses expressing CCND1 at a MOI of 10 infectious particle/cell. Twelve hours post transduction, serum free media was switched to complete Claycomb media with serum and cells were cultured for another 48 h. Control adenoviruses (Ad5-CMV vector alone) were included as controls. Retinoblastoma 1 (RB1) was

knocked down using a commercially available siRNA construct (ON-TARGET plus Rb1 siRNA construct, Dharmacon: J-047474-08-0002). Cells were transfected with 10 nM of Rb1 or control siRNAs using RNAiMax reagent (Thermo Fisher Scientific, Catalog: 13778030). DNMT1, DNMT3A, and DNMT3B were knocked down using recombinant lentiviruses expressing respective shRNAs, as described above.

The Hippo, and canonical Wnt signaling pathways were analyzed for their effects on expression levels of miR-184 [1, 6]. To activate the canonical Wnt signaling pathway, cells were treated with Wnt-3A (R&D Systems, www.rndsystems.com, cat # 1324-WN) at three concentrations of 40, 80, and 120 ng/mL for 24h. To suppress the canonical Wnt signaling pathway, HL-1 cells were transduced with recombinant lentiviruses expressing shRNA against Tcf7l2 mRNA (Lenti*:Tcf7l2*^{shRNA}), a canonical Wnt effector. Reduced levels of TCF7L2 were confirmed in the protein extracts of HL-1 cells by IB. Activation or suppression of the canonical Wnt signaling pathway was also confirmed by quantifying mRNA levels of its well-established targets, namely, *Axin2* and *Ccnd1* and a *Tcf7l2*-luciferase reporter assay.

To activate gene expression through the Hippo pathway, HL-1 cells, cultured in serum free medium, were treated with 1uM of 1-Oleoyl lysophophatidic acid (LPA, Cayman Chemical, www.caymanchem.com, cat # 62215) for 1, 2 and 4h. To suppress gene expression through the Hippo pathway, HL-1 cells were transduced with the recombinant lentiviruses expressing an shRNA against *Yap* mRNA (Lenti:*Yap*^{shRNA}). Activation or suppression of the Hippo signaling pathway was determined by quantification of YAP protein levels, transcript levels of the target genes *Ctgf* and *Cry61* by qPCR, and by a TEAD-luciferase reporter assay.

DNA methylation assay: To determine whether suppression of miR-184 was a consequence of DNA methylation dependent epigenetic silencing of the locus, genomic sequence upstream of the pre-miR-184 start site for the presence of CpG rich regions. Using EMBOSS Cpgplot (web based tool for CpG Island prediction,) 15 CpG sites with observed/expected ratio of > 0.60, located 500-800 bp upstream to the pre-miRNA start site,

were identified. This region was used for DNA methylation analysis by bisulfite conversion, cloning and sequencing of individual clones. Genomic DNA was extracted from the HL-1 and Hl-$1^{Pkp2\text{-}shRNA}$ cells using the DNeasy Blood & Tissue Kit (Qiagen, Catalog# 69504) per the manufacturer's protocol. Genomic DNA (2ug) from each sample was treated for bisulfite conversion using EpiTect Bisulfite Kits (Qiagen, Catalog# 59104,) according to the manufacturer's recommendations. Aliquots of 50-100 ng of bisulfite converted DNA was PCR amplified using primers specific to the miR-184 upstream region (Online Table I). PCR products were cloned into pCR 2.1 vector using a TA cloning strategy. After transformation, positive colonies were screened by colony PCR. Plasmids from the positive colonies were isolated and then sequenced. Methylation of CpG sites was analyzed using QUMA online tool (http://quma.cdb.riken.jp/).

Statistics: Data were presented as mean ± SD. Differences in the continuous variables between the two groups were compared by t-test or Mann-Whitney U test and among multiple groups by one-way ANOVA. Whenever applicable multiple groups Bonferroni corrected p values for pairwise comparisons were presented. Differences among the categorical values were compared by Kruskall-Wallis test. Statistical analyses were performed using Graph pad Prism or STATA 10.1 software. Statistical significance for methylation at each CpG sites was calculated by Fisher exact test (QUMA online tool).

REFERENCES

1. Chen SN, Gurha P, Lombardi R, Ruggiero A, Willerson JT, Marian AJ. The hippo pathway is activated and is a causal mechanism for adipogenesis in arrhythmogenic cardiomyopathy. *Circulation research*. 2014;114:454-468
2. Claycomb WC, Lanson NA, Jr., Stallworth BS, Egeland DB, Delcarpio JB, Bahinski A, Izzo NJ, Jr. Hl-1 cells: A cardiac muscle cell line that contracts and retains phenotypic characteristics of the adult cardiomyocyte. *Proceedings of the National Academy of Sciences of the United States of America*. 1998;95:2979-2984
3. Lombardi R, Chen SN, Ruggiero A, Gurha P, Czernuszewicz GZ, Willerson JT, Marian AJ. Cardiac fibro-adipocyte progenitors express desmosome proteins and preferentially differentiate to adipocytes upon deletion of the desmoplakin gene. *Circulation research*. 2016
4. Carlson S, Trial J, Soeller C, Entman ML. Cardiac mesenchymal stem cells contribute to scar formation after myocardial infarction. *Cardiovascular research*. 2011;91:99-107
5. Cieslik KA, Trial J, Entman ML. Defective myofibroblast formation from mesenchymal stem cells in the aging murine heart rescue by activation of the ampk pathway. *Am J Pathol*. 2011;179:1792-1806
6. Garcia-Gras E, Lombardi R, Giocondo MJ, Willerson JT, Schneider MD, Khoury DS, Marian AJ. Suppression of canonical wnt/beta-catenin signaling by nuclear plakoglobin recapitulates phenotype of arrhythmogenic right ventricular cardiomyopathy. *The Journal of clinical investigation*. 2006;116:2012-2021
7. Lombardi R, da Graca Cabreira-Hansen M, Bell A, Fromm RR, Willerson JT, Marian AJ. Nuclear plakoglobin is essential for differentiation of cardiac progenitor cells to adipocytes in arrhythmogenic right ventricular cardiomyopathy. *Circulation research*. 2011;109:1342-1353
8. Lombardi R, Dong J, Rodriguez G, Bell A, Leung TK, Schwartz RJ, Willerson JT, Brugada R, Marian AJ. Genetic fate mapping identifies second heart field progenitor cells as a source of adipocytes in arrhythmogenic right ventricular cardiomyopathy. *Circulation research*. 2009;104:1076-1084
9. Shukla V, Coumoul X, Wang RH, Kim HS, Deng CX. Rna interference and inhibition of mek-erk signaling prevent abnormal skeletal phenotypes in a mouse model of craniosynostosis. *Nature genetics*. 2007;39:1145-1150
10. Shukla V, Coumoul X, Deng CX. Rnai-based conditional gene knockdown in mice using a u6 promoter driven vector. *International journal of biological sciences*. 2007;3:91-99
11. Moses KA, DeMayo F, Braun RM, Reecy JL, Schwartz RJ. Embryonic expression of an nkx2-5/cre gene using rosa26 reporter mice. *Genesis*. 2001;31:176-180
12. Yaylaoglu MB, Titmus A, Visel A, Alvarez-Bolado G, Thaller C, Eichele G. Comprehensive expression atlas of fibroblast growth factors and their receptors generated by a novel robotic in situ hybridization platform. *Dev Dyn*. 2005;234:371-386

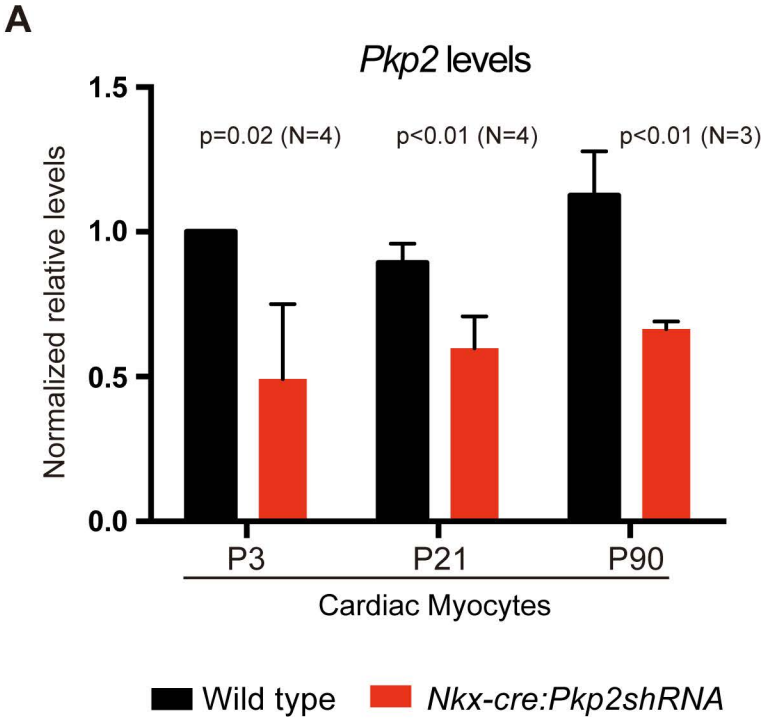

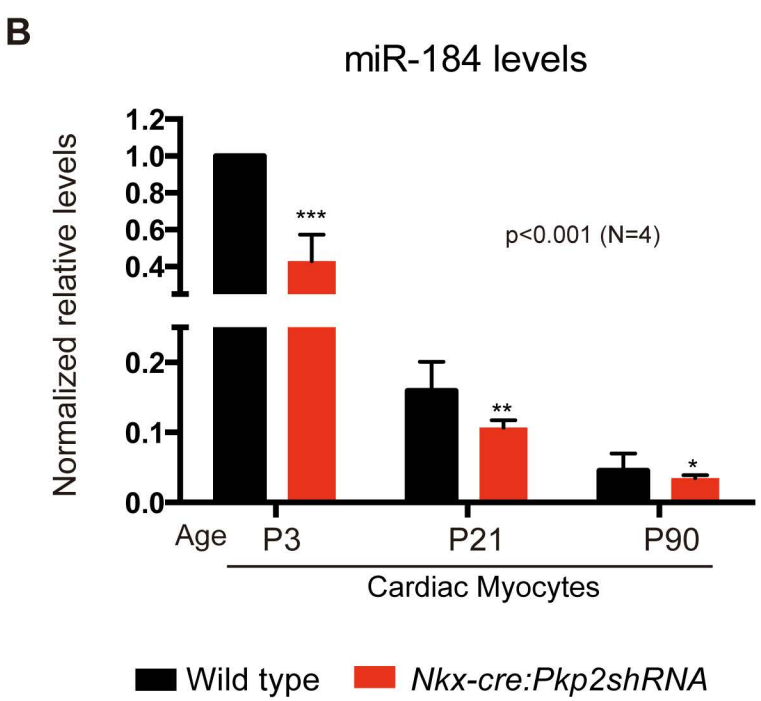

Online Figure I

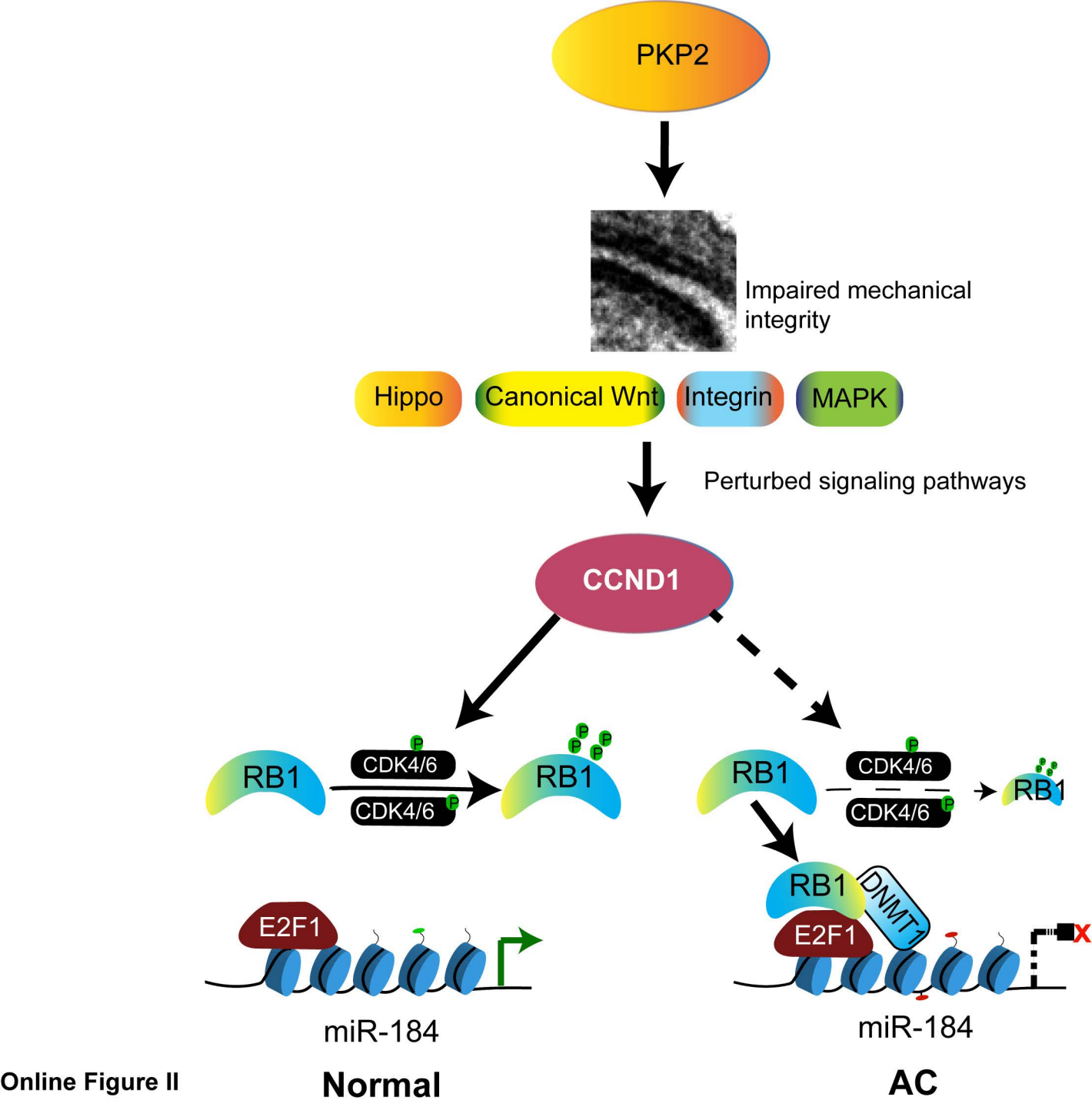

Online Figure II

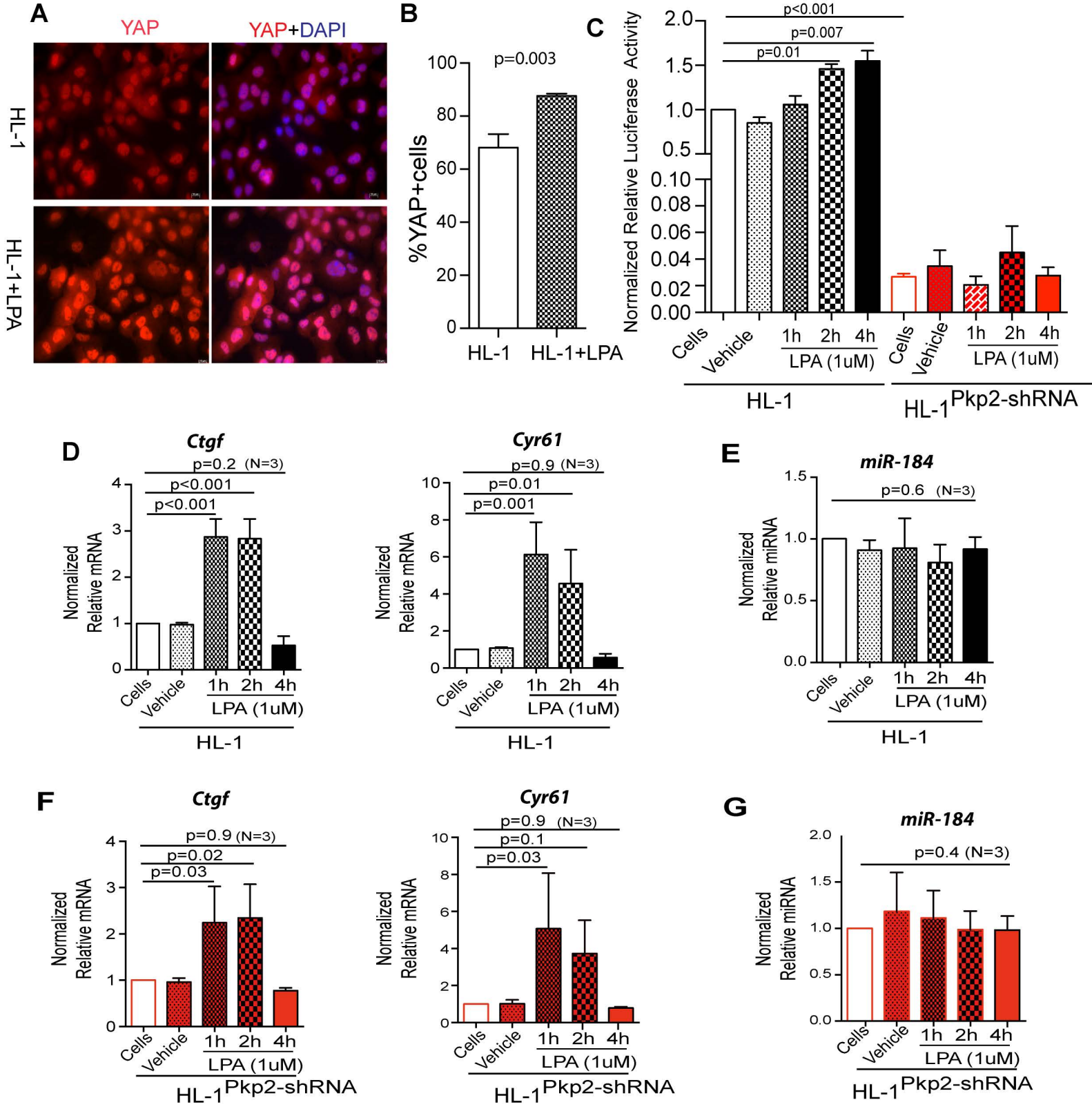

Online Figure III

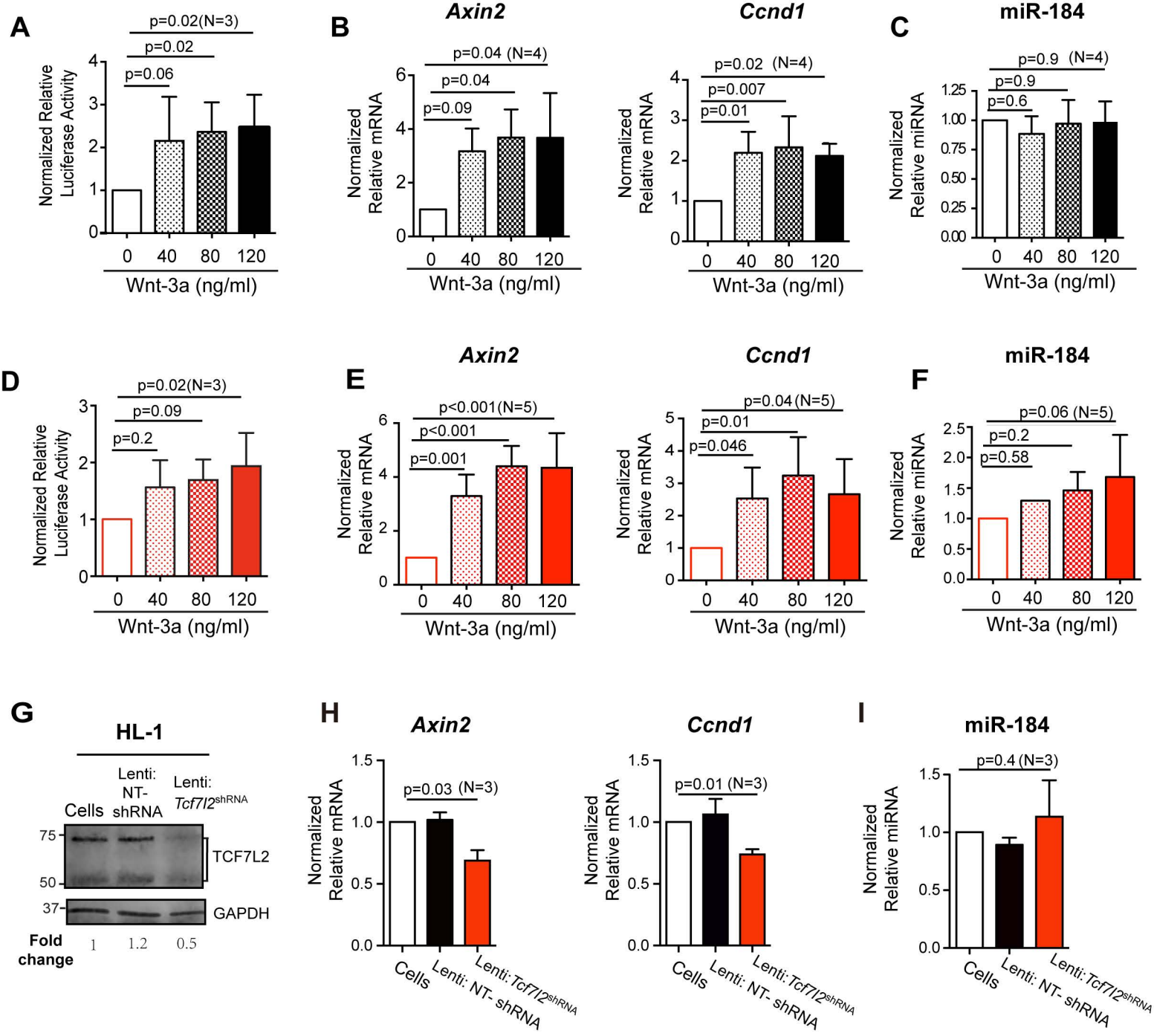

Online Figure IV

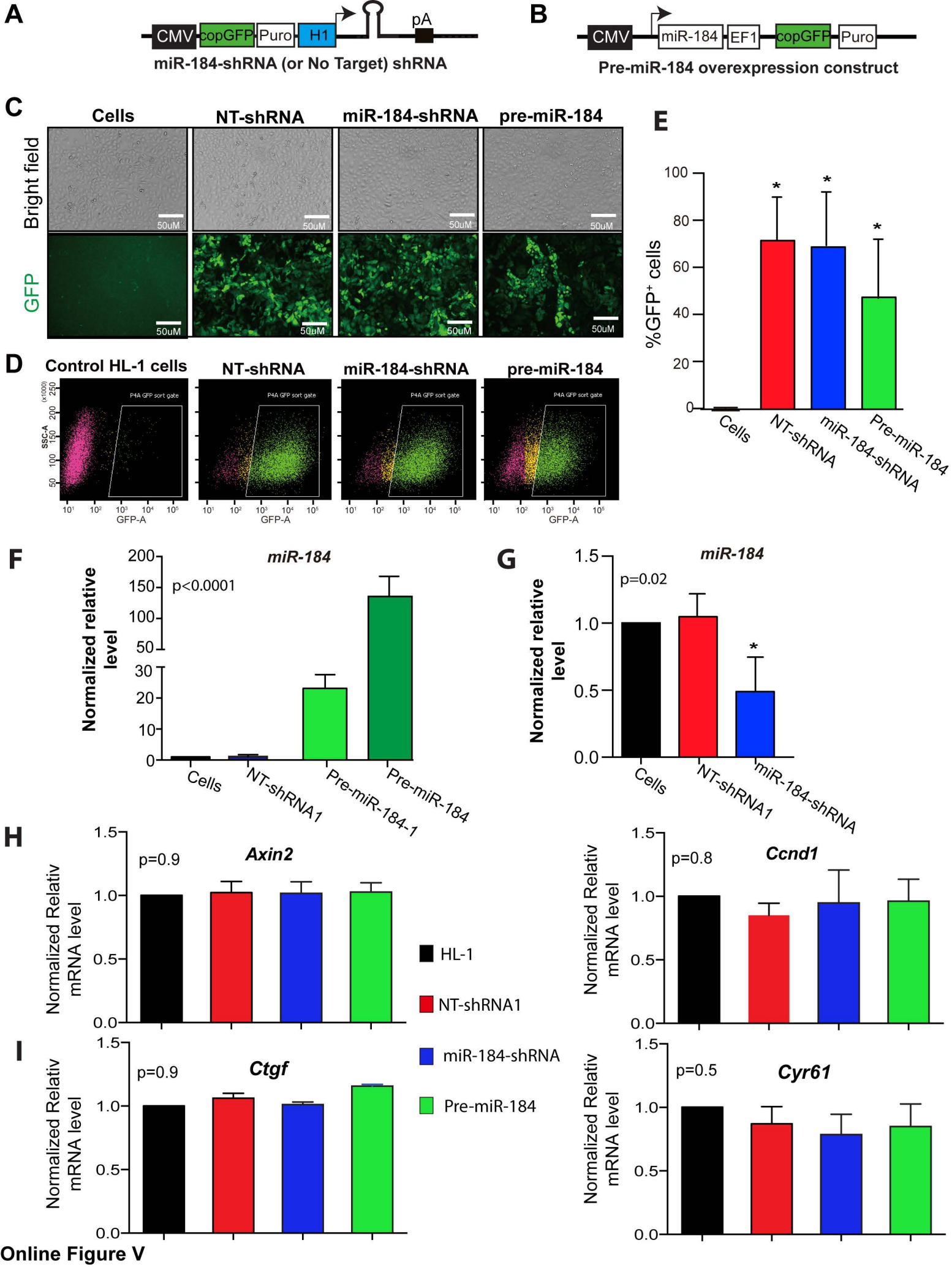

Online Figure V

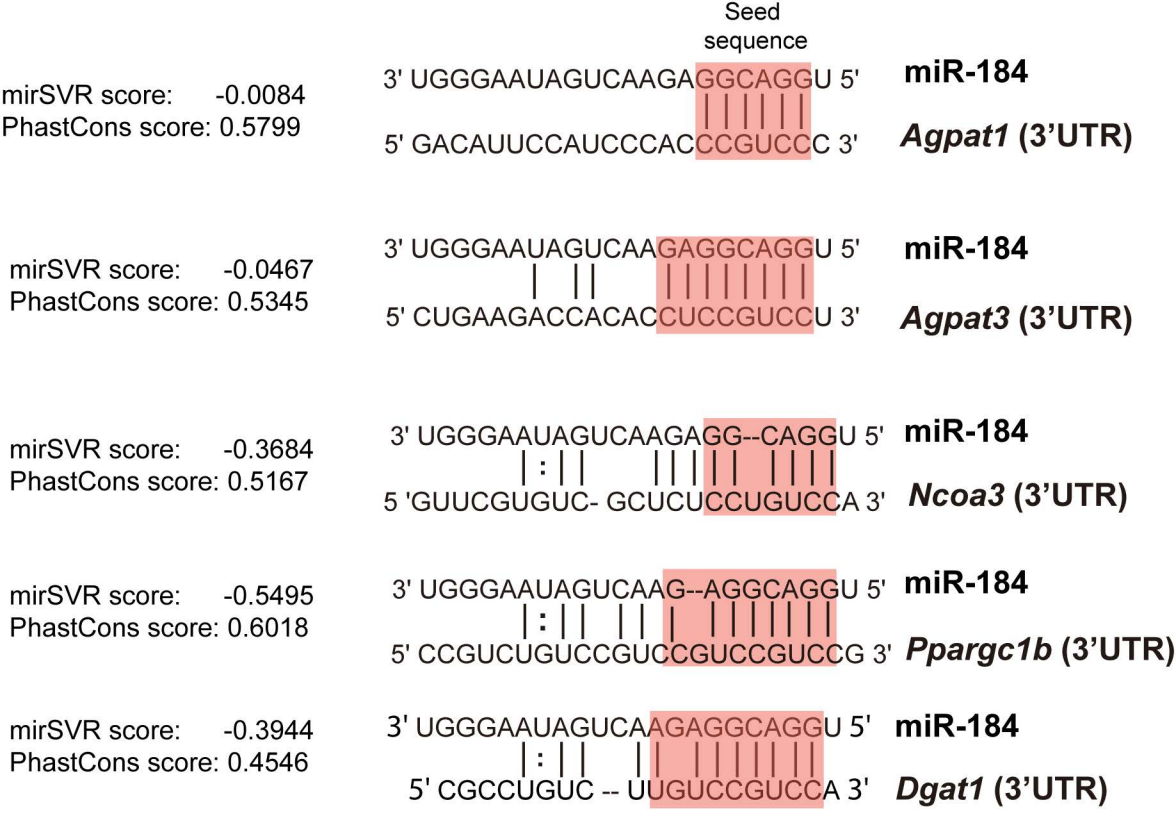

Online Figure VI

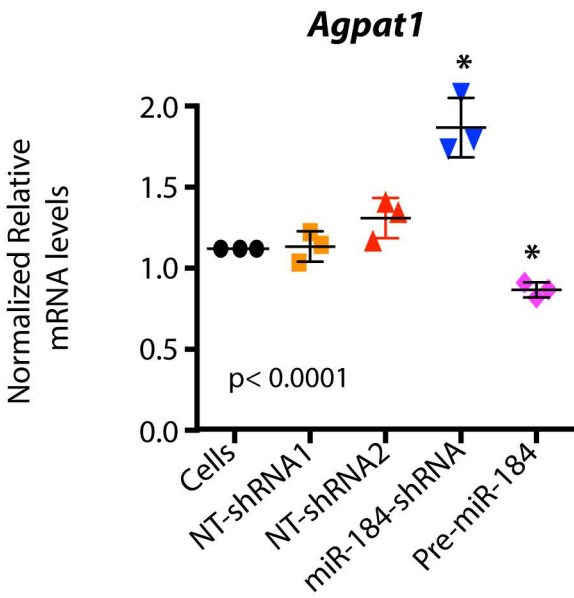

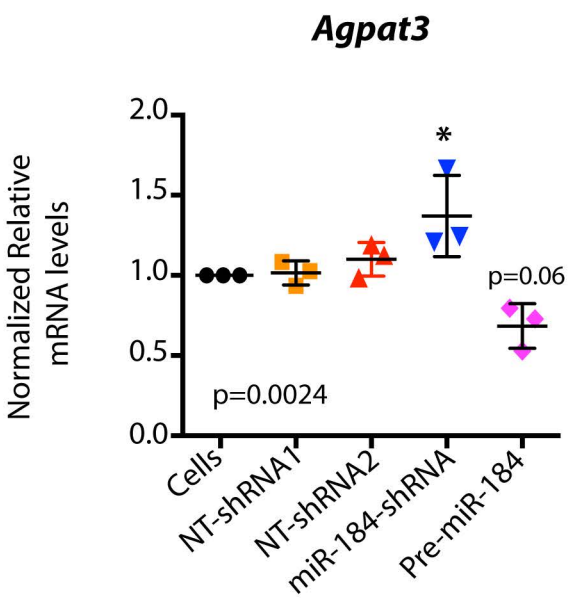

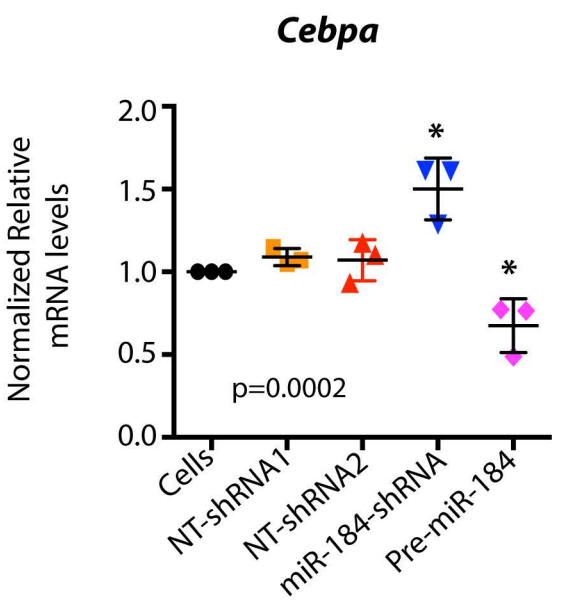

Online Figure VII

ONLINE FIGURE LEGENDS

Online Figure I. Development downregulation of miR-184 in isolated cardiac myocytes and its differential expression in the PKP2-deficient myocytes:

A. Levels of *Pkp2* mRNA were consistently lower in P3, P21 and P90 myocytes isolated from the *Nkx-2.5-Cre:Pkp2*^{shRNA} mouse hearts than the wild type myocytes, indicating effective knock down of *Pkp2* (N=3 to 4 per group). **B**) Expression of miR-184 levels in P3, P21, and P90 cardiac myocytes isolated from wild type and *Nkx-2.5-Cre:Pkp2*^{shRNA} mice. As shown, miR-184 levels were suppressed in cardiac myocytes isolated from the *Nkx-2.5-Cre:Pkp2*^{shRNA} mice in all three stages of development, as compared to myocytes isolated from the wild type mice (N=3 to 4 per group)

Online Figure II. Hypothesis tested to explain the mechanisms responsible for suppression of miR-184 in AC: Deficiency of PKP2 protein at the intercalated discs (and desmosomes) impairs mechanical integrity of the myocytes and activates mechanosenstive transduction pathways, such the Hippo, canonical Wnt and integrin signaling pathways. Perturbed mechanosensitive signaling pathways result in suppression of cyclin D1 (CCND1) expression, which is a co-activator of cyclin-dependent kinases (CDK) 4 and 6. Reduced CDK4/6 activity leads to hypophosphorylation and activation of retinoblastoma protein (RB1), which inhibits the E2F transcription factors and the ensuing suppressed gene expression through E2F1 transcription factor. The RB1/E2F1 complex is known to recruit DNMT1 to the genomic regions, which then leads to hypermethylation of the CpG rich sites and further suppression of gene expression.

Online Figure III. Effects of the Hippo pathway on miR-184 expression: A and **B)** Immunofluorescence panels and the corresponding quantitative data showing expression of the Hippo effector protein YAP in the control cells and cells treated with LPA for 1 hour. Treatment with LPA led to increased nuclear localization of YAP (N=2, 68±2% vs. 87±0.5, p=0.0039). **C)** TEAD–luciferase reporter assay showing activation of YAP/TEAD –mediated transcription in HL-1 cells treated with 1uM of LPA for 3 different time points (N=3, corrected p values for pairwise comparisons to control cells are shown). **D)** Quantification of transcript levels of selected YAP/TEAD targets showing induction of *Ctgf* and *Cyr6*1 (maximum induction of 2.87±0.38 and 6.13±1.73 -fold, respectively, N=3, p<0.001) after treatment with 1uM LPA at 3 different time points. **E)** Quantitative PCR data of miR-184 levels in the experimental groups showing no effect of activation of YAP/TEAD pathway on miR-184 expression. **F)** Transcript levels of YAP/TEAD targets in the HL-1$^{Pkp2:shRNA}$ cells treated with 1uM of LPA and analyzed at 3 time points after treatment. *Ctgf* and *Cyr61* transcripts show a maximum induction of 2.34±0.72 and 5.06±3.01 –fold, respectively (N=3, p<0.001). **G)** Transcript levels of miR-184 showing no change upon activation of the YAP/TEAD pathway. **H)** Immunoblot showing knock down of YAP (~ by about 40%) upon transduction of HL-1 cells with Lenti:Yap^{shRNA}. **I)** Transcript levels of YAP/TEAD targets *Ctgf* and *Cyr61* showing reduced levels (31±0.1% and 40±0.1%, respectively, N=3, p<0.01). **J)** Transcript levels of miR-184 showing no change upon suppression of expression of YAP in the HL-1 cells.

Online Figure IV: Effects of canonical Wnt on miR-184 expression A) Dose-dependent activation of the canonical Wnt signaling pathway upon treatment with an increasing dose of recombinant Wnt-3A protein (40-120ng/ml) in HL-1 cells as measured by the TCF7L2–luciferase reporter assay (N=3, p<0.05 as compared to untreated control

HL-1 cells). **B)** Increased mRNA levels of selected canonical Wnt target genes *Axin2* (maximum induction of 3.84±1.40 –fold, N=4, $p<0.05$) and *Ccnd1* (maximum induction of 2.32±0.76 –fold, N=4, $p<0.05$) in a dose dependent manner upon treatment of HL-1 cells with Wnt-3A. **C)** Transcript levels of miR-184 in the same set of experiments as in III-B showing no change. **D)** Activation of the canonical Wnt pathway in the HL-1$^{Pkp2\text{-}shRNA}$ cells as measured by TCF7L2-luciferase reporter assay (N=3, $p<0.05$ as compared to untreated control HL-1 cells. **E**) A dose-dependent increase in the transcript levels of the canonical Wnt targets *Ccnd1* (maximum induction of 3.24 ±1.18 -fold, N=5, $p<0.05$) *and Axin2* (maximum induction of 4.39±0.75 -fold, N= 5, $p<0.01$). **F)** Transcript levels of miR-184 showing a modest dose-dependent increase upon activation of canonical Wnt signaling (N=5, $p=0.06$ as compared to untreated HL-1$^{Pkp2\text{-}shRNA}$ cells). **G)** Immunoblot showing reduced levels of the canonical Wnt effector TCF7L2 in HL-1 cells transduced with Lenti:*Tcf7l2*^{shRNA}. **H)** Data showing reduced transcript levels of *Axin2* and *Ccnd1* upon transduction of HL-1 cells with Lenti:*Tcf7l2*^{shRNA}. **I)** Transcript levels of miR-184 as detected by qPCR showing no change upon suppression of TCF7L2 (N=3, $p>0.05$).

Online Figure V: Effects of miR-184 on the Canonical Wnt and Hippo signaling activities: Panel **A** shows schematic presentation of Lenti:*miR-184*^{shRNA} (knock down) and Lenti:*Non-target*^{shRNA} (NT-shRNA1). The *miR-184-shRNA* construct expresses an shRNA hairpin from a RNA polymerase III H1 promoter. The vector also expresses copGFP (variant of EGFP, henceforth GFP). This gene serves as a fluorescent reporter for the transfected or transduced cells. Panel **B** represents Lenti-*Pre-miR-184* over-expression construct. CMV promoter drives Pre-miR-184 expression in the construct. Lenti:*Non-target*^{shRNA} (NT-shRNA2) in this backbone served as control.In the over-expression construct, a 500 bp genomic fragment of miR-184 was cloned downstream to a CMV promoter for pre-miR-184 expression. In this construct the EF1 promoter drives

GFP expression. **C).** Bright field (upper panel) and direct fluorescence (lower panels) showing expression of GFP as an indicator of transduction efficiency and a surrogate marker for shRNA or pre-miRNA expression (changes in the transcript levels of miR-184 were also determined by qPCR). Control HL-1 cells, HL-1 cells transduced with Lenti-NT^{shRNA}, Lenti:*miR-184*^{shRNA} and Lenti:*pre-miR-184* are shown. **D)** FACS of HL-1 cells in the experimental groups showing gating strategy for GFP^{+} cells isolation. X-axis depicts the GFP fluorescence intensity and Y-axis cells side scatter. Green dots within the selected area represents the GFP^{+} cells that where collected for the subsequent experiments. **E)** Transduction efficiency in HL-1 cells infected with the recombinant Lenti-NT^{shRNA} (71±18.3%), Lenti-*miR-184*^{shRNA} (68±21%) and Lenti-*pre-miR-184* (48±25%) in four independent experiments. The transduced fraction, identified by GFP expression was used in the subsequent experiments.

F) Quantitative PCR data showing 23±4.5 and 135±33 -fold increase in the expression levels of miR-184 in the control HL-1 and HL-1 cells transduced with Lenti-Pre-miR-184 (N=3, *p<0.001). **G)** Expression levels of miR-184 upon transduction of HL1 myocytes transduced with Lenti:*miR-184*^{shRNA}. As shown miR-184 transcript levels were reduced by 41±19% in Lenti:*miR-184*^{shRNA} group, indicating effective knock down of miR-184 (N=3, *p=0.02).

HL-1 cells were infected with Lenti-NT^{shRNA}, Lenti-*miR-184*^{shRNA} and Lenti-*pre-miR-184* followed by assessment of the transcript levels of the canonical Wnt and Hippo/YAP/TEAD pathway selected targets. **H**) Quantitative PCR analyses of the transcript levels of *Axin2* and *Ccnd1*, established targets of the canonical Wnt signaling, showing no change upon over-expression or suppression of miR-184 levels (N=3, p>0.05). **I)** Quantitative PCR data on transcript levels of Hippo/TEAD/YAP downstream targets *Ctgf* and *Cyr61* showing no change upon over-expression or suppression of miR-184 levels (N=3, p>0.05).

Online Figure VI: miR-184 seed sequence paired with the 3' UTR target sequence of genes involved in triglyceride synthesis: Schematic diagrams of binding sites of miR-184 in the 3' UTR of genes involved in the lipid biosynthesis. Mature miR-184 sequence and Watson Crick pairing of 3′ UTR of *Agpat1*, *Agapt3*, *Ncoa3*, *Ppargc1b* and *Dgat1* with miR-184 are also shown. Core of the miR-184 seed sequence is highlighted by a shaded rectangle. MiRNA target site ranking and conservation score where obtained from webtool at microrna.org and presented for each miRNA;target pair.

Online Figure VII: Effect of control shRNAs on expression of selected miR-184 targets and *Cebpa*:

To rule out confounding effects of non-targeting shRNAs on miR-184 target gene expression, MPCs where transduced with lentiviruses expressing control shRNA used for knockdown experiment (Lenti-NT^{shRNA1} or NT-shRNA1) or overexpression experiments (Lenti-NT^{shRNA1} or NT-shRNA2). **A)** QPCR analysis showed no difference in expression of *Agpat1*, *Agpat3* and *Cebpa* in NT-shRNA controls as compared to the non transduced cells after 5 days of adipogenic stimulation. Knockdown or overexpression of miR-184 showed enhanced and reduced levels of corresponding RNAs (N=3, *$p<0.05$).

ONLINE SUPPLEMENTARY TABLE I

A. Primers for cloning of miR-184:

184-F: 5'-GCTAGCGAATTCGGCTGGGAGTTTCTGTGTGTCT-3'

184-R: 5'-GGATCCGCGGCCGCGAACAGATCCTAAGCCCAGGT-3'

B. Primers for miR-184 promoter ChIP:

miR-184-F-pro	CGGGAAACTGAGGCTCAAC
miR-184-R-pro	AACCGTTCCGTTTACCACAG

C. Primers for SYBR Green QPCR analysis:

mmu-Rb1-Sybr-F1	ACCTGATAACCTTGAACCTGC
mmu-Rb1-Sybr-R1	GCTTGTGTCTCTGTATTTGCAG
mmu-Actb-Sybr-F1	ACCTTCTACAATGAGCTGCG
mmu-Actb-Sybr-R1	CTGGATGGCTACGTACATGG
mmu-Gapdh-Sybr-F1	CTTTGTCAAGCTCATTTCCTGG
mmu-Gapdh-Sybr-R1	TCTTGCTCAGTGTCCTTGC
mmu-DNMT1-Sybr-F1	CCACTAAACGGAAACCCAAGG
mmu-DNMT1-Sybr-R1	CCTCTTCCAGTTTCTCCACAG
mmu-DNMT3a-Sybr-F1	ACCACGGCAATTCCTTCTC
mmu-DNMT3a-Sybr-R1	CTTCCTTTCGATCATCCTCCC
mmu-DNMT3b-Sybr-F1	ACCACGGCAATTCCTTCTC
mmu-DNMT3b-Sybr-R1	CTTCCTTTCGATCATCCTCCC
hCcnd1-Sybr-F1	CCTCGGTGTCCTACTTCAAATG
hCcnd1-Sybr-R1	GCGGTCCAGGTAGTTCATG
hGapdh-Sy-F1	ACATCGCTCAGACACCATG

hGapdh-Sy-R1 TGTAGTTGAGGTCAATGAAGGG

D. Primers for bisulfite sequencing

Bis-F1: 5’-GGGTTAATTGAATATTATTTTATGGGT-3’

Bis-R1: 5’-AAAAAAACTAACCTCAATCCAAAAC-3’

E. shRNAs

NT-shRNA	SHC002	5’-CCGGCAACAAGATGAAGAGCACCAACTC-GAGTTGGTGCTCTTCATCTTGTTGTTTTT-3’
Pkp2#1	TRCN0000123350	5’-CCGG-GCCTTGAGAAACTTGGTATTT-CTCGAG-AAATACCAAGTTTCTCAAGGC-TTTTTG-3’
Pkp2#2	TRCN0000123351	5'-CCGG-CCTGAGTATGTCTACAAGCTA-CTCGAG-TAGCTTGTAGACATACTCAGG-TTTTTG-3'
NT-shRNA1/2		5’-CTAAGGTTAAGTCGCCCTCGCTCTA GCGAGGGCGACTTAACCTTAGGTTTTT-3’
Tcf4	TRCN0000012094	5'-CCGG-GCTGAGTGATTTACTGGATTT-CTCGAG-AAATCCAGTAAATCACTCAGC-TTTTT-3'
Yap1	TRCN0000238436	5'-CCGG-TGAGAACAATGACAACCAATA-CTCGAG-TATTGGTTGTCATTGTTCTCA-TTTTTG-3'
Dnmt1	TRCN0000225697	5'-CCGG-TGAGAACAATGACAACCAATA-CTCGAG-TATTGGTTGTCATTGTTCTCA-TTTTTG-3'
Dnmt3A	TRCN0000039034	5'-CCGG-CCAGATGTTCTTTGCCAATAACTCGAG TTATTGGCAAAGAACATCTGG-TTTTTG-3'
Dnmt3B	TRCN0000071069	5'-CCGG-GCTCTGATATTCTAATGCCAACTCGAG

TTGGCATTAGAATATCAGAGC-TTTTTG-3

F. Antibodies:

Antibody	Company	Catalog Number	Working dilution
Plakophilin2	Progen	651101	1:300
α-Tubulin	Cell Signaling	2125	1:1000
GAPDH	Abcam	8245	1:10000
YAP	Cell Signaling	4912	1:1000(IB) 1:300(IF)
TCF4	Cell Signaling	2569	1:1000
FABP4	Cell Signaling	3544	1:1000(IB) 1:1000(IF)
PPARγ	Santa Cruz	7273	1:200(IF)
CEBPA	Cell Signaling	8178	1:500(IF)
E2F1	Santa Cruz	sc-193X	5ug/ChIP
DNMT1	Active Motif	39204	5ug/ChIP
NKX2.5	Santa Cruz	sc-14033	1:1000
Anti-Rabbit IgG, Alexa Fluor 594	Life technology	21207	1:1000
Anti-Mouse IgG, Alexa Fluor 594	Life technology	21203	1:1000
Anti-Rabbit IgG, HRP linked	Cell Signaling	7074	1:2000
Anti-Mouse IgG, HRP linked	Cell Signaling	7076	1:3000
V450 Mouse Lineage Antibody Cocktail, with Isotype Control	BD Pharmingen	561301	20μl:10^6cells(FC)
APC Anti-Human/Mouse CD44	eBioscience	17-0441-82	2μg:10^6cells(FC)
PE Mouse Anti-Human CD140a	BD Pharmingen	556002	1μg:10^6cells(FC)

G. Taqman gene expression and microRNA assays (from life technology)

Ankrd1	Mm00496512_m1
Axin2	Mm00443610_m1
Agpat1	Mm00479699_g1
Agpat3	Mm00474003_m1
Ctgf	Mm01192932_g1
CyclinD1	Mm00432359_m1
Cyr61	Mm00487499_g1
Dgat1	Mm00515643_m1
Dgat2	Mm00499536_m1
Fabp4	Mm00445878_m1
Gapdh	Mm99999915_g1
Hes1	Mm01342805_m1
Hey1	Mm00468865_m1
Inhba	Mm00434339_m1
Jup	Mm00550256_m1
Lpl	Mm01345523_m1
Ncoa3	Mm00500775_m1
Pkp2	Mm00503159_m1

Pparg	Mm01184322_m1
Ppargc1b	Mm00504720_m1
hsa-miR-184	000485
snoRNA202	001232
hsa-miR-200b	002251
mmu-miR-429	001077
hsa-miR-188-5p	002320
hsa-miR-487b	001285
mmu-miR-881	002609

	miRNA-Ct				U6RNA-Average Ct				delta CT				Expression(RQ)				Fold change	T-Test
Assay	HL-1-1	HL-1-2	Pkp2-1	Pkp2-2	HL-1-1	HL-1-2	Pkp2-1	Pkp2-2	HL-1-1	HL-1-2	Pkp2-1	Pkp2-2	HL-1-1	HL-1-2	Pkp2-1	Pkp2-2		
mmu-miR-184-000485	28.9684	28.9583	32.9373	32.973	18.8978	18.7472	18.8836	18.7598	10.0706	10.2111	14.0537	14.2132	0.000929924	0.000843631	5.881E-05	5.26503E-05	*-15.913*	*0.002698*
mmu-miR-881-002609	32.9708	32.9713	35.9839	35.9759	18.8978	18.7472	18.8836	18.7598	14.073	14.2241	17.1003	17.2161	5.80236E-05	5.2254E-05	7.117E-06	6.56807E-06	*-8.058*	*0.003581*
mmu-miR-574-3p-002349	29.9959	29.9623	32.9698	32.0157	18.8978	18.7472	18.8836	18.7598	11.0981	11.2151	14.0862	13.2559	0.000456183	0.000420648	5.75E-05	0.00010223	*-5.490*	*0.006287*
mmu-miR-465b-5p-002485	28.976	28.9985	31.9815	30.9607	18.8978	18.7472	18.8836	18.7598	10.0782	10.2513	13.0979	12.2009	0.000925038	0.000820448	0.0001141	0.000212404	*-5.347*	*0.010081*
mmu-miR-100-000437	26.9706	26.9786	29.2046	28.9767	18.8978	18.7472	18.8836	18.7598	8.0728	8.2314	10.321	10.2169	0.003714027	0.003327375	0.0007818	0.000840246	*-4.341*	*0.005166*
mmu-miR-470-002588	32.9495	32.9938	34.9827	35.0141	18.8978	18.7472	18.8836	18.7598	14.0517	14.2466	16.0991	16.2543	5.88866E-05	5.14453E-05	1.425E-05	1.27929E-05	*-4.081*	*0.008184*
mmu-miR-671-3p-002322	32.9559	32.9605	34.9567	34.9619	18.8978	18.7472	18.8836	18.7598	14.0581	14.2133	16.0731	16.2021	5.8626E-05	5.26466E-05	1.45E-05	1.32642E-05	*-4.007*	*0.005306*
mmu-miR-10a-000387	30.9874	31.0972	32.8671	33.0322	18.8978	18.7472	18.8836	18.7598	12.0896	12.35	13.9835	14.2724	0.000229439	0.000191549	6.174E-05	5.05335E-05	*-3.750*	*0.015989*
mmu-miR-741-002457	33.947	33.9677	35.1433	36	18.8978	18.7472	18.8836	18.7598	15.0492	15.2205	16.2597	17.2402	2.94944E-05	2.61923E-05	1.275E-05	6.45926E-06	*-2.900*	*0.035854*
mmu-miR-34b-3p-002618	31.9649	31.9735	33.9735	33.0068	18.8978	18.7472	18.8836	18.7598	13.0671	13.2263	15.0899	14.247	0.000116523	0.000104349	2.867E-05	5.14311E-05	*-2.757*	*0.03201*
mmu-miR-23b-000400	31.97	31.9729	34.0044	32.9768	18.8978	18.7472	18.8836	18.7598	13.0722	13.2257	15.1208	14.217	0.000116112	0.000104392	2.807E-05	5.25118E-05	*-2.737*	*0.035547*
mmu-miR-99a-000435	26.964	26.9851	28.96	27.9847	18.8978	18.7472	18.8836	18.7598	8.0662	8.2379	10.0764	9.2249	0.003731057	0.003312417	0.0009262	0.0016712	*-2.712*	*0.035015*
mmu-miR-196b-002215	27.9228	27.9637	29.9329	28.9318	18.8978	18.7472	18.8836	18.7598	9.025	9.2165	11.0493	10.172	0.001919571	0.001680959	0.0004719	0.000866808	*-2.690*	*0.039186*
mmu-miR-1939-121180_mat	31.9913	31.9443	32.9691	32.9933	18.8978	18.7472	18.8836	18.7598	13.0935	13.1971	14.0855	14.2335	0.00011441	0.000106482	5.752E-05	5.19146E-05	*-2.018*	*0.007506*
mmu-miR-1198-002780	33.0248	33.9671	31.9936	31.997	18.8978	18.7472	18.8836	18.7598	14.127	15.2199	13.11	13.2372	5.58919E-05	2.62032E-05	0.0001131	0.000103563	*2.639*	*0.049728*
mmu-miR-133a-002246	24.9589	23.9697	22.9849	22.9883	18.8978	18.7472	18.8836	18.7598	6.0611	5.2225	4.1013	4.2285	0.014977078	0.026783717	0.058262	0.053345116	*2.673*	*0.031932*
mmu-miR-200a-000502	35.0536	36	34.0215	34.0464	18.8978	18.7472	18.8836	18.7598	16.1558	17.2528	15.1379	15.2866	1.36968E-05	6.40309E-06	2.774E-05	2.50193E-05	*2.625*	*0.052384*
mo-miR-351-002063	30.9921	29.9996	29.0056	28.9843	18.8978	18.7472	18.8836	18.7598	12.0943	11.2524	10.122	10.2245	0.000228693	0.000409911	0.0008974	0.000835832	*2.714*	*0.029236*
mmu-miR-20b-001014	34.9551	33.9497	32.9517	32.9473	18.8978	18.7472	18.8836	18.7598	16.0573	15.2025	14.0681	14.1875	1.46646E-05	2.65211E-05	5.822E-05	5.35966E-05	*2.715*	*0.030965*
mmu-miR-132-000457	30.9572	30.008	28.9813	28.9784	18.8978	18.7472	18.8836	18.7598	12.0594	11.2608	10.0977	10.2186	0.000234293	0.000407532	0.0009126	0.000839257	*2.730*	*0.027543*
mmu-miR-342-3p-002260	28.9676	27.9805	26.9624	26.9563	18.8978	18.7472	18.8836	18.7598	10.0698	9.2333	8.0788	8.1965	0.00093044	0.001661498	0.0036986	0.003408848	*2.742*	*0.029016*
mmu-miR-362-5p-002614	31.9503	31.9776	29.9523	29.9421	18.8978	18.7472	18.8836	18.7598	13.0525	13.2304	11.0687	11.1823	0.000117708	0.000104053	0.0004656	0.000430321	*4.040*	*0.00313*
mmu-miR-1-002222	28.9827	28.9938	26.9521	26.9758	18.8978	18.7472	18.8836	18.7598	10.0849	10.2466	8.0685	8.216	0.000920752	0.000823125	0.0037251	0.003363083	*4.065*	*0.004887*
mmu-miR-676-001959	33.0019	31.982	29.9673	29.9792	18.8978	18.7472	18.8836	18.7598	14.1041	13.2348	11.0837	11.2194	5.67862E-05	0.000103736	0.0004608	0.000419396	*5.483*	*0.007475*
mmu-miR-429-001077	34.9879	34.0145	31.9758	31.9765	18.8978	18.7472	18.8836	18.7598	16.0901	15.2673	13.0922	13.2167	1.4335E-05	2.53562E-05	0.0001145	0.000105045	*5.532*	*0.006462*
mmu-miR-188-5p-002320	34.9684	32.9176	30.9058	30.9105	18.8978	18.7472	18.8836	18.7598	16.0706	14.1704	12.0222	12.1507	1.45301E-05	5.42356E-05	0.0002404	0.000219925	*6.694*	*0.012771*
mmu-miR-487b-001306	34.8681	33.6375	31.2131	31.1089	18.8978	18.7472	18.8836	18.7598	15.9703	14.8903	12.3295	12.3491	1.55762E-05	3.29286E-05	0.0001943	0.000191668	*7.957*	*0.002694*
mmu-miR-200b-002251	33.9966	33.8358	30.9523	30.9592	18.8978	18.7472	18.8836	18.7598	15.0988	15.0886	12.0687	12.1994	2.84976E-05	2.86998E-05	0.0002328	0.000212625	*7.787*	*0.002687*

Endogenous Control U6			
Assay	Sample	Ct	Average Ct
U6 snRNA-001973	HI-1-1	18.60538	18.89779367
U6 snRNA-001973	HI-1-1	18.948936	
U6 snRNA-001973	HI-1-1	19.139065	
U6 snRNA-001973	HL-1-2	18.96761	18.74718933
U6 snRNA-001973	HL-1-2	18.718025	
U6 snRNA-001973	HL-1-2	18.555933	
U6 snRNA-001973	Pkp2-1	18.745995	18.883584
U6 snRNA-001973	Pkp2-1	18.941477	
U6 snRNA-001973	Pkp2-1	18.96328	
U6 snRNA-001973	Pkp2-2	18.601871	18.75983867
U6 snRNA-001973	Pkp2-2	18.704176	
U6 snRNA-001973	Pkp2-2	18.973469	

Differentially expressed miR-184 target genes				
	Average FPKM			
Gene	**HL-1Pkp2shRNA**	**HL-1WT**	**Log2(fold_change)**	**q_value**
Bche	7.18765	0.182685	-5.29809	0
Rnf128	13.475	1.16229	-3.53524	0
Krt8	13.4598	1.22695	-3.45551	0
Acta1	21.2341	2.19407	-3.2747	0
Pgm5	16.8003	1.96903	-3.09293	0
Timp3	1.47509	0.217448	-2.76206	0
Cpne7	2.23906	0.352132	-2.6687	3.03E-09
Susd2	3.09541	0.527068	-2.55407	0
Slc12a8	1.48679	0.274184	-2.43898	6.91E-09
Camk2a	2.78699	0.657959	-2.08264	0.00000805
Alpk3	6.61629	1.69478	-1.96493	0
30419L09F	3.77173	0.982668	-1.94045	0
Tspan12	24.2752	6.35904	-1.9326	0
Lifr	68.9826	20.0837	-1.78021	0
30009J07F	1.47478	0.439042	-1.74807	3.82E-11
Foxo6	1.03285	0.330945	-1.64196	0.00000582
Itpr3	1.52355	0.501522	-1.60305	0.0000011
Epha4	6.82689	2.25461	-1.59835	0
Mmp15	7.19126	2.40599	-1.57961	0
Phf19	1.08629	0.368164	-1.56098	0.000044
Myo1e	1.35488	0.462543	-1.5505	1.4E-11
Gja1	40.8661	13.9774	-1.54781	0
Reep6	1.75803	0.604189	-1.54089	0.00030009
Des	166.135	58.4776	-1.5064	0
Plau	1.21106	0.426294	-1.50635	0.0000117
Dtna	3.60552	1.2871	-1.48608	5.69E-08
Reep2	1.59462	0.577592	-1.46509	0.00106525
Ttc39c	2.33354	0.846378	-1.46315	0.00000182
P2rx7	5.70427	2.1211	-1.42723	1.48E-09
Plxnd1	5.83042	2.36769	-1.30012	0
Fkbp1b	6.69655	2.73217	-1.29337	0.000000787
Fhl1	45.9353	18.7723	-1.291	0
Hspb6	15.3368	6.28087	-1.28796	1.52E-13
Homer1	14.9404	6.16123	-1.27792	0
B4galt5	14.9524	6.31875	-1.24267	0
Slc25a45	1.07376	0.458784	-1.22678	0.000863125
Camta1	3.94044	1.68675	-1.22411	0.00296505
Ctsb	43.1553	18.5806	-1.21574	0
Ppargc1b	2.2353	0.97627	-1.19512	7.43E-08
Wnk1	14.0242	6.16628	-1.18545	0

	Average FPKM			
Gene	**HL-1Pkp2shRNA**	**HL-1WT**	**Log2(fold_change)**	**q_value**
Erc1	4.46447	2.04052	-1.12956	0
Ift81	21.9487	11.2211	-0.967923	0
Ppm1l	2.14053	1.10562	-0.953113	0.000015
Sfrs2ip	8.30357	4.36609	-0.927391	0
Notch3	1.40772	0.750137	-0.908139	0.00000203
Gmpr	19.1434	10.2531	-0.900785	9.97E-15
Slc25a13	7.12667	3.82016	-0.899594	1.47E-11
E2f2	2.74558	1.47449	-0.896893	9.45E-08
30096C10I	10.5486	5.71959	-0.883066	3.49E-11
Plec1	8.87601	4.83008	-0.877864	0
Usp28	7.87013	4.32568	-0.863459	6.45E-12
Itsn2	38.9886	21.8394	-0.836117	0
Fyn	1.39747	0.786108	-0.830017	0.00571784
Fkbp1a	54.624	30.7503	-0.828933	6.13E-14
Ppp2r5a	84.1606	47.4009	-0.82823	0
Ncapd2	52.1172	29.6066	-0.815842	0
Pde4a	3.19065	1.82114	-0.809003	0.0000367
Tmem206	15.9482	9.16305	-0.799496	0.000023
Relt	1.73732	1.00561	-0.788796	0.0107498
Osbpl2	42.3954	24.6716	-0.781056	0
Gtpbp1	21.3908	12.5751	-0.766422	2.44E-14
Parvb	3.27314	1.9417	-0.753355	0.000000574
Pphln1	6.20395	3.70645	-0.743147	0.00000176
Arhgap1	39.3447	23.5983	-0.737488	2.04E-13
Ptpn1	10.5216	6.34852	-0.728854	2.48E-12
Gnai2	70.4007	42.7777	-0.71873	4.31E-14
Celsr1	1.31033	0.799046	-0.713578	0.000103875
Btg2	13.5459	8.30973	-0.704984	5.03E-11
Efnb3	11.7891	7.28746	-0.693969	3.06E-10
Nlgn2	1.23296	0.763012	-0.692353	0.0382146
Suv39h2	2.35694	1.48458	-0.666865	0.00471024
Aox1	3.23485	2.0424	-0.663434	0.0000587
Tspan9	28.8491	18.4191	-0.647324	5.38E-11
Gfod1	5.05447	3.2292	-0.646383	0.000000017
Rnf19a	6.45643	4.13549	-0.642678	3.39E-08
Plagl2	1.75117	1.1247	-0.638779	0.000611053
Cds2	12.9936	8.34736	-0.63841	2.04E-12
Shisa4	10.7935	6.94245	-0.636653	0.00244198
Egln3	2.15463	1.40127	-0.620708	0.00293974
Map3k7ip1	10.0817	6.57077	-0.617607	5.38E-08
Chmp4b	76.0544	49.6398	-0.615535	8.09E-12
Prdm16	1.10749	0.725943	-0.609367	0.0275819
Uros	6.63778	4.38663	-0.597588	0.0063327

	Average FPKM			
Gene	**HL-1Pkp2shRNA**	**HL-1WT**	**Log2(fold_change)**	**q_value**
Rassf2	3.76131	2.48682	-0.596936	0.000201564
10008F13F	82.0565	54.2787	-0.596233	0.000000233
Stom	40.9747	27.1166	-0.595557	4.87E-11
Agpat3	31.3299	21.224	-0.561839	0.0000202
Add3	61.3926	41.6302	-0.560433	0.00000001
Aes	119.153	80.977	-0.557234	3.7E-10
Rab22a	23.1848	15.8083	-0.5525	0.0000103
Abca2	3.90995	2.6662	-0.552367	0.0000692
Hap1	6.1726	4.2157	-0.550107	0.000821441
Phyhip	5.25173	3.59641	-0.546237	0.00177599
Mlf2	104.378	72.0158	-0.535432	1.05E-09
Adrm1	88.1664	61.0166	-0.531026	0.0000013
Gnas	276.045	191.265	-0.529328	0.000000235
Tmem65	12.2641	8.52289	-0.525024	0.00000474
Prepl	4.28386	3.00702	-0.51058	0.00543301
Ddx19b	3.29131	2.31734	-0.506191	0.0000498
Zfp217	2.60392	1.83642	-0.503787	0.014816
Clptm1	19.6691	13.8762	-0.503316	0.00000011
Grina	54.5078	38.5993	-0.497889	0.000000923
Flot2	20.9001	14.8178	-0.496181	0.0000017
Rap1gap	3.71311	2.63369	-0.495541	0.0497323
Herc3	7.57815	5.41718	-0.484302	0.000179938
Necap1	14.7376	10.5439	-0.483091	0.0000144
Dtd1	28.7091	20.5948	-0.47923	0.0000131
Ncoa3	6.91483	4.97248	-0.475729	0.00288118
Tnrc6b	4.08116	2.9566	-0.465038	0.0000113
Trak1	26.8557	19.5511	-0.457975	0.000255254
Eif2s2	82.4258	60.0259	-0.45751	0.000000423
Rttn	3.65003	2.65896	-0.457044	0.016585
Hexim1	3.74769	2.73294	-0.455552	0.00268384
Plekhb2	20.26	14.8364	-0.449493	0.00000583
Cdc25a	7.90853	5.79464	-0.448691	0.000947718
Qk	45.1224	33.0746	-0.448119	0.0000926
Abhd2	5.86796	4.31097	-0.444845	0.000330587
Dntt	9.27984	6.89315	-0.428937	0.0268039
Crlf3	11.576	8.63942	-0.422128	0.000994636
Impdh1	8.26037	6.17293	-0.420251	0.00228326
Bcl2l1	6.61097	4.94057	-0.420182	0.0162744
Ncam1	5.95839	4.46629	-0.415846	0.00221263
Ccdc47	25.5732	19.1693	-0.415832	0.0000587
P4ha2	15.2851	11.4591	-0.415632	0.000811737
Eif6	89.3775	67.1054	-0.413483	0.00000751
Pycrl	31.7469	23.931	-0.407733	0.000185982

	Average FPKM			
Gene	**HL-1Pkp2shRNA**	**HL-1WT**	**Log2(fold_change)**	**q_value**
Otub2	8.79144	6.67148	-0.398093	0.0051228
Stat3	26.6951	20.2806	-0.396474	0.0000432
Tmbim1	32.8753	25.0106	-0.394466	0.00294546
Pxk	4.86869	3.74129	-0.379996	0.0209646
Ttc7	6.50792	5.01552	-0.375796	0.0178865
Ndrg3	9.82643	7.62726	-0.365503	0.00652351
Pif1	6.24946	4.86279	-0.361947	0.03434
Glod4	17.7501	13.8217	-0.360895	0.000800396
Tgm2	153.283	119.651	-0.357359	0.00038769
30402H24I	8.55627	6.69332	-0.35426	0.00611627
Immt	100.744	78.8821	-0.352921	0.000847821
Fbxo5	12.2012	9.55714	-0.352372	0.0065312
Stxbp1	3.46954	2.72297	-0.349565	0.0454547
Ppp2r5c	32.8134	25.7968	-0.347093	0.00509571
30437P03I	19.2244	15.1389	-0.344671	0.00346517
Fbxl14	8.31429	6.55489	-0.343022	0.00362404
Etv3	5.05205	3.98485	-0.342341	0.0294552
30007P12I	4.6192	3.64918	-0.340071	0.0177828
Gpr107	7.53659	5.96096	-0.338367	0.0120154
Agpat1	22.1647	17.5468	-0.337052	0.00299628
Trpc4ap	26.558	21.2228	-0.323529	0.00147103
Rabac1	76.4841	61.1202	-0.323512	0.00222761
Sesn2	6.70153	5.37039	-0.319462	0.0355186
Fuca1	11.7854	9.51583	-0.3086	0.0105506
Tmco1	20.3214	16.4921	-0.301223	0.0021039
Efhd2	28.3418	23.0265	-0.299632	0.0035384
Snd1	65.9376	53.6005	-0.298856	0.00179138
Cpsf2	17.9054	14.6963	-0.284942	0.0398121
Ube2s	218.02	179.102	-0.28368	0.00348826
Vps28	39.7244	32.8968	-0.27208	0.0224055
Rnd3	25.898	21.472	-0.27038	0.00830042
Kif13a	8.18896	6.79208	-0.269826	0.041871
Rbm9	11.2996	9.39513	-0.266289	0.0225842
Map2k2	21.0763	25.4699	0.273169	0.0329056
Utp18	14.5414	17.5739	0.27327	0.0138249
Klf6	3.61879	4.40357	0.283163	0.0426405
Aldh9a1	5.43675	6.61758	0.28356	0.0414963
Fzd7	5.56072	6.77598	0.28516	0.0299117
Clspn	6.90761	8.43472	0.288153	0.0203161
Ezr	37.6539	46.093	0.291747	0.00489464
Igf1r	3.50723	4.29541	0.292466	0.0161783
Chst11	5.44226	6.69914	0.29977	0.0257837
Bri3bp	7.07894	8.72764	0.302057	0.00372025

	Average FPKM			
Gene	**HL-1Pkp2shRNA**	**HL-1WT**	**Log2(fold_change)**	**q_value**
Mafk	7.88271	9.75648	0.30767	0.0129525
Khdrbs3	35.6764	44.1891	0.308721	0.00184476
Slc30a9	16.292	20.2784	0.315779	0.00180849
Tsen54	8.31619	10.3704	0.318482	0.0171115
Sdad1	6.88164	8.58401	0.318898	0.00364032
Gkap1	11.2729	14.0949	0.322314	0.0257262
Ppme1	13.0903	16.3706	0.322611	0.00416102
Mynn	5.41005	6.77289	0.324128	0.0161771
Dmtf1	6.88943	8.63541	0.32588	0.0300308
Lrba	4.50586	5.64973	0.32638	0.00578848
Stam2	4.92933	6.19835	0.330493	0.00784183
Kcne1	12.7449	16.063	0.333827	0.00757547
Csnk1g2	15.9732	20.1998	0.338687	0.00654851
Hist1h1d	57.2306	72.4386	0.339971	0.000296371
3426M11	4.96142	6.28594	0.341375	0.00370132
Grsf1	26.8789	34.1605	0.345851	0.000796476
Snip1	9.02986	11.4808	0.34645	0.0045251
Dhcr24	24.3793	31.0877	0.350685	0.000212991
Tfip11	4.608	5.87662	0.350847	0.00887897
Trim27	12.3214	15.7316	0.352499	0.00352907
Commd8	9.43025	12.0481	0.353443	0.00326279
Rhot1	10.6988	13.6842	0.355073	0.00354039
Srpk2	6.68819	8.57715	0.358882	0.00231383
Prkag2	17.5485	22.5327	0.360673	0.00802484
Cdk5rap2	8.64296	11.1187	0.36339	0.0011822
Ppp1cc	91.8111	118.227	0.364825	0.000108068
Angptl2	5.36597	6.92252	0.367459	0.00454977
Lzts2	13.7228	17.7626	0.372271	0.00328512
30402E16F	6.59864	8.54369	0.372692	0.0228557
Fez2	9.1833	11.8907	0.37275	0.00277474
Hand2	35.2424	45.6481	0.373242	0.0000942
Stoml2	39.9616	51.8021	0.374395	0.000117519
Ehd1	13.1415	17.0679	0.377156	0.000249857
Prpf4	3.54253	4.62208	0.383762	0.00180725
Rab8b	4.55478	5.96006	0.387944	0.0011904
Gatad2b	3.68573	4.82435	0.388382	0.0029591
Snx27	5.36361	7.02758	0.389826	0.00357497
Cenpn	12.3774	16.2404	0.391877	0.000857838
10007L01F	12.5688	16.5444	0.396496	0.000283719
Slc2a4	10.4982	13.8309	0.397753	0.000660017
S100pbp	7.01874	9.27879	0.402724	0.0187618
Adcy1	4.14109	5.47678	0.403316	0.000089
Rnf38	4.45878	5.8996	0.403967	0.0116983

	Average FPKM			
Gene	**HL-1Pkp2shRNA**	**HL-1WT**	**Log2(fold_change)**	**q_value**
Hiat1	18.5944	24.6116	0.404474	0.0000476
Clcn7	10.085	13.3627	0.406	0.000339104
Chn2	2.86535	3.81855	0.414317	0.00788841
Ptma	494.34	661.475	0.420185	0.000352282
Siah2	4.33343	5.80164	0.420951	0.00540006
Zbtb5	4.28377	5.73626	0.421229	0.00511846
Mesdc2	14.4489	19.3804	0.423633	0.00000821
Zfp523	3.23738	4.34472	0.42444	0.0233668
Foxj3	3.76025	5.05006	0.425471	0.004748
Rsu1	22.4104	30.1662	0.428762	0.0000538
Rprd1a	11.0659	14.9217	0.431293	0.000888883
Lrrc40	9.09783	12.2794	0.432646	0.000052
Ap2m1	85.454	115.406	0.433503	0.0000277
Uso1	7.35254	9.93125	0.433732	0.0488176
Lasp1	5.90933	7.98442	0.434191	0.000615207
Ctdsp2	9.25499	12.5682	0.441474	0.000041
10007L15R	25.3471	34.4267	0.441707	0.0000067
Pkd1	3.02045	4.10483	0.442559	0.000100402
Cisd2	11.3547	15.4399	0.44337	0.000032
Lrrc8a	5.26049	7.15393	0.443537	0.000349672
Git1	5.76638	7.86489	0.447761	0.00034135
Prps2	13.1199	17.8994	0.448155	0.00000535
Tmem38b	5.21345	7.12526	0.450705	0.00226968
Map3k7ip3	2.17961	2.98339	0.452885	0.010106
Ndel1	22.2054	30.4238	0.454289	0.0000112
Dgcr2	12.4284	17.0328	0.45467	0.0000372
Slc38a7	3.22256	4.42308	0.456844	0.0232542
Cdc42se1	11.7828	16.1752	0.457096	0.0166723
Sec24a	1.68479	2.31976	0.461405	0.0178956
Depdc5	4.03246	5.55242	0.461457	0.00259283
Gsk3b	4.55819	6.3074	0.468585	0.00000237
Trim33	3.40074	4.71093	0.470165	0.0000746
Lrp5	3.42889	4.76555	0.474899	0.0000717
Qtrtd1	3.30968	4.60913	0.477804	0.0116028
Nhlrc3	2.57938	3.59672	0.479659	0.0285968
Nav1	1.61206	2.2504	0.481272	0.000808437
Stx4a	7.07951	9.90182	0.484044	0.00103332
Sh3bgrl	18.4929	25.9037	0.486192	0.0000028
Gosr2	21.6459	30.4314	0.491466	0.000000203
Magi3	20.9888	29.5984	0.495898	0.000000159
Tmem9b	17.6794	24.9734	0.498326	0.00000344
Alg2	2.60922	3.68817	0.499285	0.0217726

	Average FPKM			
Gene	**HL-1Pkp2shRNA**	**HL-1WT**	**Log2(fold_change)**	**q_value**
Psd3	2.99693	4.25742	0.506492	0.0000113
Golga7	22.1062	31.4288	0.507634	0.00000456
Ube2b	12.4352	17.7028	0.509553	0.0000912
Eif4ebp1	132.455	189.434	0.516189	1.13E-08
Acaca	10.342	14.8388	0.520867	0.000000012
Nsun2	11.3894	16.3433	0.521001	4.82E-08
Ppm1f	8.85045	12.7059	0.52168	0.000000667
Stat5a	3.89012	5.60474	0.526832	0.000409877
Arl13b	1.74948	2.52115	0.527153	0.0131759
Med28	18.4746	26.6465	0.528404	0.0000227
Hspb8	74.1552	106.972	0.528616	4.64E-09
Ubn1	7.68909	11.1048	0.530299	0.00000149
Prkx	3.11768	4.50421	0.530799	0.000141575
Vti1a	3.79004	5.49522	0.535966	0.0101381
Rufy3	3.41061	5.00296	0.552753	0.00010987
Rcc1	14.8404	21.7885	0.554033	0.000000691
Vac14	10.8879	15.9871	0.554183	4.19E-08
Atp8a1	1.15358	1.69707	0.556929	0.00382542
Ankrd27	6.23947	9.18958	0.558575	0.0000506
Cog2	10.9619	16.1836	0.562036	0.000000622
Csf1	2.93014	4.3338	0.564663	0.00111966
Rhobtb1	5.193	7.71348	0.570814	0.0000389
Sppl3	7.30415	10.8599	0.572224	0.000000808
Zfx	6.01484	8.95205	0.573692	0.000000964
Phka1	4.4586	6.64111	0.574835	6.04E-08
Stx2	4.59373	6.87874	0.582479	0.0000837
Tshz1	7.8165	11.7441	0.587346	1.88E-10
Slc25a23	3.98215	5.9858	0.587995	0.00000251
Slc35d1	1.21917	1.83434	0.589362	0.0147459
Zc3h18	20.4354	30.769	0.590403	4.25E-09
Myo1c	21.8872	32.9665	0.590911	7.06E-09
Vps33a	9.3297	14.076	0.593333	2.65E-08
Sntb2	10.6918	16.1459	0.594665	0.000000725
Stag1	5.15035	7.78656	0.596317	4.14E-08
Klhl30	17.1329	25.9396	0.59839	3.91E-10
Ntan1	16.9553	25.6738	0.598565	0.0120666
Golm1	9.24917	14.024	0.600496	2.12E-09
Smarca2	5.72859	8.74303	0.609953	0.0000104
Cyp26b1	3.24365	4.95423	0.611044	0.000215367
Mllt3	2.25428	3.44633	0.612394	0.000000915
BC026590	1.35679	2.07722	0.614459	0.0309912
Zc3hav1l	1.235	1.89703	0.619226	0.00193683
Tgds	2.77539	4.27181	0.622159	0.000837248

	Average FPKM			
Gene	**HL-1Pkp2shRNA**	**HL-1WT**	**Log2(fold_change)**	**q_value**
30308A19I	2.51454	3.87142	0.622569	0.00097306
Amotl2	7.59634	11.6992	0.623032	3.03E-09
Tcfap4	2.42517	3.73932	0.624688	0.000559256
Ulk1	2.6981	4.17013	0.628147	0.0000123
Ddc	4.34114	6.71783	0.629921	0.0209351
Pitpnm2	2.40873	3.72907	0.630542	0.0000326
Zmym3	6.15621	9.54036	0.632002	0.000238875
Ssr4	63.1764	97.9716	0.632978	0.000924503
Slc6a9	2.76266	4.2863	0.633674	0.000543717
Cggbp1	18.3801	28.5347	0.634569	1.41E-10
Akap12	5.31297	8.26123	0.636839	6.25E-11
Lgr6	1.75462	2.7312	0.638378	0.00204083
Pdzd11	19.0583	29.7085	0.640453	2.48E-08
Zyx	7.50933	11.8415	0.657095	0.00000148
16H22S68(	6.82468	10.7687	0.658011	0.000251981
Lpp	5.715	9.06197	0.665071	0.0000152
Eif4ebp2	3.72194	5.91511	0.66835	2.08E-08
Rab3d	3.91844	6.23315	0.669683	0.000000373
Slc7a5	33.8847	53.9569	0.671171	6.13E-14
Ube2a	5.99807	9.5643	0.673161	0.00000244
00021P15F	2.70222	4.31177	0.674132	0.00000493
Nhlrc1	0.708634	1.13532	0.679993	0.0293141
Galnt2	49.5119	79.354	0.68053	2.39E-13
Arhgef7	10.1573	16.3109	0.68332	8.11E-10
Trim2	9.48078	15.2279	0.683638	4.85E-09
Arl8b	21.9304	35.2698	0.685504	8.39E-14
Gca	3.6729	5.91609	0.687725	0.00000479
Evc2	2.31374	3.73256	0.68994	0.000120975
Trim32	3.6717	5.92368	0.690045	0.0000778
Unc5b	2.11803	3.42076	0.691595	4.79E-08
Smap1	5.10739	8.25614	0.692881	0.000000213
Xiap	3.8873	6.292	0.694749	9.73E-09
Hspa12a	1.37513	2.22916	0.696929	0.0000416
10003E01F	14.1719	23.001	0.698659	6.36E-09
Rap2c	4.28078	6.94812	0.69875	0.00000389
Tmco4	3.8143	6.20056	0.700978	0.0000036
Cyb5b	85.6909	140.642	0.71481	3.88E-13
10079N02I	14.3283	23.55	0.716864	0.000000554
Gm672	0.633588	1.04511	0.722039	0.00740348
Prkacb	9.1291	15.0611	0.722279	2.43E-13
Phc2	6.82271	11.3158	0.729923	2.03E-08
Nkap	2.58239	4.287	0.731263	2.24E-08
Rab35	13.0823	21.7274	0.731895	1.2E-12

	Average FPKM			
Gene	**HL-1Pkp2shRNA**	**HL-1WT**	**Log2(fold_change)**	**q_value**
Anp32b	18.0306	30.3016	0.748946	2.9E-13
Ubap2	4.29899	7.24903	0.753791	2.22E-10
B3galtl	4.68305	7.90049	0.754493	0.000574043
Ikzf2	0.600872	1.01535	0.756848	0.00182296
Frmd4a	1.75317	2.97443	0.762648	0.0000274
Arid5b	0.874966	1.49693	0.774706	0.000273738
Psip1	30.4575	52.1098	0.774759	7.25E-12
Lmln	1.09753	1.87886	0.775593	0.00134896
Acp1	37.6977	64.5909	0.776853	3.84E-14
Tns3	5.04133	8.65095	0.779055	8.75E-10
Ndst1	10.3663	17.7921	0.779328	5.86E-08
Dlg1	8.97271	15.4104	0.78029	1.29E-13
Zfp777	1.7013	2.92336	0.780989	0.000961136
Dcun1d3	1.53924	2.64866	0.783043	0.0000367
Clec16a	4.71317	8.11649	0.784159	0.000000221
Man2a1	21.9623	37.8567	0.785522	0
30012A19I	0.896076	1.54743	0.788178	0.00419915
Zmiz1	3.90357	6.75544	0.791257	1.86E-11
Polr2h	15.4563	26.9964	0.804567	5.29E-10
Syngr1	59.6451	104.178	0.804573	2.77E-12
Zdhhc7	15.8681	27.7296	0.805302	0
Rab1	17.0928	29.9282	0.808118	2.9E-13
Fmnl3	1.86109	3.27672	0.8161	0.00000189
Tpcn1	1.81871	3.21064	0.819949	4.63E-09
Src	2.38475	4.21674	0.822287	0.000000819
Unc119b	12.7833	22.7393	0.830928	0
Nkrf	1.43065	2.55094	0.834358	0.0000878
Eif2c1	1.62511	2.90242	0.836719	2.2E-09
Abcd3	15.4632	27.752	0.843755	0
Ebna1bp2	15.4597	27.7592	0.84445	0
Numbl	1.78365	3.2046	0.845313	0.0000513
Itsn1	10.9789	19.8432	0.853914	0
Cmtm4	34.6902	63.0881	0.86284	8.85E-09
Slc36a1	1.77944	3.23858	0.863942	0.000000039
Arcn1	55.9444	102.189	0.869176	0
Man1c1	4.125	7.58175	0.878137	0
Wwc2	8.44927	15.5533	0.880325	0
Ap3m1	20.8433	38.8272	0.897481	0.0000256
Plekhh2	1.22372	2.30248	0.91192	8.17E-12
B4galt1	19.2274	36.8513	0.938552	0
Ankrd52	2.28336	4.38337	0.940879	3.41E-13
Prkab2	2.23211	4.31122	0.94969	0.000000026
Tmeff1	1.75827	3.4029	0.95261	0.000581989

	Average FPKM			
Gene	**HL-1Pkp2shRNA**	**HL-1WT**	**Log2(fold_change)**	**q_value**
Rragc	13.616	26.8488	0.979552	0
Fdxr	5.93116	11.7548	0.986863	1.14E-12
Pldn	2.9115	5.81315	0.997559	4.58E-12
Ets2	1.45826	2.91833	1.0009	6.92E-10
Ifnar1	5.44487	10.9245	1.0046	0
Zmat3	1.82303	3.70689	1.02387	0
Fkbp10	2.99023	6.08279	1.02448	0.000000141
Tbc1d1	17.4479	35.5546	1.02699	0
Dcun1d4	2.55462	5.2147	1.02947	4.09E-12
Tsr2	3.74483	7.78295	1.05542	0
Emp1	6.37309	13.2902	1.06029	0
Eomes	1.37992	2.87835	1.06066	2.82E-08
Gpr173	0.730241	1.5334	1.07029	0.000193332
Mkl1	0.990183	2.08555	1.07466	0.000000273
Hadh	24.97	52.7265	1.07833	0
Smad1	4.84538	10.2973	1.08759	0
Lnx1	6.92823	14.8936	1.10413	1.04E-10
Hyou1	71.1844	153.51	1.1087	0
Slc46a1	1.00192	2.21289	1.14316	0.00000645
Rab3il1	1.02032	2.26818	1.15251	0.00000261
Smad9	1.14491	2.57333	1.16841	3.63E-11
Chst12	2.62819	5.99552	1.18982	7.72E-09
Swap70	7.49665	17.3222	1.2083	0
Tpm2	98.7529	228.234	1.20862	0
Sh3d19	1.64833	3.83051	1.21653	0
Adcy9	0.767446	1.83414	1.25697	0.00000401
Trdmt1	1.21295	2.90562	1.26033	0.000000334
Dapk1	2.73712	6.61069	1.27214	0
Zcchc14	3.91959	9.73433	1.31238	7.21E-11
10022B05I	24.0457	59.7878	1.31407	0
Rgl1	4.58922	11.4586	1.32011	0
Fzd2	4.4711	11.1768	1.3218	0
Dact3	4.28795	10.811	1.33413	0
Serinc5	2.86411	7.37083	1.36374	0
Nfyc	15.079	39.0877	1.37418	0
Zc3h12a	0.473779	1.25035	1.40004	0.000546588
Eif5a2	6.3424	16.9485	1.41805	0
Zfp704	0.837377	2.28699	1.4495	0
Klhl24	8.04856	22.1236	1.45879	0
Foxo1	0.528515	1.48563	1.49106	2.93E-10
Pink1	9.75375	27.9903	1.5209	0
Col4a4	7.27376	22.0527	1.60018	0
30224M15I	0.35314	1.20048	1.7653	0.0000888

	Average FPKM			
Gene	**HL-1Pkp2shRNA**	**HL-1WT**	**Log2(fold_change)**	**q_value**
Cabp1	1.18317	4.47632	1.91966	6.59E-09
Mmp14	5.81187	22.6551	1.96276	0
Emilin1	1.4939	5.9846	2.00217	0
Tgfb2	1.12864	4.55554	2.01304	0
Etv5	1.54098	6.38705	2.0513	0
Hs3st3b1	0.580553	2.57901	2.15132	0
Runx1	0.930973	4.55359	2.29019	0
Nipsnap1	0.832757	4.31912	2.37477	0
Gper	0.665631	3.56461	2.42095	8.17E-10
Ppap2b	3.0782	17.8475	2.53556	0
Rasgef1b	1.5352	9.19842	2.58296	0
Crispld2	0.42764	2.64117	2.62671	4.91E-11
Mcf2l	1.57594	11.5779	2.87709	0
Igfbp4	6.85319	53.3595	2.9609	0
Reck	0.56863	4.61862	3.0219	0
Lypd1	0.18629	1.95914	3.3946	5.68E-08
Ltbp1	0.15593	1.71335	3.45785	0
Tmem86a	1.12874	13.6796	3.59924	0
Arhgdib	1.25911	26.747	4.4089	0
Eln	0.0409468	1.18427	4.85411	8.73E-12

Online TABLE III

Echocardiographic Data

	Wild type	***Pkp2*^{shRNA} (no promoter)**	***Nkx-2-5-Cre:Pkp2*^{shRNA}**	**p**
N	12	12	19	
Male/Female	6/6	5/7	9/10	0.915
Age (months)	9.0±2.1	8.4±1.5	8.1±0.9	0.284
Body weight (g)	32.7±3.6	35.5±4.3	33.9± 4.3	0.267
HR (bpm)	565± 106	582 ±84	576±70	0.885
IVST (mm)	0.99 ±0.11	0.92± 0.16	0.76± 0.06*	≤0.001
PWT (mm)	0.99± 0.07	0.94± 0.07	0.73 ±0.08*	≤0.001
LVEDD (mm)	3.01±0.26	3.20±0.22	3.80± 0.46*	≤0.001
LVEDDi (mm/g)	0.09±0.11	0.09±0.01	0.11± 0.02*	≤0.001
LVESD (mm)	1.07±0.22	1.26± 0.30	2.10± 0.55	≤0.001
FS (%)	64±6	61±9	46±9*	≤0.001
LVM (mg)	85±27	98±22	95±19	0.358
LVMi (mg/g)	2.6±0.8	2.8±0.5	2.8±0.5	0.753

Abbreviations: *Pkp2*^{shRNA}*:* shRNA against *Pkp2* mRNA without a promoter; *Nkx-2-5-Cre:Pkp2*^{shRNA}*:* shRNA against *Pkp2* mRNA expressed under the transcriptional control of *Nkx2-5* promoter. HR, heart rate; bpm, beats per minutes; IVST, interventricular septal thickness; PWT, posterior wall thickness; LVEDD, left ventricular end diastolic diameter; LVEDDi, LVEDD divided for the body weight; LVESD, left ventricular end systolic diameter; FS, fractional shortening; LVMass, left ventricular mass; LVMi, LVMass divided for the body weight.*p≤0.005 vs WT and *Nkx2-5-Cre:Pkp2*^{shRNA}.

Summary of information	
Number of CpGs analyzed	15
Number of clones used for bisulfite sequencing (HL-1)	17
Number of clones used for bisulfite sequencing (HL-1$^{Pkp2\text{-}shRNA}$)	20

CpG position	1	58
Number of methylated CpGs (HL-1)	4	5
Number of CpGs (HL-1)	17	17
ratio of methylation (%) (HL-1)	23.5	29.4
Number of methylated CpGs (HL-1$^{Pkp2\text{-}shRNA}$)	16	20
Number of CpGs (HL-1Pkp2-shRNA)	20	20
ratio of methylation (%) (HL-1$^{Pkp2\text{-}shRNA}$)	80	100
Number of methylated CpGs (total)	20	25
Number of CpGs (total)	37	37
ratio of methylation (%) (total)	54.1	67.6
P-value of Fisher's exact test	0.000913	3.34E-06
P-value of Mann-Whitney U-test	0.000001	
S.D. of % methylated (between CpGs, HL-1)	10.3	
S.D. of % methylatied (between sequences, HL-1)	35.8	
S.D. of % methylatied (between CpGs,HL-1$^{Pkp2\text{-}shRNA}$)	7.1	
S.D. of % methylatied (between sequences, HL-1$^{Pkp2\text{-}shRNA}$)	4.3	
S.D. of % methylatied (between CpGs, total)	7	
S.D. of % methylatied (between sequences, total)	43.1	

Condition to exclude low quality sequences	
Upper limit of unconverted CpHs	5
Lower limit of percent converted CpHs	90.00%
Upper limit of alignment mismatches	25
Lower limit of percent identity	90.00%

Methylation status of each CpG site

151	156	177	183	187	192	221	281
5	5	8	5	5	5	3	2
17	17	17	17	17	17	17	17
29.4	29.4	47.1	29.4	29.4	29.4	17.6	11.8
18	20	19	20	20	20	18	20
20	20	20	20	20	20	20	20
90	100	95	100	100	100	90	100
23	25	27	25	25	25	21	22
37	37	37	37	37	37	37	37
62.2	67.6	73	67.6	67.6	67.6	56.8	59.5
0.00021	3.34E-06	0.00198	3.34E-06	3.34E-06	3.34E-06	1.06E-05	1.45E-08

287	304	357	371	385	Total
3	1	3	2	3	59
17	17	17	17	17	255
17.6	5.9	17.6	11.8	17.6	23.14
20	18	18	16	19	282
20	20	20	20	20	300
100	90	90	80	95	94
23	19	21	18	22	341
37	37	37	37	37	555
62.2	51.4	56.8	48.6	59.5	61.44
1.11E-07	1.95E-07	1.06E-05	4.73E-05	1.47E-06	9.90E-73